Physics of Complex Plasmas: Some fundamental problems.

Robert Sütterlin

München 2010

Physics of Complex Plasmas: Some fundamental problems.

Robert Sütterlin

Dissertation
an der Fakultät für Physik
der Ludwig–Maximilians–Universität
München

vorgelegt von
Robert Sütterlin
aus München

München, den 18.6.2010

Erstgutachter: Gregor Morfill
Zweitgutachter: Victor Steinberg
Tag der mündlichen Prüfung: 27.9.2010

Contents

List of Figures

Acknowledgments

Dear Greg, I would like especially to thank you for inviting me on this demanding, adventurous and unique journey. When I came to MPE in 1998, "complex plasmas" had been freshly entitled "colloidal plasmas" by you, and the "Plasmakristall" group consisted of six people: Hubertus Thomas, Alexei Ivlev, Uwe Konopka, Dirk Goldbeck, Milenko Zuzic — and me. From then on you managed to get the *who is who* of complex plasmas, plasma physics, plasma-diagnostics, -engineering and -application, and dusty plasmas in geosciences to collaborate with our group, join our group as postdocs or senior scientists, and to grow it into something that most people would consider a research institute. Thanks for this opportunity.

Many thanks go to the Max-Planck-Gesellschaft and the Institute for Extraterrestrial Physics who supported my PhD studies in many ways, and which provided a unique basic research environment for the emerging field of complex plasmas.

To all my friends at work, all of you fellow scientists I am proud to share my time with, I'd like to say, that this is the best time of my life. My work would not have been the same without your individual scientific prowess and your support and encouragement as colleagues. I believe that our complex plasma group is the best and most successful group in the world, because all of us tried hard to improve collectively our research, instead of improving our individual CVs. Hubertus, thanks for trusting in me, and involving me in the Plasma Crystal projects — and not to forget the financial support.

Last but not least I would like to thank my friends and family who might have suffered some collateral damage along the way, but never blaming me or holding a grudge against me, for bad tempers when I was stressed, overworked, or just not satisfied with my scientific success. I enjoy my life around you.

Summary

Physics of complex plasmas is a wide and varied field. In the context of this PhD thesis I present the major results from my research on fundamental properties of the plasma sheath, the plasma dust interaction, non-Hamiltonian dynamics, and on non-equilibrium phase transitions, using complex plasmas as a model system.

The first chapter provides a short overview of the development of physics of Complex Plasmas. From fundamental plasma physics, properties of dust in plasmas, to the exceptional and unique features of complex plasmas. A summary of twenty years of research topics is also presented. This is followed by three chapters that illustrate publications based on experiments I did during my PhD. These publications, in my opinion, reflect nicely the large diversity of complex plasma research.

- The investigation of nonlinear vertical oscillations of a particle in a sheath of an rf discharge was a simultaneous test of (pre-)sheath models and parameters. The nonlinear oscillations were shown to derive from a (strong) nonlinearity of the local sheath potential. They could be described quantitatively applying the theory of anharmonic oscillations, and the first two anharmonic terms in an expansion of the sheath potential were measured. On top of that we provided a simple experimentally, theoretically and mathematically based method that allows for in situ measurement of these coefficients for other experimental conditions.

- The vertical pairing of identical particles suspended in the plasma sheath demonstrated some of the unique features that complex plasmas have as an open (non-Hamiltonian) system. Particle interaction becomes non-reciprocal in the presence of streaming ions. The symmetry breaking allows for mode-coupling of in plane and out of plane motion of particles.

- Lane formation is a non-equilibrium phase transition. I summarize the main result of my papers on the dynamics of lane formation, i.e., the temporal evolution of lanes. This is followed by an outlook on my future research on non-equilibrium phase transitions, how they relate to our research of systems at the critical point, and how they allow us to test fundamental theories of charging of particles and the shielding of the resulting surface potential.

Finally there is an appendix on the scaling index method. A versatile mathematical tool to quantify structural differences / peculiarities in data, that I used to define a suitable order parameter for lane formation.

Zusammenfassung

Die Physik komplexer Plasmen ist ein sehr vielgestaltiges Forschungsfeld. Im Rahmen dieser Dissertation möchte ich die wichtigsten Ergebnisse meiner Experimente mit komplexen Plasmen zu Eigenschaften der Plasmarandschicht, der Wechselwirkung zwischen Plasma und Staubteilchen, nicht konservativen Systemen und Nichtgleichgewicht-Phasenübergangen präsentieren.

Im ersten Kapitel gebe ich eine kurze Hinleitung zur Physik komplexer Plasmen. Angefangen mit grundlegender Plasmaphysik, über die wichtigsten Wechselwirkungen zwischen Staub und Plasma, bis zu den speziellen und einzigartigen Eigenschaften komplexer Plasmen. Zudem zeige ich kurz die Schwerpunkte aus den letzten 20 Jahren Forschung an komplexen Plasmen.

Danach folgen drei Kapitel in denen ich ausgewählte Publikationen aus der Zeit meiner Doktorarbeit vorstelle, die meiner Ansicht nach in besonderer Weise den Umfang und die Vielschichtigkeit meiner Forschung und des Forschungsgebietes belegen.

- Mit Hilfe der Untersuchung nichtlinearer Schwingungen von Staubteilchen in der Plasmarandschicht konnte ich einen Test für Randschichtmodelle durchführen und gleichzeitig wichtige Parameter der Randschicht messen. Meine Kollegen und ich haben gezeigt, dass die Ursache der nichtlinearen Schwingungen in einer stark nichtlinearen Struktur der Randschicht begründet ist. Die Theorie anharmonischer Schwingungen liefert eine gute quantitative Beschreibung, und ich konnte die ersten beiden anharmonischen Terme der Entwicklung des Randschichtpotenzials bestimmen. Die Arbeit stellt zudem eine einfache Methode bereit, um diese Parameter auch für andere experimentelle Bedingungen in situ zu bestimmen.

- Komplexe Plasmen in der Plasmarandschicht sind offene, nicht konservative Systeme. Eine daraus resultierende Besonderheit ließ sich mit den Experimenten zur Staubpartikel-Paarbildung klar nachweisen und quantitativ bestimmen. Die Wechselwirkung von Staubpartikeln, die von strömenden Ionen umgeben sind, unterliegt nicht länger dem dritten Newtonschen Gesetz. Es tritt eine Symmetriebrechung auf, die die Kopplung von Moden ermöglicht. Dies führt zu einer völlig neuen Instabilität.

- Ein weiteres Merkmal offener / getriebener Systeme sind sog. Nichtgleichgewicht-Phasenübergänge. Ich habe im speziellen die Entstehung von Strukturen in gegeneinander getriebenen Teilchenströmen untersucht. Komplexe Plasmen ermöglichen uns hier die zeitliche Entwicklung der Strukturen zu untersuchen. Ich gebe einen Ausblick auf zukünftige Experimente zu Nichtgleichgewicht-Phasenübergängen, und gehe auf deren generelle Bedeutung, die Forschung über Systeme am kritischen Punkt, und die Möglichkeit, Staubladungs- und Abschirmungs-Modelle damit zu überprüfen, ein.

Den Abschluss bildet ein Anhang über die Skalierungsindex-Methode (SIM). Ein vielseitig einsetzbares nichtlineares Maß für Struktureigenschaften von Daten. Mit Hilfe der SIM habe ich einen sensitiven Ordnungsparameter für die Bildung von Strukturen in komplexen Plasmen definiert.

Chapter 1

Introduction

Modern plasma physics started in the 1920s, when Langmuir coined the terms sheath [106] and plasma [107], Schottky defined ambipolar diffusion [177], and Tonks and Langmuir detected plasma oscillations [201] and published their general theory of the plasma [200].

With Alfvén waves [4] providing some explanation for cosmic ray acceleration, the discovery of collision free Landau damping [104], plasma physics input to theoretical astrophysics, the exploration of the solar system, plasma fusion devices, the increasing application of plasma devices and of plasma processing in engineering, plasma physics has become a very influential field of physics.

Dust in plasma was in the beginning never considered an important player in plasma physics. Even though dust in the discharge was already reported by Langmuir [108], and despite Alfvén's work "on the origin of the solar system" [3]. Similar to the neutral gas component, dust's influence on the plasma was neglected as long as possible [26, 46, 27], and mainly the influence of a plasma environment on the dust was considered important, e.g., in early work on using dust as a plasma probe [7], and for the interstellar medium [187].

In the 1980s the interest in dust in a plasma reemerged from three different directions.

- It was discovered that dust grains, contaminating silicon substrates in plasma processes, were growing inside the processing plasmas, instead of coming from outside. The dust was levitating and agglomerating above the processed wafers, until it either grew too heavy, or the plasma itself — or in the case of etching applications the applied voltage to the wafer — was shut down [183, 45].

- The Voyager mission recorded the so called spokes. Huge radial structures across Saturn's rings, which were attributed to clouds of dust elevated above the ring plane, due to dust plasma interaction [127].

- Ikezi published a paper [68], estimating that the mean potential energy of dust in the plasma of the dual plasma device [194] at his lab would exceed its mean thermal energy. This would provide for a strongly coupled Coulomb system, and allow for crystallization of the dust species.

While this was all "just" physics of dust in a plasma, Complex Plasma research took off in 1994, when three groups independently reported the realization of 2D Coulomb crystals and liquids in a dusty plasma [196, 62, 35]. Since then complex plasma has emerged as a truly interdisciplinary research field.

1.1 Plasma Physics

Highly ionized gases, with free electrons, positive ions and neutral gas atoms, are good conductors of electricity. The charged particles interact with the local electromagnetic field, and collective motion of these charges can generate electric and magnetic fields. In the presence of a static electric field free charges react like any conductor by quickly rearranging to shield most of the gas from the field. The large mostly field free regions of the gas with almost perfectly balanced positive and negative space charges were called plasma by Langmuir [107].

The coupling of charged particle collective motion via the electric field leads to an interesting phenomena called ambipolar diffusion [177]. Naively one could expect, that the transport of different plasma species, i.e., electrons and ions, happens independently. Especially for low temperature plasmas the diffusion of electrons, due to their high temperatures and low inertia, should happen much faster than for the relatively cold and heavy ions. In a localized plasma without magnetic fields, the electrons would initially diffuse outwards relatively quickly, leaving behind the much slower ions. This will result in an electric field pointing outward, decelerating the electrons and pulling the ions after the electrons. Effectively ions and electrons will leave the system with the same velocity, which will be lower than expected for the thermal diffusion of the electrons, but faster than the thermal diffusion of the ions.

When plasma comes into contact with surfaces a boundary layer is formed. This boundary was called a sheath by Langmuir [106] and first described for real macroscopic solid surfaces, in the context of Debye shielding. As the electrons have higher mobility than the ions all surfaces in contact with the plasma charge up negatively compared to the plasma potential. This potential drop starts attracting ions and repelling electrons. A volume of positive space charge develops above the surface. This sheath cancels the electrostatic fields from the surface, shielding the plasma from it. Its size is given by the Debye length. The negative charge of the surface increases, until some equilibrium surface potential is attained, when the ion and electron currents to the surface are the same. A similar boundary, called a double layer, is generated between plasmas of different characteristics, i.e. electron temperatures. Along the boundary more electrons from the hotter plasma will cross over into the colder plasma than vice versa because of their higher thermal velocity. Thus on the side of the colder plasma an excess negative, on the side of the hotter plasma an excess positive space charge will build up. This generates an electric potential drop which decelerates the hot electrons and accelerates the cold ones. Fewer and fewer electrons from the hot plasma will penetrate the boundary but more from the cold plasma, until finally both currents are equal, and the double layer is formed.

Closer inspection of the conditions necessary for forming a stable sheath, [1] by Bohm [16] revealed that ions must enter the sheath region with at least sound speed $v_s = (k_B T_e/m_i)^{1/2}$, which can usually not be generated by ion thermal velocities. Therefore Bohm's criterion requires the existence of a pre-sheath region where an electric field extends from the sheath into the quasi-neutral plasma and accelerates the ions. This pre-sheath is large compared to the sheath itself, depending strongly on the conditions of the plasma source, and the geometry of the plasma surface transition. In technical applications the pre-sheath can be expected to penetrate the whole plasma.

Even without taking into account additional influences, such as magnetic fields, frictional coupling, plasma wall interaction, mixtures of gases, negative ions, etc. plasma physics allows for all kinds of interesting phenomena. E.g., a huge variety of waves can be observed in plasmas. The most well known are the plasma oscillations of the electrons, originally detected by Langmuir and described by Tonks and Langmuir [201], the corresponding ion acoustic waves, and the Alfvén [4] and magnetosonic magnetohydrodynamic waves. The coupling between the electromagnetic field and the charged particles, gives rise to the collision free Landau damping [104]. Fundamental problems — like the sheath — are still not solved or fully understood after almost 100 years of research. Real world problems leave a lot of space for future investigation, better mathematical tools and theories, and of course more experiments.

1.2 Dust in Plasma

Dust is a macroscopic particle with respect to the plasma species. It consists of hundreds of thousands or millions of atoms and is at least nanometers in size. Dust can grow in plasma processes, like sputtering or reactive plasmas, and accordingly in fusion plasmas. These dusty plasmas and the transport of dust in these systems, have been studied in great detail, especially because of the many beneficial technical applications, but also because of possible health risks and hazardous influence during continous operation (e.g., in fusion machines) [19, 24, 17, 18, 21, 23, 189, 171, 22, 20, 209, 12, 44, 185, 152]. In most complex plasma experiments spherical particles with a diameter of 1–10 μm are used. They collect several thousand elementary charges and acquire a substantial surface potential. Charging of dust, initially considered in the context of interstellar space (e.g., by Spitzer [187]), and the shielding of the surface potential from the plasma are actively researched in laboratories and theory.

When an isolated dust grain enters a plasma it is charged negatively, and its electric potential is shielded from the plasma, by a process very similar to the formation of a Debye sheath [43]. The dust is subjected to electron and ion currents, leading to a dynamic

[1] The Debye sheath is ideally considered to be very thin, i.e., collisionless and free of ionization and recombination, thus the energy and flux of ions must be conserved. Then Poisson's equation $d^2\Phi(x)/dx^2 = \frac{e}{\epsilon_0}(n_e(x) - n_i(x))$, relating the curvature of the electrostatic potential to the local space charge density, is solved (in part numerically), where the density of electrons inside the sheath is assumed to be given by the Boltzmann relation $n_e(x) = n_0 \exp(e\Phi(x)/k_B T_e)$.

equilibrium surface potential, which is negative compared to the plasma potential, due to the higher mobility of the electrons [49, chapter 3]. Charging time is on the order of 10^{-6}-10^{-5}s for typical laboratory plasmas. As the surface potential of a dust particle depends strongly on local plasma conditions, the particle charge will adjust to changes in the surrounding plasma conditions. In addition the charge on the dust is subject to statistical fluctuations [41], that cannot be neglected for sub micron sized particles, and the coupling to the local plasma environment can result in instabilities for dust several micrometers in size [203, 71]. The exact dynamics of charging is still under discussion, as is the type and structure of the shielding of the particle surface potential, which is often considered to be described by a Debye Hückel potential distribution, even though investigations over the last ten years generally predict deviations from this theory [34].

The first and simplest charging model, applied to Langmuir probes by Mott-Smith and Langmuir [141], for a collisionless plasma with finite electron and ion temperature, is the so called orbital motion limited (OML) theory. Initially solved under the assumptions of Debye shielding, the probe radius being small compared to the Debye length, and the sheath being surrounded by an otherwise undisturbed plasma. OML takes into account the angular momentum of the plasma species, which results in an effective (centrifugal) potential barrier, preventing charges from reaching the probe (or dust). (It is described in the context of impact parameter of electrons and ions, calculating the distance of closest approach to the dust. Only electrons and ions coming closer than the grazing radius, equal to or smaller than the dust grain, are considered to be captured, and to contribute to the charging. Sometimes the angular momentum of electrons is ignored in calculations.)

OML as a probe theory has been criticized, from theoretical and experimental considerations (e.g., [5], proposing the orbital motion (OM) theory), and even been considered generally inapplicable to dust grains in Maxwellian plasmas [6]. Closer inspection of this work has shown, that OML closely approximates the exact solution of the dust surface potential in the limit of small dust grains [100] and low pressure [89], and allows accurate calculation of ion currents to the grains, while not reproducing Debye Hückel shielding at distances of the order of the Debye length under all circumstances. Recently full OM theory was solved analytically in the context of small probes and dust, taking into account the disturbance of the ion distribution by ion absorption on the grain surface [85], also supporting the OML results for surface potential, but giving corrections to the Debye Hückel shielding.

Another important factor in charging theory is the mean free path of ions and trapping of ions. OML and OM are only applicable in the collisionless regime, as collisions will lead to a loss of angular momentum. In a strongly collisional regime ion currents will be limited by mobility, lowering the flow of ions as the mean free path gets shorter. In a weakly collisional regime basically all ions that approach a dust particle and collide with neutral gas atoms, especially in charge exchange collisions, will be captured by the negatively charged dust particle [216, 221]. In addition trapping (i.e capturing without absorption) of ions is possible and an important process in all cases of finite ion neutral collision frequency [55, 101, 102]. This results in an increased space charge around the dust grain, substantially influencing the shielding of the potential, the currents and the

charging of the dust in a plasma.

Charging of a dust particle and shielding of its potential gets even more interesting with streaming ions, as it is the case, e.g., for dust in the sheath or pre-sheath of a plasma, for dust particles moving through a plasma, or for an induced ion flow through external potentials. This produces three main effects [70]:

- The ion currents to the dust grain are reduced, as can be derived from OML due to higher angular momentum of the ions. This will decrease the equilibrium surface potential and thus increase the negative charge of the dust. OML predicts an optimum Mach number of the ion flow for which the most negative charge of a particle is attained.

- The velocity distribution of ions is no longer isotropic, thus absorption of ion fluxes on the dust grain will result in a net momentum transfer onto the dust, a drag from the ions, similar to neutral drag force. The ion drag on a charged dust particle also has to take into account the momentum loss of ions that are not absorbed, but merely deflected, while passing by the charged dust. The ion drag force depends critically on the shielding of the dust surface potential [87], as does plasma production and loss on the particles [30]. In the highly collisional, weakly ionized regime ion drag can even accelerate slowly moving dust, due to absorption of ions by the particle [86].

- The deflection of streaming ions by the charged particle results in a complicated structure of the space charge around the particle, no longer approximating the Debye sphere, called an ion wake [174, 206, 115, 69, 99, 111, 109, 210, 110, 32, 31]. The ion wake is an important and unique feature of dust in plasma, resulting in many interesting phenomena in complex plasma, and is recently being applied to design the interaction potential of complex plasma.

For a full description of charging, one must also consider secondary emission of electrons due to electron and ion impacts, as well as photo emission, field emission, and thermoionic emission, as well as collisions with neutral gas atoms, in addition to electron and ion fluxes from the plasma.

1.3 Complex Plasma

A complex plasma is a self consistent system of (highly) charged dust particles immersed in a plasma. The transition from "physics of dust in plasma" to "physics of complex plasma" happens when either the charged dust grains can no longer be treated individually, or the plasma can no longer be considered undisturbed by the presence of dust. The first transition was noted by Ikezi [68], the second happens when the charging and shielding of many particles interact strongly with the embedding plasma, and interfere with each other.

Complex plasmas are typically described in terms of the so called coupling parameter Γ, denoting the ratio of potential energy of the dust to its thermal energy, and $\kappa = \Delta/\lambda$

the ratio of mean distance Δ between dust grains to the range λ of the grain interaction potential. It is clear that these two parameters depend strongly on the exact nature of the particle interaction potential, which is defined by particle charging and the shielding of particle potential. In the case of Debye Hückel shielding with the range of the interaction potential given by the Debye length λ_D (assuming identical particles and mean thermal energy $E_{th} = \frac{3}{2}k_BT$) the coupling parameter can be expressed as $\Gamma = \frac{Z^2e^2\exp(-\kappa)}{6\pi\epsilon_0\Delta k_BT}$, where Ze is the average dust charge, with vacuum permittivity ϵ_0, Boltzmann constant k_B, and mean dust temperature T. [2]

This coupling of dust allows complex plasmas to, e.g., attain liquid and crystalline states [68, 35, 196, 62, 117, 59, 61, 137, 136, 222], supporting the investigation of flows, crystallization and melting [195, 181, 168, 134, 90], makes it an interesting model for strongly coupled Coulomb systems (SCCS) (or Yukawa type systems), allows for the study of wave phenomena [158, 114, 11, 112, 223, 151, 198, 65, 84, 130, 50, 82, 146, 144, 207, 172, 51, 180, 64, 217], e.g., dust-acoustic, dust-lattice and solitary waves, and shocks, etc. All this research depends on the knowledge of complex plasma parameters, inspiring basic research, employing laboratory and numerical experiments, to measure particle charge [117] and inter particle potential in situ, and if possible independently of local plasma conditions [94, 9, 10, 144, 162]. This is especially important as the theoretical study of real complex plasmas is impossible to solve analytically, and as such strongly depending on model assumptions, that can either not be provided, controlled, or verified experimentally, preventing efficient model testing. [3]

As noted in section 1.2 the charging of dust depends strongly on the local plasma environment, and vice versa, especially when there are not just isolated dust grains, but in a complex plasma with $\kappa \sim 1$, and in anisotropic plasma conditions. This gives rise to a whole new set of complex phenomena, like enhanced ion charging currents [113], electron depletion [170], self-excited waves and auto-oscillations [179, 220], classic tunneling [139], charging instabilities [145], instabilities of the discharge (often found with huge numbers of grown particles) [155, 119, 122, 121, 28], the decharging of particles (after plasma switch-off) and charge buffering [80, 15, 36, 40, 39], current driven waves and instabilities, and interference of plasma waves and particle charging [166, 42, 170, 71, 74, 73, 118], altered complex plasma configurations [98], electro- and magneto-rheology [25], non-newtonian fluids [77], and charge enhanced dust agglomeration [75] with its implications for planet formation. Mixtures and boundaries between complex plasmas of different characteristics

[2] Even for this relatively simple model it is difficult to estimate Γ from experimental measurements: Dust temperature can be difficult to measure and is often assumed to be that of the neutral gas. Dust particles are further defined spherical and to have three degrees of freedom. λ depends on the mobility of electrons and ions, and their energy and density distribution (measuring these values in a plasma is tedious and a science of its own — applying these measurements to a complex (dusty) plasma is not straight forward). This also limits the possibility of calculating the charge of dust.

[3] E.g., theoretical models show divergence from simple OML (with Debye shielding) for distances smaller than λ or beyond 6 λ. But up to now experiments allow to probe the inter particle potential only for distances between 1 and 5 λ. As for example Uwe Konopka's investigation of charging and shielding in the sheath of an rf-discharge, using self consistent two particle collisions [94], eliminating as much as possible many-particle influences and removing the need to know local plasma conditions.

can lead to interesting phenomena, similar to double layers between plasmas of different electron temperature [214].

Complex plasmas have additionally been used as model systems to investigate particle clusters [49, section 12.1] and atomistic systems like nano-fluids [49, section 12.2], i.e., systems dominated by boundary effects and on the edge of collective behavior.

Recently complex plasmas are perceived as "The Plasma State of Soft Matter" [133]. Soft matter is a term introduced by de Gennes for materials that are "supramolecular, exhibit macroscopic softness, have metastable states and a sensitivity of their equilibrium to external conditions". Usually theses materials have temperatures well above the quantum limit. Other members of the soft matter family are granular media, colloids and foams. (de Genne in 1991 recieved the Nobel Prize in physics for his generalization of the order parameter from simple thermodynamical to more complex systems. In his Nobel lecture he gives a nice introduction to soft matter.)

Current research in complex plasma physics is mainly in the fields of basic physical processes, collective behavior, waves and shocks, dust growth, manipulation and control (in processing and fusion plasmas), magnetized complex plasma, star birth rates, formation of solar systems and planets, geosciences (e.g., dust in the solar system, planetary rings [127] and dust in earth's mesosphere [54, 60, 165]), phase transitons, the vapor-liquid critical point, soft matter, self-confinement, surface tension, self-organization as, e.g., in non-equilibrium phase transitions, either liquid-liquid (e.g., lane formation and phase separation, with corresponding liquid-liquid critical point) or solid-solid (e.g., electro- or magneto-rheology), charging and de-charging, the dust grain interaction potential (even speculating on collective attraction [33]), and plasma medicine [135]. Complex plasma is first and foremost an interdisciplinary research field [138].

The use of well defined, manufactured, micrometer sized particles as dust grains in typical complex plasma experiments allows for several features that turn it into an interesting basic research topic and model system:

- The dust grains are usually illuminated by a laser. The scattered light of individual dust grains is visible by eye, and can be recorded by cameras. This allows fully resolved particle dynamics to be studied.

- The dust in a complex plasma fills only a very small portion of the whole volume (i.e., particle size $\ll$ mean particle separation), making them almost perfectly transparent, and thus making it possible to identify and track individual dust grains throughout the system (even up to 10^9 particles).

- All kinetic processes of the dust happen below 1kHz. Thus the full kinetics can be temporally resolved (unlike for ions and electrons, where the typical kinetic frequencies are mega- or giga-hertz).

- The dust is frictionally coupled to the neutral gas, as described by Epstein damping [47]. I.e., in the pressure range from 0.1 Pa to 1000 Pa, typical for complex plasma experiments, we cover the full range of dissipative kinetics from fully undamped to

over-damped systems. (Below 100 Pa inter particle kinetics are virtually undamped, still long term dynamics follow fluid patterns.)

- The dust can be manipulated in many ways without disturbing the plasma conditions. E.g., laser manipulation [66], and (in non-reactive plasmas) neutral gas drag and thermophoresis [167], UV-light (to change dust charge), etc.
- The inter particle potential of the dust is modified by anisotropies in the plasma (cf. the description of the wake in section 1.2). Current research [91] investigates the application of wakes to design the inter particle potential.

These features open up the possibility to conduct complementary research with ionic crystals and colloids, to use complex plasmas as slow motion model for real fluids and solids, and (under some conditions) to make comparisons with one-component plasmas (OCP). Complex plasmas offer us the opportunity to investigate phenomena on a fully kinetic level, that until now are only understood and described statistically. Examples are the transition from laminar to turbulent flow, self-organization, crystallization, viscosity, non-equilibrium phase transitions like phase separation, critical phenomena, and 2D/3D phase transitions.

Chapter 2

Nonlinear Vertical Oscillations of a Particle in the Sheath of a Radio Frequency Discharge

The idea to perform this experiment stemmed from previous experiments on dust lattice waves by Milenko Rubin-Zuzic, trying to measure the in plane dispersion relation of two-dimensional (2D) plasma crystals, during his PhD work. His experimental setup featured a wire across the GEC [1] chamber located slightly below — Milenko Rubin-Zuzic had discovered that it was very difficult to excite the dust particles using a wire located at the same height as the dust or higher — and to the side of a crystalline dust monolayer, levitated in the (pre-)sheath of the rf-discharge. Applying a sinusoidal voltage of varying frequency he noted four things:

- The particles would move horizontally, not as a wave but oscillating as a whole, showing a resonance as expected for the strength of the horizontal confinement of ∼2–3 Hz.
- When he, just out of curiosity, increased the excitation frequency well beyond this resonance, at around 15 Hz the dust particles would gain thermal energy and the crystal structure would break up. Increasing the frequency even further would again stabilize the crystal.
- He continued increasing the excitation frequency, until the crystal sublimated at ∼30 Hz, the dust going into some kind of gaseous phase, with large out of plane amplitude. Increasing the frequency to about 40 Hz, the crystal reappeared.
- Increasing the frequency further would not disturb the dust particles in any noticeable way.

[1] The Gaseous Electronic Conference (GEC) rf reference cell [148], is a standard capacitively coupled radio frequency gas discharge chamber, defined at a workshop at the 1988 GEC, as a baseline to allow for repeatable and comparable plasma experiments.

Unfortunately Rubin-Zuzic had no time to look more deeply into the phenomenon. Fortunately he recorded the event and all parameters in his lab-book. Something similar was reported by Schollmeyer et al. [176], without giving a conclusive insight to the underlying physics.

I was told about this most extraordinary dust behavior by Alexey Ivlev, a theoretician of the "Plasmakristall" group, during the first year of my PhD thesis, while I was working together with Beatrice Annaratone, Alexei Khrapak and Victor Steinberg, investigating the behavior of rod-like particles in a plasma [8], and trying to create a 2D plasma "glassy state". Ivlev and Rubin-Zuzic convinced me of the importance to investigate the exact dynamics of this phenomenon and to identify its physical origin. Alexei Ivlev and Victor Steinberg supported my experiments and analysis with all their physical insight and by providing the theoretical background to relate my numbers and curves to plasma sheath physics. At the same time Uwe Konopka was finishing his PhD thesis [92], measuring single particle horizontal oscillations and dual particle collisions in the sheath [93]. This resulted in the first comprehensive experimental survey on the dust particle surface potential. Fortunately Konopka used exactly the same GEC chamber as Rubin-Zuzic had — which had previously been used by Hubertus Thomas for his plasma Coulomb crystal and 2D phase transitions experiments — operating it at very similar plasma conditions. Konopka's experiment also inspired me to using a single particle for my measurements after successfully repeating Rubin-Zuzic's experiment with a dust monolayer, verifying the experimental conditions.

For the single particle investigation I implemented only two changes to the experiment from Rubin-Zuzic's setup. First I put the wire much lower than in his case, so that the electrically floating wire would not disturb the dust particle. And second I put the wire exactly below the particle to prevent the overlap of vertical and horizontal oscillation of the particle. Analyzing the horizontal and vertical motion of the particle from the same recording was impossible, as the horizontal motion (due to much weaker horizontal confinement) was an order of magnitude larger than the vertical motion. At that time digital (high speed) cameras could only record for a few seconds, and I used a standard PAL camera to record the particle motion to a VHS tape. A single recording of a resonance curve, going up from 0.1 Hz to 40 Hz and back down took about half an hour. The analysis of one recording to extract all particle images (resulting in position and velocity measurements for slow excitation frequency, but only allowing amplitude measurements for frequencies beyond 12 Hz) took approximately one day.

Later I found, that using a wire was not necessary, the same oscillations could be reproduced applying the low-frequency excitation directly to the lower (driven) electrode of the rf chamber. And Ivlev and I devised a scheme how to measure the next higher nonlinear coefficient of the sheath expansion. Unfortunately, just like Rubin-Zuzic, I did not have the time to do the obvious follow up experiments, already proposed in the original paper, to measure the full sheath potential using particles of different size and density, and to proceed with the model testing of (pre-)sheath theories. I had just attained the position of Project Scientist for the PKE Nefedov project. At that time this was to be the first permanent plasma science facility onboard the International Space Station (ISS). I had

already been involved part time during the development of this experimental setup, but now Hubertus Thomas hired me and I became responsible for managing data acquisition, storage and post-processing in the project. This responsibility also resulted in me working with Milenko Rubin-Zuzic on a fully digital video acquisition for our laboratory setups — as mentioned before, we mainly used analog PAL video tape for recording.

Just shortly after our publication Zafiu et al. published results on nonlinear oscillations in the plasma sheath [215], attributing this to a parametric instability driven by nonlinear variations of the particle charge, in an otherwise linear sheath. Both results do not contradict our paper as Zafiu et al. used much bigger particles, levitating much closer to the electrode, possibly in a different (pre-)sheath region, of a gas discharge with ten times higher pressure and six times higher discharge power. In addition Uwe Konopka's results on the particle charge supported that in the regime of our measurements the nonlinearity could not be caused by a nonlinear variation of the particle surface potential.

2.1 Results

The results of these experiments and their interpretation were published in Physical Review Letters (PRL) [78] (attached).

The paper reports first of all a simple method to measure in situ the potential distribution of the sheath in the vicinity (1–2 mm in height) of the dust particles. It is very important to note that these measurements can deviate strongly from probe measurements, as probes can influence the gas discharge at large, and might not provide the same spatial resolution.

As theoretical model for the interpretation of the nonlinear oscillations we used anharmonic oscillations. We expanded the potential energy of the particle in the sheath around its equilibrium position $z = 0$, i.e., where the particles weight is balanced by the electrostatic force $Q(0)E(0) = Q_0E_0$, with particle charge Q(z) and sheath electric field E(z). In general the charge of a particle could depend on its position but for our conditions the charge changes weakly with z, one order of magnitude less than the electric field [93, 92], so we consider $Q(z) \simeq Q_0 = const.$ From these assumptions we expand the potential energy of a particle $U = Q\phi$ around $z = 0$ in a series $U(z) = U_0'z + \frac{1}{2}U_0''z^2 + \frac{1}{6}U_0'''z^3 + \frac{1}{24}U_0^{(4)}z^4 + O(z^5)$. We could describe all peculiarities of the nonlinear oscillations keeping only the first two anharmonic coefficients [105, 142], still we needed to verify that our series really converges. In addition we considered the force, driving the particles, to depend not only on the external disturbance, but also on the position of the particle. We derived this dependence self-consistently from the local sheath structure.

Applying my experimental method and the above mathematical model we got three main results. First, the sheath potential is strongly nonlinear (cf. figure 2.1) for our conditions, which are similar for all complex plasma experiments at very low neutral gas damping. We determined a sheath potential proportional to the potential energy of the dust particle at a distance z (in mm) from its equilibrium position $\Phi(z) \propto U(z) \simeq M\omega_0^2(-0.9z + \frac{1}{2}z^2 - \frac{1}{3}0.5z^3 + \frac{1}{4}0.07z^4)$. Second, judging from the magnitude of the second anharmonic

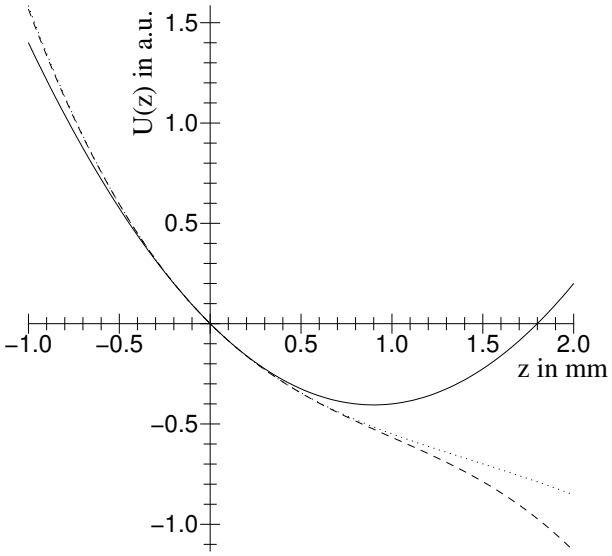

Figure 2.1: Nonlinear sheath potential. The potential energy (in arbitrary units) of a dust particle, depending on its distance from the equilibrium height within the sheath. The usually assumed parabolic potential well (solid) is compared to a nonlinear sheath, evaluated with the first (dashed) and first and second (dotted) anharmonic terms of the expansion of the potential energy, as determined by my measurements.

coefficient, i.e., 0.07, the expansion series converges quickly, justifying our expansion of the potential energy to only fourth order. Third, I could measure the dependence of the ratio between driving force and the externally applied electrical signal, on the particle position. To my knowledge this dependence has been ignored by all previous publications on electrical manipulation of particles.

These ideas have subsequently been tested and used in more than 40 publications (e.g., [215, 208, 186, 219, 67, 150, 96, 173, 95, 184]).

2.2 Outlook

Knowledge about the plasma sheath is not only of interest to the basic research in complex plasmas, but is of crucial importance to plasma processing and in fusion devices, e.g., etching, film growth, plasma wall interaction, loss of plasma from magnetic confinement, etc., and in rf-engineering, e.g., of antennas, and for satellite based experiments, ...

Accordingly there is active research on the sheath and on the measurement methods themselves. Most prominent is the development of better probes and spectroscopic measurements. But there is a steady research in probing the plasma sheath using dust test particles and analytical models for the sheath and particle surface potential [13, 211], and there are recently some interesting experiments utilizing hypergravity with centrifuges [14].

Chapter 3

Vertical Pairing of Identical Particles Suspended in the Plasma Sheath

Victor Steinberg asked me to join him in his experiments on two-dimensional (2D) plasma glass — as opposed to plasma crystals — using binary mixtures of complex plasmas. He experimented on levitating particles of different size at the same height in the sheath of a radio frequency (rf) discharge, using particles made from varying materials. He had succeeded in creating relatively stable single layer systems but not in finding the glassy state of complex plasma. Instead he had noticed during his scanning of the experimental parameter space, that while lowering rf power, his single layer would abruptly change into a double layer configuration, with one particle in the upper layer apparently being paired to one particle in the lower layer. In addition Steinberg had found that he could restore the single layer configuration by increasing the power. I should help him to get rid of these annoying pairings to finally realize plasma glass.

Vertically aligned structures, e.g, so called "polarization" or "stacking" of 3D plasma crystals [35, 193] vertical strings of dust particles [52, 147], and the vertical pairing of two particles of different size [116], had been reported before in complex plasma. This had been attributed to an ion wake [182] and used to predict some kind of "binding" force and "dust molecule" formation [163]. In all these cases the vertical structure was already present, and there was no transition from horizontal to vertical alignment or vice versa. And the dynamics of pairing were not yet investigated at all.

Steinberg and I initially had two assumptions what would cause, and thus how we could get rid of, the vertical pairing. First, Victor Steinberg thought, that the confining potential of the dust particles might vary qualitatively while changing rf power. Thus we changed the setup to use a physical glass tube inside the GEC to provide the confinement for the particles, instead of "Poisson confinement", that relies on the propagation of the geometry of the lower electrode into the sheath region. Second, I suspected Steinberg's binary mixture of being not perfect for all plasma parameters. Especially when rf power would be reduced, as the plasma sheath expands and particles would levitate deeper and deeper in the sheath, invalidating the assumptions he used in calculating the size to density ratios of his binary mixture. So we repeated the experiment using just one kind of dust particles.

To our surprise we were still able to switch from single to double layer configuration by changing the rf power of the discharge.

At the same time Victor Steinberg was working on measurements of 2D particle clusters of identical dust particles, investigating the structure of such clusters depending on particle number, the possible changes of configurations, and dependence of these configurations and transitions on plasma or discharge parameters. Usually we would only look at and record these configurations from top, as we "considered" them to be 2D. One day Victor changed the setup and tried to record a two particle system from the side. He saw two particles apparently levitated at slightly different height, perpetually passing above and below each other. He called me to the lab and we set up a second camera to look at the particles from top, finding that the particles were not passing above and beneath, but randomly rotating around a common center. The side view had only shown the projection of this motion. But still it was interesting that two identical particles could be levitated at different heights. Victor advised me to continue the investigation of this phenomenon and continued his work on particle clusters.

While trying to get back to Victor's experimental conditions and varying plasma parameters, I noticed that the height difference of the particles depended on rf power. (As did the absolute height, which was well known at that time.) I decided to record the evolution of height difference, while lowering the rf power down till plasma switched off. With increasing height difference, the radial distance varied. Then suddenly the lower particle dropped. I had expected it to drop all the way to the electrode, but it just jumped exactly below the upper particle (see right pane of figure 3.1). Trying to get back to the initial configuration I found that the system had some substantial hysteresis. From here I just recorded pairing and unpairing events at different pressures and using statistically independent pairs, charting the parameter space where this phenomenon occurs. For very low pressure (<2–3 Pa), the lower particle would usually drop all the way to the lower electrode. But in the cases when particles formed pairs, these pairs could not be undone, even applying an rf power higher than necessary for a perfectly horizontal initial condition. Figure 3.1 shows several particle configurations depending on rf power for low pressure.

The experiment supplied two self consistency checks: First, the rotation of the particles around a common center was random, going clockwise or counterclockwise at random but low velocity. Inter particle distance and levitation height of the particles were independent of the rotation of the system. The rotation center was independent of rf power. This demonstrated the symmetry of the confinement potential. Second, repeating the experiment with the same pair of particles, which particle went down was random, during early stages of the continuos bifurcation upper and lower particle could also spontaneously change roles, proving that particles were indeed identical. In addition the unpairing events showed, that the upper particle in a pair is levitated higher up, than the exactly same unpaired particle. And of course the experiment could fully explain our multi particle experiments showing spontaneous change from single to double layer configuration.

At that time I was also investigating in detail particle oscillations in the sheath (cf. chapter 2). I found that the vertical and horizontal resonance frequency of a particle strongly depended on the rf power of the gas discharge. Even though this fact could

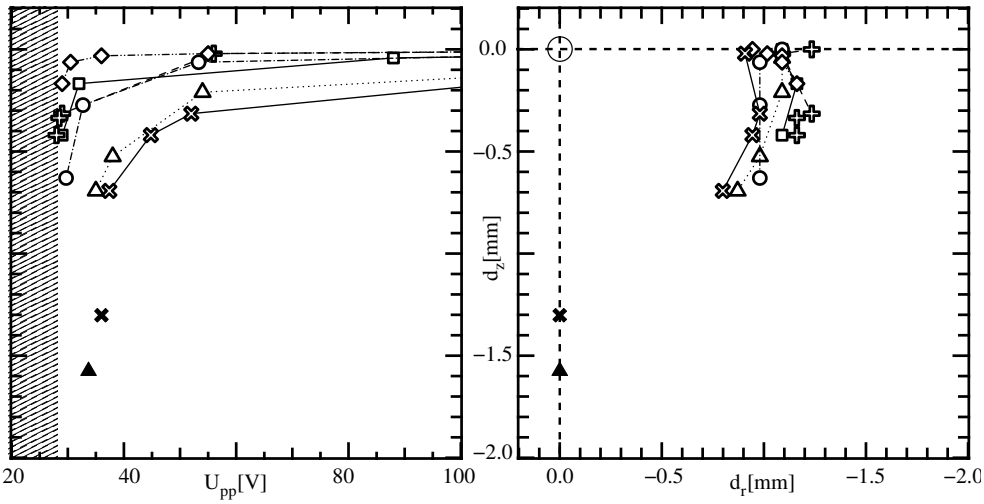

Figure 3.1: Vertical Pairing. Particle configurations at 2 Pa: dependence of vertical separation between the particles on peak to peak voltage between the electrodes of the discharge chamber (left), and the corresponding spatial configuration (right). Open symbols are used for configurations that are not paired vertically, and closed symbols for paired configurations, lines are used to guide the eye. The striped area in the left figure highlights forbidden configurations, as particles would fall to the lower electrode for such low rf power.

be considered expectable in hindsight, the details of this were unknown at that time. "Common knowledge" defined vertical confinement — confinement corresponds directly to resonance frequency — to be an order of magnitude stronger than horizontal confinement independent of experimental setup. Figure 3.2 shows the dependence of resonance frequencies on rf power. Not only do these resonance frequencies depend strongly on rf power, but they converge for lower rf power, resulting in an almost isotropic confinement!

Showing my results to Victor Steinberg he immediately recognized that the vertical pairing was an instability with rf power as control parameter. He consulted Alexei Ivlev, who together with Steinberg developed a theoretical model for the vertical pairing of identical particles. Motivated by my results on the convergence of horizontal and vertical resonance frequencies Ivlev used these to characterize the model instead of rf power. We decided to combine both experimental results and the theory in a single paper. As reported in chapter 2 I did not have the time to continue the research on particles in the sheath, as I started working as project scientist in the PKE.

3.1 Results

The article published in Physical Review Letters (PRL) [188], also attached to this thesis, gives full details of the theoretical model, and reports on the experimental facts, showing some examples and details of the experimental results. In summary the following basic findings were reported:

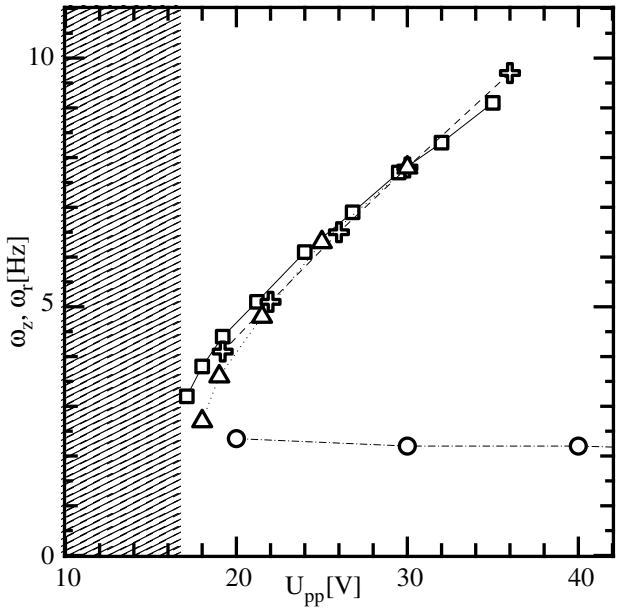

Figure 3.2: Convergence of vertical and horizontal resonance frequencies: influence of the rf peak to peak voltage on the vertical and horizontal resonance frequency of a single particle in the sheath of an rf discharge at 1Pa. The striped area highlights the minimum rf power necessary to levitate the particle in the sheath against gravity.

- The local potential well trapping a particle in the sheath of an rf discharge depends strongly on the discharge conditions. For very low power the confinement of the particle becomes almost isotropic — the vertical (ω_z) and horizontal (ω_r) resonance frequencies of a particle in the potential well converge.

- In radial direction the confinement is rotationally symmetric.

- I observed a new instability using identical particles initially levitated at the same height in the sheath. The instability first develops as a continuous bifurcation to vertically separated particles, and then results in a discontinuous vertical pairing. The pairing transition shows hysteresis — stronger for lower pressure.

- The instability is indeed symmetric in the particles, i.e. there is equal probability for either one of them to go down.

- The control parameter of the instability can be either rf power (more specific U_{pp}, the peak to peak voltage applied to the driven electrode of the GEC chamber) or gas pressure p. We describe the instability using U_{pp} for fixed pressure. (We supply a more intuitive characterization of the model using the confinement strength, i.e., resonance frequencies ω_z and ω_r of a particle, which depend on U_{pp} and p.)

- The bifurcation starts at a certain threshold $U_{pp}^{th}(p)$. This threshold increases with

increasing pressure, while the width of the pairing-unpairing hysteresis decreases with increasing pressure.

- The convergence of ω_z and ω_r cannot be responsible for the continuous bifurcation, as it develops while ω_z is still substantially larger than ω_r.

The theoretical model developed for the interpretation was a very simple sketch of an ion wake potential. As explained in the introduction on complex plasma physics ions in the plasma sheath stream towards the lower electrode, and are deflected while passing by the highly charged microspheres, forming a complicated space charge structure behind each particle. Our model approximated this situation by a constant point-like positive charge q fixed at a distance Δ exactly below each particle (constant point-like negative charges Q). Using R the radial and δ the vertical separation of the particles, and ω_z and ω_r, the vertical and horizontal resonance frequencies of a particle in the confinement, the total potential energy of the two trapped particles can be written as

$$\mathcal{W}_{\text{pair}} \simeq \frac{1}{4}M(\omega_r^2 R^2 + \omega_z^2 \delta^2) + \frac{Q^2}{\sqrt{R^2+\delta^2}} - \frac{Qq}{2\sqrt{R^2+(\Delta+\delta)^2}} - \frac{Qq}{2\sqrt{R^2+(\Delta-\delta)^2}}. \quad (3.1)$$

The last two terms describe the particle wake interaction. In the paper we additionally took into account the nonlinear structure of the sheath potential described in chapter 2.

Even though the model describes quantitatively (taking into account the dependance on U_{pp} and p) only the initial continuous part of the instability — for larger vertical displacements and the discontinuous transition into a pair one would have to take into account the real shape of the ion wake — it captures well the fact and influence of symmetry breaking induced by the streaming ions.

This paper has been cited more than thirty times. The effect of the ion wake that the paper clearly demonstrated, inspired a lot of great experimental and theoretical work and numerical investigations (e.g., [204, 63, 199, 98, 169, 213, 126]).

3.2 Outlook

The symmetry breaking I observed, and we explained in our paper, is the result of the complex plasma being a thermodynamically open system, with an external supply of energy driving the steaming ions. The anisotropy of the wakes formed by ions streaming past the particles is responsible for a nonreciprocal action between the particles, i.e., breaking of Newton's third law, invalidating the conservation of momentum. Nonreciprocal action had also been reported by Melzer [116] previously. It can be seen nicely in the asymmetry between the last two terms in equation 3.1. (It is important to note that *nonreciprocal* explicitly does not mean, that in general one particle has no influence on the other. It just means that the influence is different, e.g., has a different magnitude.) Wakes drive a whole spectrum of non-Hamiltonian dynamics, like 2D melting observed by Konopka [72] and mode coupling as observed by Samsonov [173].

Our model was simple and the paper did not state all the minute details of my experiments nor did we at that time fully understand all the implications of our results. Still I consider this paper my most important contribution to fundamental complex plasma research. I am very happy how this evolved over the years by contributions of peer scientists.

For example we did not mention that in a paired configuration the upper particle was situated higher up than an otherwise identical single particle would be for the same plasma conditions. The pair would push upwards. Lampe et al. [98] went to great efforts to investigate numerically the wake structure and the properties of pairs or strings of particles in an environment of streaming ions. They could show that such strings are able to push "upwards" against the stream of ions, among other results.

Only recently the theoretical model of Ivlev and Steinberg has been generalized to a 2D layer of particles by Sergey Zhdanov [218]. Using this generalized model he predicts a mode-coupling instability of two-dimensional plasma crystals. Lenaic Couëdel could demonstrate the extraordinary agreement between real 2D complex plasma crystals and the model of Zhdanov, by comparing his measurement of optical phonons — transverse vertical modes of self-excited waves — in 2D plasma crystals, with numerical simulations based on Zhdanov's model [38]. In addition Couëdel was able to observe the predicted mode-coupling instability [37].

The shape and influence of the ion wake is considered to be well understood by numerical simulations and theoretical models. Currently researchers use the ion wake to design custom particle interaction potentials [91], or to produce, e.g., electro-rheological complex plasma [76, 25]. Further probing the ion wake using complex plasma experiments might be possible using, e.g., driven systems, where one kind of complex plasma penetrates through a different electro-rheological complex plasma. We have tried such experiments under micro gravity using the PK-3 Plus experiment on the International Space Station. But so far these experiments could not be analyzed, because they were overlaid by another (unknown) instability.

Chapter 4

Lane Formation in Driven Binary Complex Plasmas

The experiments leading to this discovery were performed on board of the International Space Station (ISS) using the PK-3 Plus [197] experiment operated by Russian cosmonauts, a unique research opportunity for the complex plasma community operational in orbit since 2001. I was lucky enough to become hired as Project Scientist with this Russian-German collaboration during its development phase, in the second year of my PhD. The project was initially called PKE 3. "PKE" stays for Plasma Kristall Experiment because at that time the main interest was in studying the crystalline state of complex plasmas. The number "3" was given to it, because the Russian collaborators had previously flown two dedicated experimental setups for this purpose. The "Plus" was assigned when the original experimental setup was replaced by an incrementally improved system in 2005. The original setup was "baptized" PKE Nefedov [143], after the Russian PI — our colleague and friend Anatoli Nefedov — who died in February 2001. Over the past nine years we could do two to three experimental campaigns every year, each of three days, with at least 90 minutes continuous micro gravity (μG) time per day. (This amounts to over 6000 minutes of micro gravity experiments.) As mentioned above these long experimental runs were initially considered necessary to study in detail all aspects of condensed complex plasma. That is the liquid and solid state of complex plasmas and the melting and crystallization dynamics [222, 168]. These can not be investigated nicely under gravity conditions, where the whole complex plasma is compressed into the thin region of the plasma sheath — and experimental runs need minutes of continuous μG, unavailable during drop tower or parabolic flight campaigns. In addition PKE Nefedov and even more so PK-3 Plus were intended to investigate multi-component complex plasmas, with the hope of detecting a glassy state [157]. We had tried for several years to produce mixtures of complex plasma using several different approaches. But gravity and the nonlinear effects described in the previous chapters had prevented any success. Results from sounding rocket and parabolic flight experiments, theoretical estimates and numerical simulations had assured us, that we might get the necessary optimum conditions under micro gravity.

Already during the development phase PKE provided us a nice feature: the void [56,

1, 2]. A region in the geometric center of the discharge, that particles would not enter. We had expected the pre-sheath electric field to assemble all particles in the center of the chamber. Apparently we underestimated the ion drag force caused by the ions, which are mainly generated at the center of the system, and stream outwards to the walls of the discharge chamber. Before the investigation of the void using PKE Nefedov experimental data [97] it had been generally assumed, that the interaction between ions and the particles in the complex plasma would be basically limited to the Debye sphere. A picture that had to be revised in face of our experimental facts [87]. In addition the void seems to be correlated to a new instability or rather auto-oscillation of the complex plasma: the so called heartbeat-instability [120, 125, 123, 205, 124].

In the PKE laboratories instead of the sheath electric field and gravity we now have two new counteracting forces: electro static confinement and ion drag. Both depend on the diameter a of the particles in the complex plasma and the resulting net force becomes zero at some distance $R(a)$ from the center of the chamber, closer to the center for smaller particles. Important results from PKE research have been, that inside a homogeneous complex plasma electrostatic and ion drag forces seem to cancel each other [103], making the interior of such complex plasma bubbles virtually force free, and that we can control the net force magnitude by changing the discharge parameters. In the end this endowed us with a new way to manipulate the complex plasma.

The basic idea behind the lane formation experiment was to fill the setup with a background complex plasma of large particles and then inject smaller particles. These smaller particles would be pulled by the net force towards the center and would settle around the perimeter of the void. For the first such experiment we did not know what kind of interpenetration we should expect, but we had high hopes to see some kind of dissipative structure [156]. The results were better than expected: At first the complex plasma of small particles would clash against the background of larger particles pushing the whole cloud collectively. Only very few small particles would penetrate into the cloud of big particles. Then more small particles would follow behind these forerunners creating lanes of small particles instead of diffusing through the background individually. In short time the large particles would be combed into lanes by the small particles flowing past them, too. Both particle species thus forming an array of interpenetrating lanes. As the small particles approached the center, two more things happened. First, the individual lanes would come closer to each other because of the central force pulling the particles, and individual lanes would unite to larger streams. Second, the net force got weaker and weaker. At some characteristic distance from the center there were no more individual lanes of small particles, but instead they formed one big drop of complex plasma, that would move collectively through the background of big particles. This drop would deflect big particles at its bow, creating a flow of big particles around the object, and big particles captured inside the bubble of small particles would be squeezed out. When the drop "hit" the void it crawled viscously around it. Interestingly the lanes combed into the big particles persisted for more than a second after the flow of small particles subsided.

When I first saw the videos from these experiments — conceived by Hubertus Thomas and Alexei Ivlev, presented by Ivlev during a conference on castle Ringberg in 2007 — I

was thrilled. A similar event had by chance been recorded in parabolic flight experiments during the pre-development phase of PKE [139], by Uwe Konopka and me, and has later also been observed in the PK-4 experiment [202, 48]. But nothing of such detail, without the formation of a stable drop, and not even close to so much high quality data. Ivlev began to develop a model and theory for this, and Milenko Rubin-Zuzic asked me to join forces with him for the analysis of the data. I had to finish this work without him, as he took a sabbatical year shortly after. Initially our biggest interest was centered on the formation of the complex plasma droplet. This was the first experiment showing something like a surface tension for complex plasma. But as we could not explain the origin [79] of this phase separation, yet, we concentrated on the lane formation instead.

Extended numerical and theoretical investigations on lane formation in colloids had been done by Hartmut Löwen from the Heinrich-Heine-Universität Düsseldorf and collaborators [29, 212, 164], so Ivlev decided to consult him on our results. Hartmut Löwen brought a lot of insight and knowhow into our research collaboration, and Adam Wysocki provided an ample supply of MD simulations for calibration of the experimental data. Ivlev also asked Wim Goedheer for help with determining the discharge parameters from numerical simulations, and I worked together with Christoph Räth to find a suitable order parameter for laning (cf. appendix A).

Lane formation in binary complex plasma offers a unique research opportunity: to investigate the dynamics of lane formation, i.e., not the properties of the lanes themselves, nor the (temporal) asymptotic behavior and its dependence on external parameters (like driving force), but the temporal evolution of lanes and its dependence on complex plasma parameters. This is possible because for complex plasmas we can investigate the fully kinetic level of individual particle motion, and because the damping is low but finite. The particle interaction can be considered undamped, allowing the temporal resolution of all relevant frequencies. Still the system has substantial dissipation, enabling the occurrence of these nice dissipative structures in the first place.

4.1 Results

Details on the experiment and simulations, as well as on the order parameter I developed were published in PRL [191, 192]. We presented the dependence of lane formation dynamics on complex plasma parameters, based on our numerical simulations, during the 12th workshop on the physics of dusty plasma (Boulder CO, 2009). These results were published in IEEE Transactions on Plasma Physics [190]. Please find these papers attached to the thesis.

To investigate lane formation I compared the experiments to three dimensional molecular dynamics simulations at the Langevin level. The theoretical model behind these is that particle-particle interaction can be described by a Yukawa-type interaction potential, defined via the particle charge Q(a), with particle radius a, and screening length λ, that depend on each other by a fixed coupling strength Γ (cf. chapter 1).

The main results were:

- A universal order parameter to quantify this non-equilibrium phase transition in driven systems.
- The dynamical onset of lane formation can be resolved.
- Lanes of small particles form practically immediately, within inter particle distance of the background complex plasma.
- The much more inert large particles are arranged into lanes by the passing flow of smaller particles, too.
- Lanes in the background persist for times much longer than the self diffusion time of large particles.
- The dynamics of lane formation depend strongly on the internal parameters of the complex plasma, and on the initial phase of the background complex plasma.
- Internal parameters of the complex plasma that cannot be measured directly or derived theoretically, like screening length λ and particle charge Q, can be determined by varying them in the MD simulations.

4.2 Outlook

Lane formation and phase separation are a hot topic in soft-matter for two reasons. On the one hand they have been shown to be two sides of the same coin, i.e., Rayleigh-Taylor instability at the discreteness limit [212], discriminated by the ratio of surface tension to driving force. On the other hand they are dissipative structures, like, e.g., vortices, shocks or dissipative dark solitons [64]. The possibility to investigate hydrodynamics at the discreteness limit is very exciting, and complex plasmas offer a lot to investigate here, like the transition from laminar to turbulent flow or Kelvin-Helmholtz instability at the discreteness limit [140]. Still I want to give some motivation for and concentrate on the investigation of non-equilibrium phase transitions in the remainder of this outlook.

Lane Formation is a non-equilibrium phase transition. It is a form of self-organization that occurs whenever two particle species are driven through each other with sufficient but not too strong force. Lanes have been studied extensively for "intelligent" particles, i.e., pedestrians, but the occurrence of lanes has been shown to be independent of cognitive abilities or communication, i.e., potential, between the particles — even hard spheres form lanes. The phase separation of binary complex plasma seen at a later stage of the experiment is a liquid-liquid non-equilibrium phase transition, too.

Lane formation and phase separation supply us with interesting new insight into the complex plasma and new experimental venues of fundamental complex plasma research. Examples are:

- The decay of lanes in the background plasma. Which was found to take much longer than self-diffusion time. The results of my analysis for experimental data hint on the existence of meta-stable states.
- Conducting lane formation experiments in electro-rheologically altered complex plasma, to probe the wake structures using numerical simulations for model testing.
- The dependence of lane formation dynamics on the exact decomposition of the complex plasma coupling parameter into dust charge and the screening length. From numerical simulations it is obvious that this makes a significant difference, that could also be used for testing of charging and shielding models. [1]
- Phase separation indicates that the system has some kind of effective surface tension, something that could not be detected for a complex plasma with particles of only one size, yet.
- Phase separation has been shown to be driven by a non-additivity in the particle interaction potential [79]. This is a clear indication of the interaction potential being non-Yukawa.

I currently continue the investigations of lane formation, taking into account non-additivity, looking at all the lane formation events in our experimental data, to do a huge parameter space survey. Additionally we are using the dynamics of phase separation to identify the nature of the particle interaction potential, which seems to have a long range (maybe even Coulomb type) component [88].

Phase separation as a non-equilibrium phase transition is in the focus of complex plasma research also because it has a liquid-liquid critical point. Mathematically this corresponds directly to the vapor-liquid critical point for usual phase transitions. The research of physics at the critical point from a particle resolved fully kinetic point of view — as it is possible by the unique features of complex plasmas — would be a breakthrough result for science. Before investigations at the critical point are possible first the parameters to realize the critical point must be found and experiments have to be built to attain the necessary conditions: The vapor-liquid critical point requires an attractive component in the binary interaction potential. For non-equilibrium phase transitions like phase separation, that depends only on the mixing ratio of the two particle species, the search for the critical point is straight forward, and in principle reduces to a binary search — at least for numerical experiments. Experimentally these conditions are easier to attain, as phase separation works also if there is no attractive component. In contrast experiments were unable to get close to the vapor-liquid critical point for more than three years. In 2009, finally, experiments on the ISS were able to generate complex plasma conditions close to what is

[1] Current research on phase separation in binary complex plasma indicates that a weak long range interaction will result in completely different dynamics of the phase transition than a strong short range interaction potential. Even though both parameter sets result in the same coupling strength, which would result in an almost indistinguishable behavior and steady state for a complex plasma with particles of only one size.

expected by theoretical predictions, and we found methods to allow the identification of the vapor-liquid critical point in measurements available for complex plasmas.

The difficulty for real experiments is in generating extraordinarily homogenous conditions. Experiments on lane formation and phase separation in binary complex plasmas are currently only possible using the PK-3 Plus setup onboard the ISS. Unfortunately this limits severely the diagnostic possibilities and the number of parameters that can be checked systematically. This makes it necessary to rely on numerical experiments for interpretation of the data we have received so far. An important goal for the near future will be the adaption and design of ground based or parabolic flight experiments, using the full possibilities of current diagnostics, especially on plasma parameters [83, 129, 128], and recording of particle trajectories using high speed cameras, possibly in 3D.

Chapter 5

Outlook

Complex plasma research is first and foremost an interdisciplinary art. To devise, run, analyze, interpret and improve experiments in this field, one must not neglect all the knowledge gained in fundamental plasma physics over the last 80 years, its application in astrophysics, fusion plasmas, processing plasmas and engineering. These fields provide a solid scientific background needed in complex plasma research. On the other hand complex plasma is a perfect test system for these fields. Allowing model testing of plasma physics theories, like plasma sheath and pre-sheath potential, charging of surfaces, or inter particle potential. Research in complex plasma has strong implications to, e.g., astrophysics, similar to the formulation of Alfvén waves or Landau damping, especially in all magnetohydrodynamic processes, dynamics of interstellar and solar system dust, the formation of planets, etc.. The strongest impact over the last years has most likely been to the processing plasmas communities, and recently in the field of plasma medicine.

Beyond that complex plasmas provide a whole new unique research opportunity. Complex plasmas were from the very beginning entitled the "fifth state of matter", similar to plasma being the fourth. In my opinion more correctly complex plasma is finally recognized as the plasma state of soft matter, linking it with other states such as polymers, gels, foams, colloids, and granular media. All these systems share fundamental properties, while each has special unique advantages, either in application, or in its suitability to do specific experiments.

Still a lot of fundamental physics in complex plasma is not solved and we need more high precision experiments, smart experimenters and support from numerical experiments to distinguish between different theoretical models in our field. The most fundamental ones are particle charging, inter particle potential, and parameters of plasma in the presence of particles. Our knowledge of these three is the most important ingredient in all our theoretical and experimental approaches to investigate this huge field of physics. In addition a lot of complex plasma science is explorative. As long as we do not know all the details and cannot control all the system parameters, we must not neglect freak or not yet understood events that happen during complex plasma experiments.

All progress so far was achieved through iterative improvements, from former knowledge, physical principles, usage of most modern computer simulation, and international

collaborations. We need a steady and growing number of researchers who can approach complex plasma research with their own ideas not being forced to prove some predefined theory, and not having to "hurry for results" on their scientific career rally. One fine example for the application of these principles is the PK-3 Plus experiment onboard the ISS.

For the next ten years of fundamental complex plasma research I would like to see the detailed investigation of hydrodynamics at the discreteness limit, the transition from laminar to turbulent flow, dissipative structures (e.g. shocks, vortices, dissipative dark solitons), (the dynamics of) non-equilibrium phase transitions, and physics at the critical point, all at the most fundamental level of particle resolved kinetics. In addition I expect extended numerical investigation of particle charging and particle interaction potential. A whole new playground is available through custom made interaction potentials, allowing the investigation of electro- and magento-rheological systems, solid-solid phase transitions, etc.. The development of a dedicated experiment to investigate physics related to flows using complex plasma under micro gravity is already finished. The PK-4 [202] experiment, is currently manufactured, and will soon be integrated into ESA's Columbus module on board of the ISS. Furthermore the complex plasma group of the Max-Planck-Institut for extraterrestrial Physics is developing Plasma Lab, a complex plasma research facility designed to allow maximum control over discharge conditions. Including the tuning of electron temperature, changing the particle interaction potential using the ion wake effect, and making it possible to control the position of main plasma production — which is important to create homogeneous complex plasmas. Plasma Lab could replace PK-3 Plus within a few years from now.

Most of all I expect complex plasma to surprise me with new, exciting and unpredicted phenomena, applications and research possibilities.

Appendix A

Scaling Index Method

The scaling index method (SIM) is a methodology to investigate the structural properties of point distributions. It can be applied to data of any dimensionality, and is sensitive to nonlinear effects. Applying the SIM to a point distribution results in a single value for each point in the distribution that can be understood in terms of the dimensionality of local structure elements: the so called scaling index α. The original ideas behind the SIM derive from the study of attractors in chaotic systems. The scaling index method is a realization of the distribution of pointwise dimensions as used in the characterization of strange sets [58], and the investigation of anomalous scaling laws [149]. It is closely related to the calculation of the correlation dimension [57].

In this appendix I present the SIM in the context of finding patterns or nonlinearities in, and quantifying topological properties of experimental data. Most disciplines in science have standard methods for these tasks, and every physicist has expertise in several methods, he is applying in the analysis of his data. Examples are the discrete Fourier transform and the power spectrum derived from it, higher order spectral analysis instruments like the bispectrum, the pair correlation function $\mathrm{g}(r)$ and the bond angle correlation function $\mathrm{G}_6(r)$ to evaluate liquid and solid phases, and Minkowski functionals in morphological image analysis. Even though there is a large number of methodologies, I specifically recommend to evaluate the SIM, because of its conceptual and implementation simplicity, and its versatility.

Before the formal definition of the scaling index, I want to provide some motivation, by giving a rough sketch of applying the SIM. Consider the finite point set X (of 1600 discrete points) displayed in the left diagram. A quick visual inspection identifies a "square" or "sheet" of uniformly distributed random background, a "horizontal narrow band" with increased density, and a small "cluster" of very dense points close to the lower left corner.

Applying the SIM, defines for every point $\mathbf{x}_i \in X$ a value α_i, that estimates how the number of points in some neighborhood (e.g., a hypersphere) of radius a around $\mathbf{x}_i$ scales with radius. α_i is called "scaling index", its value depends in general on the specific radius a of the neighborhood for which the scaling behavior is estimated. a is referred to as "scale". From the individual scaling indices $\alpha_i(a_0)$ at one specific scale a_0 we define $P(\alpha(a_0))$ as the spectrum of scaling indices. The central diagram of figure A.1 shows $\log(P(\alpha(a)) + 1)$

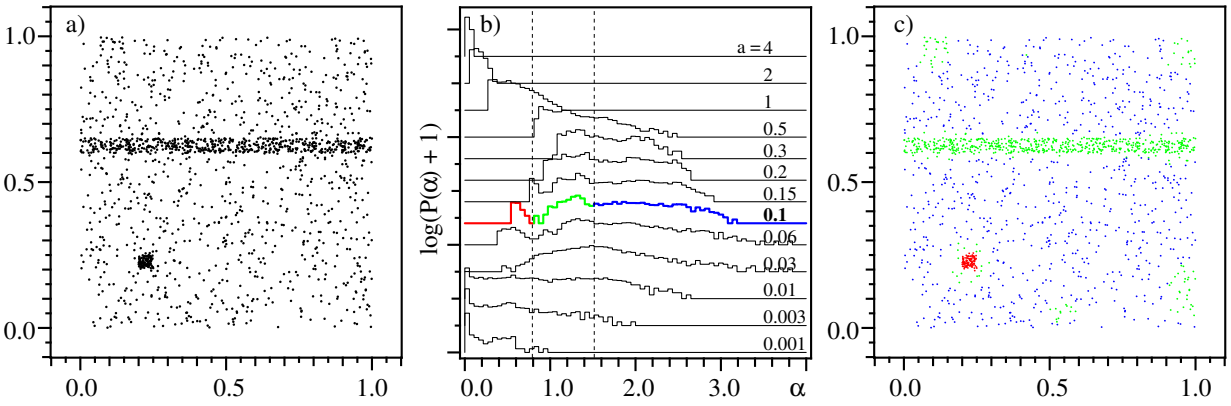

Figure A.1: Example for the scaling index method. (a) The point set X. (b) Spectra of scaling indices $\log(P(\alpha(\mathbf{x}_i, a)) + 1)$ obtained at different scales a. The graph for $a = 1.0$ is emphesized, the vertical lines highlight $\alpha = 0.8$ and $\alpha = 1.5$ respectively. (c) Points $\mathbf{x}_i \in X$ were colored by their scaling indices at scale $a = 0.1$: red for $\alpha_i < 0.8$, green for $0.8 \leq \alpha_i < 1.5$, and blue for $1.5 \leq \alpha_i$.

for several scales a. On very short scales $a < 0.01$ the SIM resolves the discreteness of X: almost all points recieve a scaling index of zero. At intermediate scales $0.03 < a < 0.15$ rich spectra of scaling indices unfold. For larger scales boundary effects become important. $P(\alpha)$ smears out, and finally almost all scaling indices become zero again. (At these scales the whole X appears as one "point".)

The right diagram in figure A.1 shall help visualize the geometric or topological meaning of specific scaling index values. For the intermediate scale $a = 0.1$, the points $\mathbf{x}_i \in X$ have been colored according to their α_i: red for $\alpha_i \in [0, 0.8[$, green for $\alpha_i \in [0.8, 1.5[$, and blue for $\alpha_i \in [1.5, \infty[$. Apparently α_i represents the dimensionality of the local (as defined by a) structure of X around $\mathbf{x}_i$: Most points "in the background" get $\alpha \simeq 2$, which is the embedding dimensionality, points "on the band" get α closer to 1, the dimensionality of a line, and those "in the cluster" have an α closer to 0, the dimensionality of a point. Please note, that several points "in the background" are colored green, which characterizes them as members of a line-like structure.

A.1 Mathematical Definition

Lets consider a set of points X embedded in a d dimensional vector space. This can but need not be an infinite set. In the following description of the scaling index method, I would rather consider point sets with a finite number of points, i.e., like all measurement results in experiments, e.g., time series, images, or point distributions.

To derive the scaling index method, I define the *mass* $M(\mathbf{x}_i, a)$ of the point set X in a neighborhood of size a around $\mathbf{x}_i$. Historically this mass function is defined by the number of points — or analogously integrated densities — within a neighborhood defined

by hypercubes or hyperspheres of size a:

$$M_\Theta(\mathbf{x}_i, a) = N_\Theta(\mathbf{x}_i, a) = \sum_j \Theta(a - ||\mathbf{x}_i - \mathbf{x}_j||),$$

where $\Theta(d) = \left\{ \begin{smallmatrix} 1 & d \geq 0 \\ 0 & d < 0 \end{smallmatrix} \right.$ is the Heaviside function, and $||\ldots||$ is the maximum or the Euclidean norm respectively. In principle there can be an unlimited number of such mass functions, or definitions of a local neighborhood, there are just three necessary constraints: $M(\mathbf{x}_i, a)$ must be strictly positive, it has to be a monotonically increasing function of a, and $M(\mathbf{x}_i, a)$ must be finite. For example, the historical M_Θ can easily be extended to a generalized mass function using the sum of weighted distances $M_{s,d}(\mathbf{x}_i, a) = \sum_j \mathrm{s}(\mathrm{d}(\mathbf{x}_i, \mathbf{x}_j)/a)$, where $\mathrm{s}(d)$ is a suitable shaping function, and $\mathrm{d}(\mathbf{x}_i, \mathbf{x}_j)$ is a general distance measure, that is normalized by the scale a.

For the definition of the scaling index $\alpha_i = \alpha(\mathbf{x}_i, a)$ we assume that $M(\mathbf{x}_i, a) \sim a^{\alpha_i}$, for some range of scales $a \in [\underline{a}, \overline{a}]$. α_i is called "scaling index", as it describes the scaling of the mass function M with the size a of a neighborhood around point $\mathbf{x}_i$. In general there can exist several regimes $[\underline{a}, \overline{a}]$ with completely different scaling properties (cf. figure A.1). For the interpretation of α_i one has to specifying the scale a.

The concrete definition of α solely depends on the exact mass function M. It can be obtained from the power law as $\alpha = \frac{\mathrm{d}\ln(M)}{\mathrm{d}\ln(a)}$. Lets take the original M_Θ as an example. As the Heaviside function $\Theta(d)$ is not differentiable in $d = 0$ one has to use an estimator for the derivative, e.g., the difference quotient with two scales $a_1 < a_2$:

$$\alpha_\Theta(\mathbf{x}_i, a_1, a_2) = \frac{\ln(M_\Theta(\mathbf{x}_i, a_2)) - ln(M_\Theta(\mathbf{x}_i, a_1))}{\ln(a_2) - \ln(a_1)}.$$

With a mass $M_b = \sum_j \exp(-(|\mathbf{x}_i - \mathbf{x}_j|/a)^b)$, $b \in \mathbb{R}^+$, i.e., a weighted sum with a Gaussian type shaping function and standard Euclidean distance $d_{ij} = |\mathbf{x}_i - \mathbf{x}_j|$ normalized by the scale a, one gets:

$$\alpha_b(\mathbf{x}_i, a) = b\frac{\sum_j (\frac{d_{ij}}{a})^b \exp(-(\frac{d_{ij}}{a})^b)}{\sum_j \exp(-(\frac{d_{ij}}{a})^b)}.$$

The scaling index α_i can be recognized as the dimensionality of the local structure of X at $\mathbf{x}_i$ discernible at some scale a. For instance, $\alpha \simeq 0$ indicates that the local structure "looks" like a point, for $\alpha \simeq 1$ like a line, for $\alpha \simeq 2$ like a plane. Scaling indices between, e.g., 1 and 2 will be obtained for points on wiggled lines or bands (i.e., wide lines). Noise will have $\alpha \simeq d$, i.e., close to the dimensionality of the embedding space — which means nearby points appear to be uniformly distributed. Interestingly scaling indices larger than the embedding dimension exist, even though this seems counterintuitive. This originates in α being defined as a derivative, and is a signature of points in under-dense regions with a size comparable to the scale a.

One often investigates $\mathrm{P}(\alpha)$ the spectrum of scaling indices realized by the point set X. $\mathrm{P}(\alpha)$ can be interpreted as a spectrum of local structure elements. It is a *global* measure comparable to the results from Fourier frequency analyses.

A.2 Features

The SIM has four advantages:

- It is very easy to implement.
- It produces point wise local structure measures α_i that provide a natural global measure $P(\alpha)$.
- It can be applied to data of any type.
- It is sensitive to nonlinear effects.

The last two points do not come for free and need careful evaluation of the problem and the SIM. I will discuss this in the relevant sections below.

Simple Implementation and Adaption

The SIM can be implemented using the naive $\mathrm{O}(N^2)$ algorithm. The method is very easy to apply to data of arbitrary dimensionality. For example $\alpha_2(\mathbf{x}, a)$, with $\mathbf{x} \in \mathbb{R}^d$, would look like this in pseudo code:

```
point = array(real, N, d)
alpha = array(real, N)
for i = 1, N do begin
   num = 0.
   den = 0.
   for j = 1, N do begin
      dist2 = 0.
      for k = 1, d do begin
         dist2 = dist2 + (point(i, k) - point(j, k))^2
      endfor
      dist2 = dist2 / a^2
      wght = exp(- dist2)
      num = num + dist2 * wght
      den = den + wght
   endfor
   alpha(i) = 2 * num / den
endfor
```

Of course this algorithm scales unfavorably with the number of data points, but all techniques that have been developed for numerical simulations can also be applied to the SIM. Depending on the shaping function used in the definition of M and α, and on the data representation (e.g., gridded or continuos) different strategies can be applied to speed up computation: for example lookup tables, cutoffs, cell lists, clustering tree codes or distance

trees, heavily parallel computing. Unlike, e.g., with molecular dynamics simulations, these techniques can be applied very aggressively, as errors do not accumulate over time. Additionally scaling indices are of the order of one, and for all applications I know absolute errors of 0.01 are negligible.

Beyond that the scaling index method allows to change the meaning of "local neighborhood" elegantly by using different shaping functions and special purpose distance measures — or correspondingly state space transformations. This will not change the concept of scaling indices, and also will not change the algorithms used to calculate them. Another possible extension of the SIM is to use partial or directional derivatives to obtain the concrete definition of α from the mass function. That way the scaling index attains a vector quality, possibly changing the meaning of its magnitude from scaling to scaling contrast. Examples for this are given in the subsection on suitability and the section on applications below.

Local and Global Structure Measure

On their own the individual α_i provide interesting new information about each individual point $\mathbf{x}_i$, that could, e.g., be used directly as an additional state space dimension. Their spectrum $P(\alpha)$ is a natural global measure of the structural properties of the point set. Statistical analysis of the α-spectrum of different datasets can be used to discriminate between different classes of events. An important application is, e.g., model testing, where the $\mathrm{P}(\alpha)$ of experimental data is compared to the $\mathrm{P}(\alpha)$ of simulations based on different models.

Because each $\mathbf{x}_i$ contributes exactly one α_i to $P(\alpha)$, the SIM allows to identify all individual points that contributed to some peculiarity of the spectrum. For example one can filter the point set in state space by selecting ranges of scaling indices, as has been demonstrated in the introduction (cf. figure A.1). This structural decomposition allows to distinguish if some peculiarity results from macroscopic or microscopic patterns in the point set. For instance, a peak in $P(\alpha)$ close to $\alpha = 1$, means that lots of points appear to be on some line-like structure. This could result from lots of points really sitting on some macroscopic string, or it could be a signature of lots of microscopic strings scattered throughout state space, or some combination of both.

Structural decomposition is missing from a lot of well established measures, like the power spectrum, bispectrum, $\mathrm{g}(r)$, $\mathrm{G}_6(r)$ and Minkowski functionals. In the case of power spectra one can achieve some kind of locality by masking spectral bands and performing the inverse Fourier transform. Comparison of the original data, e.g., a time series or image, to the result of the filtered back transform, can identify which parts (temporal or spatial regions) contributed the most to that spectral band. Yet this is not exactly the same, as all parts of the original data will contribute to the whole power spectrum, and vice versa.

In principle it is possible to devise local measures from global measures by simply limiting the calculations to some temporal or spatial region. Examples are the short time

Fourier transform, Gabor filters[1], or localized versions of the Minkowski functionals. The latter will produce spectra very similar to $P(\alpha)$, representing different topological aspects of the point set. Still these extensions and modifications are not trivial and unlike the SIM they are not easily adaptable to data of arbitrary dimensionality.

Suitable for any Type of Data

As the SIM operates on arbitrary point sets, it can be applied to any type of data, e.g. time series, images and point sets. One embeds the data in some state space of suitable but arbitrary dimensionality, selects a scale, defines a mass function that counts points, and receives scaling indices. For numerical processing this means, that basically the same computer program can analyze all datasets. This simplicity and versatility of the SIM does not come for free, the complexity is just transferred to identifying the relevant scale(s), building the correct embedding, and tuning the mass function — and of course data mining the resulting scaling indices.

Scale

Even though the selection of the relevant scale might seem trivial or even arbitrary, it is a crucial part of the scaling index method.

In the definition of the scaling index α, we assume the existence of a range of sizes $a \in [\underline{a}, \overline{a}]$, for which the mass function can be expressed by a power law $M \sim a^{\alpha}$. It is not obvious that such a range exists! More likely such a range does not exist at all, or there need not be one range that produces the same scaling behavior for all $\mathbf{x} \in X$. Additionally for every $\mathbf{x}$ there might exist several ranges, each with its own power law dependance. In general it is neither necessary nor expected and not even desired for a point set to show the same scaling behavior on all scales. This property is immanent only in point sets that are dense in some subspace of the embedding space and are uniformly distributed, like for example white noise. Often one is interested in point distributions that display varying scaling behaviour on different scales. These are called multi-fractal sets, the typical pictures for them are, e.g., coastlines or a plate of spaghetti[2].

Usually one will have to do a multi scale analysis to get a good understanding of the real meaning of individual α values and their spectrum P(α). This involves an investment of time, computing resources and data storage. It will generate a new data space that will have to be analyzed or data mined. This may lead to the discovery of one or more natural scales (like the size of the plate or the diameter of the spaghetti in footnote 2) and can produce unexpected results.

[1] Gabor filters are linear filters used in image processing. An application of the Gabor transformation, a spatially localized version of the Fourier transformation, named after Nobel laureate Dennis Gábor.

[2] When looked at from a great distance a plate of spaghetti will look like a point ($\alpha \simeq 0$). Coming closer it will start to look like a fairly homogeneous plane ($\alpha \simeq 2$), until we are able to distinguish individual spaghettis, that are more like curly lines ($\alpha \simeq 1-2$). When the scale becomes smaller than the spaghetti diameter we will start to resolve the spaghetti surface ($\alpha \simeq 2-3$) and the homogeneous dough inside ($\alpha \simeq 3$).

Embedding

While choosing a good data representation is a necessary step in any analysis methodology [175], it is crucial for the SIM. Data will come with some natural meaning and units, like distances in meters, or time in hours, that are not directly comparable. Equally important, information need not be distributed uniformly within one dimension or over the whole state space, e.g., noise could be distributed unevenly over the dynamic range of a measurement or might depend systematically on time or location. As the SIM compares everything on one common scale, the embedding has to provide for a globally valid relevance of this scale.

Consider for example a digital image, recorded by a CCD with an $M \times N$ matrix of pixels p_i as some charges Q_i, and digitized to intensities I_i by individual analog digital converters (ADCs). One can use a simplistic three dimensional embedding space, where each p_i would be represented by one point $\mathbf{x}_i = (r_i, c_i, I_i)$, where $r_i = row(p_i)$ and $c_i = column(p_i)$. Row and column seem to be compatible as both refer to spatial coordinates, still their relative mapping depends on several factors, e.g., possibly non-square pixels in the camera or the (nonlinear) mapping function of some optics. The individual intensities are also not directly comparable as they depend on the sensitivity of the real pixels and the transfer function of their ADCs, additionally each pixel can have a different noise characteristic. All these intradimensional mappings can be corrected. More (maybe even prohibitively) complicated is the interdimensional mapping between spatial coordinates and intensities. This could be solved by using a two dimensional embedding, where for each pixel p_i, one creates I_i points $\mathbf{x}_{i,j} = (r_i, c_i)$, for $j \in [1, I_i]$.[3] As an additional benefit the resulting scaling indices would retain the same dimensionality as expected from images, i.e., $\alpha_{i,j} \in [0, \sim 2]$.

Usually it's not possible to transform all variables of a measurement to a common unit from a priori knowledge. In these cases one will have to do some information centered analysis first. Lets consider two examples. First, the time series of some voltage $U(t)$. The problem one faces here is mapping time to voltage. Commonly this is solved by using delay coordinates, where each pair of t_i and $U(t_i)$ is represented by one point $\mathbf{x}_i = (U(t_i + dt), U(t_i))$ in the state space (which is in general only possible for a periodic $U(t)$). Of course one could select any delay dt, but its not obvious how to find the optimal value. Well established choices are, e.g., the first zero of the autocorrelation function, or the first minimum of the mutual information [53]. Second, one can do global and possibly nonlinear information based rescaling of axes, analogous to (itensity-)histogram equalization used in image processing. The axes are stretched in such a way that equal distance means same amount of information. This can help in cases when, e.g., noise is not equally distributed over the full dynamic range. Infomation based rescaling can allow for automated interdimensional mapping (like position to velocity or intensity), as it replaces the individual natural meaning of the scale a with an abstract global meaning of information content.

[3] Instead of creating a number of points equal to the intensity of the pixel, one could alternatively use intensity as a weight. The mass function would then accumulate weights instead of simply counting points in the neighborhood. Even though the resulting α_i are identical to the $\alpha_{i,j}$ their spectrum $P(\alpha)$ will be very different.

Tuning

Depending on the original problem or question, one might have to tune the concrete definition of α. Usually this will happen if one is interested in some kind of directionality, as is often the case in, e.g., pattern recognition or texture detection. Even though the unmodified SIM is able to identify anisotropies, it is by construction insensitive to directions. To introduce directionality to the SIM one can, e.g., use a directional derivative instead of a total derivative in the definition of α, limit the SIM to subspaces of the embedding space, or one applies local transformations of the state space in every data point.

Let's deliberate on local state space transformations. For the calculation of every α_i one can allow for arbitrary transformations of the embedding space using rotations, linear and nonlinear stretching. There are two methods to do this: Either one identifies the "correct" local transformation by pre-analyzing the point set using some other tool, or one performs a multi-parameter study, similar to the multi-scale investigation proposed to identify relevant scale(s). For example, to characterise anisotropies in an image, one could use some image filter (e.g., Gabor filters) to find preferred directions θ_i in every pixel p_i of the image, then one would stretch the point set around the corresponding $\mathbf{x}_i$ before the calculation of α_i, to correct for or emphasize the anisotropy. Alternatively one could stretch the image in a large number of directions θ, by a lot of factors ϵ, calculate all $\alpha(\mathbf{x}_i, a, \theta, \epsilon)$, and characterize the anisotropies in $\mathbf{x}_i$ by comparing perpendicular directions. With both methods the individual α_i and the scale a will only have meaning in the context of the applied transformations. Usually one will neglect the topological meaning of α in such investigations, and uses some scaling index contrast instead.

Sensitivity to Linear and Nonlinear Effects

In this section I treat *linear* to mean "noticeable by the two point correlation function" or "expressed by the power spectrum", and *nonlinear* to be synonymous with higher order correlations or "correlations of the phases of the Fourier transform".

For the demonstration of this feature see figure A.2 which shows the time series $\mathrm{x}(t)$[4] and $\mathrm{x_a}(t)$ and $\mathrm{x_p}(t)$, two crude surrogates [178, 159] derived from it: First, I calculated $x' = \mathrm{F}(x)$ the Fourier transform of the original time series. Then I created x'_a by shuffling the amplitudes of the positive frequencies in x', and replicating them for the negative frequencies in such a way that the inverse Fourier transform will result in a real function. This destroys the power spectrum, but preserves the energy and all the phase information. Finally, $x_a = \mathrm{F}^{-1}(x'_a)$ is calculated applying the inverse Fourier transformation. x_p is generated analogously by shuffling the phases of the Fourier transform x'. This will randomize the phase correlations, but preserves the full power spectrum. I.e., naive investigation of these surrogates using only the Fourier amplitudes — neglecting the phase information — will claim that $\mathrm{x}(t)$ is identical to $\mathrm{x_p}(t)$.

[4] $\mathrm{x}(t)$ was obtained from the simulation of a pressure shock wave along a tube. It is an arbitrary example for data obtained from a nonlinear process.

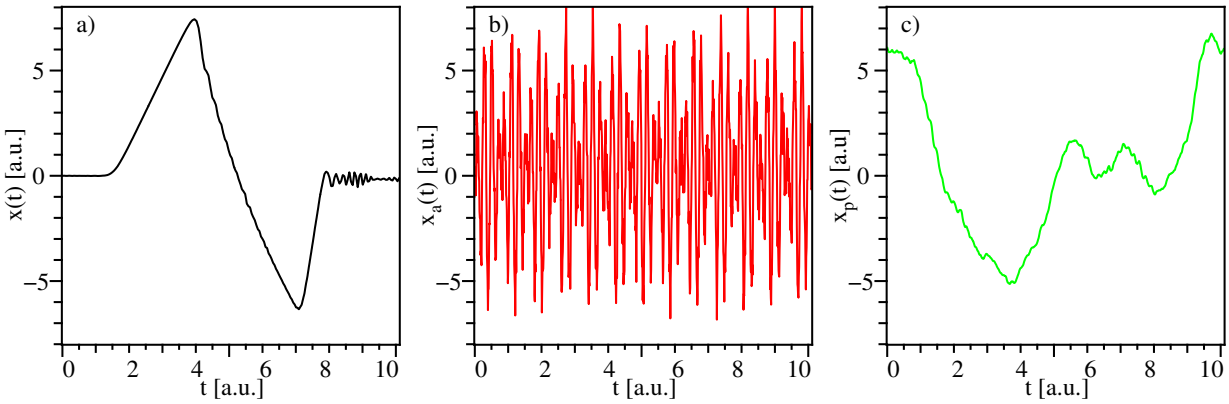

Figure A.2: Illustration of linear and nonlinear effects. (a) The original time series $\mathrm{x}(t)$. (b) $\mathrm{x_a}(t)$ derived from $\mathrm{x}(t)$ by randomizing the Fourier amplitudes. (c) $\mathrm{x_p}(t)$ derived from $\mathrm{x}(t)$ by randomizing the Fourier phases.

To analyze the time series $\mathrm{x}(t)$ and its surrogates $\mathrm{x_a}(t)$ and $\mathrm{x_p}(t)$ using the SIM, I transformed them into point set X, X_a and X_p in a 2D embedding using delay coordinates. That means for every $\mathrm{x}(t_i)$ I created a point $p_i = (\mathrm{x}(t_i + dt), \mathrm{x}(t_i))$ in X, where dt is a fixed time delay. X_a and X_p were derived analogously from $\mathrm{x_a}(t_i)$ and $\mathrm{x_p}(t_i)$. The time delay $dt = 0.7$ was chosen by visual inspection of the resulting X. Figure A.3 shows the resulting point sets. The point set X from the original time series obviously differs from X_a that represents the randomized fourier amplitudes. But the point set for randomized fourier phases X_p displays similarity to the original. For each of these sets, I calculated the scaling indices using $\alpha_2(\mathbf{p}, a)$ and the identical scale $a = 1$. The resulting spectra $\mathrm{P}(\alpha)$ are displayed in figure A.4. Comparing the peculiarities of these spectra one can clearly separate all three point sets.

The SIM as a nonlinear filter has two main drawbacks. First, as can be seen from this example, the SIM does not separate linear and nonlinear effects nicely, as for instance the Fourier transformation does. That means, one cannot distinguish nonlinear and linear effects using the SIM, without the help of additional methods, like surrogates. Second, it is not bijective, i.e., you cannot recreate a point set X from the scaling indices α_i or the $\mathrm{P}(\alpha)$ spectrum.

A.3 Applications

Even though the scaling index method is a realization of the distribution of pointwise dimensions, and thus is related to the characterization of attractors in phase space, my view of the SIM results from its application as a nonlinear filter in data processing, and by the interpretation of $\mathrm{P}(\alpha)$ as the spectrum of the dimensionality of local structure elements. In this section I present a chronological sketch of the application of the SIM to different problem domains, that formed my picture of the SIM. I will emphasize the main concepts

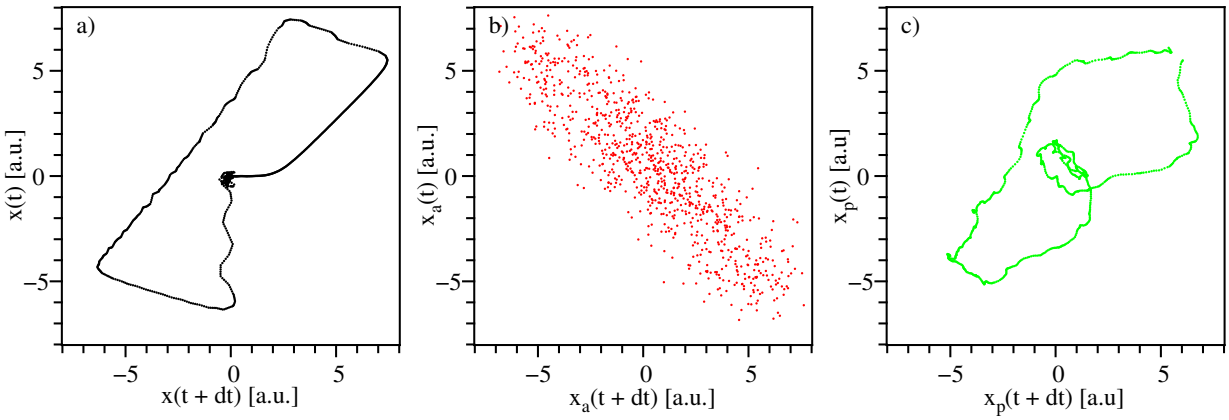

Figure A.3: 2D embedding using delay coordinates. (a) Original $\mathrm{x}(t)$ plotted vs. $\mathrm{x}(t+dt)$. (b) Randomized Fourier amplitudes $\mathrm{x_a}(t)$ vs. $\mathrm{x_a}(t+dt)$. (c) Randomized Fourier phases $\mathrm{x_p}(t)$ vs. $\mathrm{x_p}(t+dt)$. All three graphs use the same delay $dt = 0.7$.

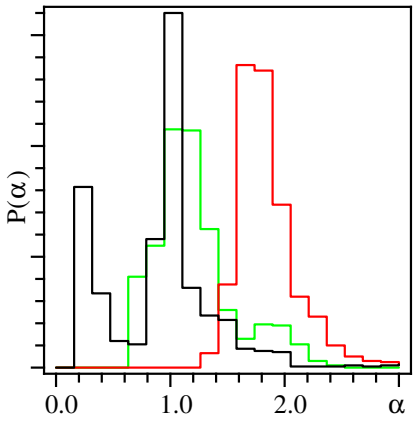

Figure A.4: Spectrum of scaling indices obtained from the delay coordinate representation. $\mathrm{P}(\alpha)$ was calculated using $\alpha_2(\mathbf{x}, a = 1)$. The black curve shows the spectrum of the original data, the red curve represent the randomized Fourier amplitudes, and green the randomized Fourier phases.

and refinements each of these applications added to this picture.

In 1997 Räth and Morfill [160] applied the SIM to image processing, defining a nonlinear filter to identify textures. They used three different mass functions and scaling indices. The then standard

$$M_\infty(\mathbf{p}_i, a) = \sum_j \Theta(a/2 - ||\mathbf{p}_i - \mathbf{p}_j||_\infty),$$

which results in

$$\alpha_\infty(\mathbf{p}_i, a_1, a_2) = \frac{\ln(M_\infty(\mathbf{p}_i, a_2)) - ln(M_\infty(\mathbf{p}_i, a_1))}{\ln(a_2) - \ln(a_1)}$$

and two "anisotropic" versions,

$$M_x(\mathbf{p}_i, a) = \sum_j \Theta(a/2 - |x_i - x_j|)\Theta(a_2/2 - ||\mathbf{p}_i - \mathbf{p}_j||_\infty)$$
$$M_y(\mathbf{p}_i, a) = \sum_j \Theta(a/2 - |y_i - y_j|)\Theta(a_2/2 - ||\mathbf{p}_i - \mathbf{p}_j||_\infty),$$

with $\mathbf{p}_i = (x_i, y_i)$, that result correspondingly in

$$\alpha_{\mathrm{x}}(\mathbf{p}_i, a_1, a_2) = \frac{\ln(M_x(\mathbf{p}_i, a_2)) - ln(M_x(\mathbf{p}_i, a_1))}{\ln(a_2) - \ln(a_1)}$$
$$\alpha_{\mathrm{y}}(\mathbf{p}_i, a_1, a_2) = \frac{\ln(M_y(\mathbf{p}_i, a_2)) - ln(M_y(\mathbf{p}_i, a_1))}{\ln(a_2) - \ln(a_1)}.$$

That is, the authors define "anisotropic" scaling indices, by replacing the total derivative with a directional or partial derivative in the definition of α. On top of the orthogonal α_{x} and α_{y} the authors create a new concept of anisotropic difference or contrast, by calculating $E\Delta\alpha = E\alpha_x - E\alpha_y$ the difference between the expectation values of the anisotropic scaling indices for small regions of the image. This new nonlinear filter is used to discriminate the image into areas of predominantly vertical and horizontal structures. The geometric interpretation of α is completely neglected.

Related to texture detection, but much closer to application, is the quantification of image content for automatic evaluation of (malignant) melanoma — skin cancer — investigated by René Pompl in his PhD [153]. His thesis — written in German — contains an extended chapter on the scaling index method, that introduces two important modifications to the SIM. First, the use of "fuzzy" neighborhoods in the mass function, i.e., generalizing the Heaviside function and maximum norm to a differentiable shaping function and a general distance measure. Second, the development of a locally self-adaptive state space transformation to allow for rotationally invariant anisotropic scaling indices. The general idea is similar to the anisotropic contrast defined by Räth et al., but additionally Pompl determines the direction of derivation by analyzing the local image structure. This approach is basically equivalent to finding the scaling index vector gradient. Additionally, he gives a simple example to illustrate the geometrical interpretation of the scaling index, and to explain the meaning of the local scale a.

The direct use of the topologic meaning of scaling indices in the registration of images of different modality is described by Jamitzky et al. [81]. They clearly demonstrated the ability of the SIM to identify the dimensionality of local structure elements in images, and interpreted the scaling index as topological information about objects in the image.

As final example for using the SIM in image processing I'd like to mention the removal of noise, as applied by Poppe in his PhD [154]. His thesis — published 2001 in German — demonstrates the use of scaling indices to remove noise from medical images and of course provides a general introduction to the SIM.

The sensitivity of the SIM to nonlinear features of the data was used in the analysis of the large scale structure of the universe. First of all Räth et al. [159] extended the idea of iteratively refined surrogates [178] to apply it to a three dimensional point set (distribution of galaxies). Then they used the SIM to show significant deviations between the original point set and its surrogates (which preserved basically all linear features, i.e., power spectrum in the Fourier space and the pair correlation function $g(r)$ in configuration space). In addition the paper provides a concise definition of the SIM and "weighted scaling indices" — called "fuzzy SIM" by Pompl, and "suitable shaping function" in this appendix.

The idea of an anisotropic scaling index method, that would use smoothly deformed local neighborhoods, instead of a directional derivative, was developed in a series of publications by Monetti et al. and Räth et al.. They continuously refined anisotropic scaling indices to quantify trabecular bone structure [132, 131, 161]. The resulting method was called "scaling vector method" (SVM), to highlight the possibility to use different anisotropies at each point of the distribution. The SVM was used directly in the analysis of electro-rheological complex plasma [76].

For our papers on lane formation [191, 192, 190], we used the local vectors that came out of the SVM to transform our point set into a set of rods, akin to liquid crystals. We consequently defined a "nematic" order parameter to investigate the laning phase transition in driven binary complex plasma — which is conceptually identical to a mesophase in soft matter.

Bibliography

[1] M. R. Akdim and W. J. Goedheer. Modeling of voids in colloidal plasmas. *Phys. Rev. E*, 65:015401, 2001.

[2] M. R. Akdim and W. J. Goedheer. Modeling of dust voids in electronegative discharges under microgravity. *IEEE Transactions on Plasma Science*, 32(2):680–690, April 2004.

[3] H. Alfvén. *On the Origin of the Solar System*. Oxford University Press, Oxford, 1954.

[4] H. Alfvén. Existence of electromagnetic-hydrodynamic waves. *Nature*, 150(3805):405–406, Jul 1992.

[5] J. E. Allen. Probe theory - the orbital motion approach. *Physica Scripta*, 45(5):497–503, 1992.

[6] J. E. Allen, B. M. Annaratone, and U. de Angelis. On the orbital motion limited theory for a small body at floating potential in a maxwellian plasma. *Journal of Plasma Physics*, 63:299–309, 2000.

[7] T. C. Anestos and C. D. Hendricks. Injection of small macroscopic particles into plasmas as a diagnostic technique. *J. Appl. Phys.*, 45(3):1176–1178, 1974.

[8] B. M. Annaratone, A. G. Khrapak, A. V. Ivlev, G. Söllner, P. Bryant, R. Sütterlin, U. Konopka, K. Yoshino, M. Zuzic, H. M. Thomas, and G. E. Morfill. Levitation of cylindrical particles in the sheath of an rf plasma. *Phys. Rev. E*, 63(3):036406, Feb 2001.

[9] C. Arnas, M. Mikikian, and F. Doveil. High negative charge of a dust particle in a hot cathode discharge. *Phys. Rev. E*, 60:7420, 1999.

[10] C. Arnas, M. Mikikian, and F. Doveil. Micro-sphere levitation in a sheath of a low pressure continuous discharge. *Physica Scripta*, T89:163–167, 2001.

[11] A. Barkan, R. L. Merlino, and N. D'Angelo. Laboratory observation of the dust–acoustic wave mode. *Physics of Plasmas*, 2(10):3563–3565, 1995.

[12] M. S. Barnes, J. H. Keller, J. C. Forster, J. A. ONeill, and D. K. Coultas. Transport of dust particles in glow-discharge plasmas. *Phys. Rev. Lett.*, 68(3):313–316, Jan 1992.

[13] R. Basner, G. Thieme, F. Sigeneger, H. Kersten, G. Schubert, and H. Fehske. Micro particles of different sizes as electrostatic probes in rf-plasma. *APS Meeting Abstracts*, October 2006.

[14] J. Beckers, W. W. Stoffels, T. Ockenga, M. Wolter, and H.; Kersten. Microparticles in a rf plasma under hyper gravity conditions. *ICOPS 2009, IEEE Conference on Plasma Science*, 2009.

[15] J. Berndt, E. Kovacevic, V. Selenin, I. Stefanovic, and J. Winter. Anomalous behaviour of the electron density in a pulsed complex plasma. *Plasma Sources Sci. Technol.*, 15:18–22, 2006.

[16] D. Bohm, E. H. S. Burhop, and H. S. W. Massey. *Characteristics of Electrical Discharges in Magnetic Fields*. McGraw-Hill, New York, 1949.

[17] A. Bouchoule and L. Boufendi. Particule formation and dusty plasma behaviour in argon-silane rf discharge. *Plasma Sources Sci. Technol.*, 2:204–213, 1993.

[18] A. Bouchoule and L. Boufendi. High concentration effects in dusty plasmas. *Plasma Sources Sci. Technol.*, 3:292–301, 1994.

[19] A. Bouchoule, A. Plain, L. Boufendi, J. Ph. Blondeau, and C. Laure. Particle generation and behavior in a silane-argon low-pressure discharge under continuous or pulsed radio-frequency excitation. *J. Appl. Phys.*, 70:1991, 1991.

[20] André Bouchoule. *Dusty Plasmas: Physics, Chemistry and Technological impacts in Plasma Processing*. Wiley, New York, 1999.

[21] L. Boufendi and A. Bouchoule. Particle nucleation and growth in a low-pressure argon-silane discharge. *Plasma Sources Sci. Technol.*, 3:262, 1994.

[22] L. Boufendi, J. Gaudin, S. Huet, G. Viera, and M. Dudemaine. Detection of particles of less than 5 nm in diameter formed in an argon–silane capacitively coupled radio-frequency discharge. *Appl. Phys. Lett.*, 79(26):4301–4303, 2001.

[23] L. Boufendi, J. Hermann, A. Bouchoule, B. Dubreuil, E. Stoffels, W. W. Stoffels, and M. L. deGiorgi. Study of initial dust formation in an ar-sih4 discharge by laser induced particle explosive evaporation. *J. Appl. Phys.*, 76:148, 1994.

[24] L. Boufendi, A. Plain, J. Ph. Blondeau, A. Bouchoule, C. Laure, and M. Toogood. Measurements of particle size kinetics from nanometer to micrometer scale in a low-pressure argon-silane radio-frequency discharge. *Appl. Phys. Lett.*, 60:169, 1992.

[25] Philip C. Brandt, Alexei V. Ivlev, and Gregor E. Morfill. Solid phases in electro- and magnetorheological systems. *The Journal of Chemical Physics*, 130(20):204513, 2009.

[26] A. C. Breslin and K. G. Emeleus. Effects of dust in a bounded positive column. *Physics Letters A*, 31:23–24, January 1970.

[27] A. C. Breslin and K. G. Emeleus. The distinction between negative ions and charged dust in plasmas. *International Journal of Electronics*, 31(2):189–190, 1971.

[28] M. Cavarroc, M. C. Jouanny, K. Radouane, M. Mikikian, and L. Boufendi. Self-excited instability occurring during the nanoparticle formation in an ar/sih_4 low pressure radio frequency plasma. *J. Appl. Phys.*, 99:064301, 2006.

[29] J. Chakrabarti, J. Dzubiella, and H. Löwen. Reentrance effect in the lane formation of driven colloids. *Phys. Rev. E*, 70(1):012401, Jul 2004.

[30] M. Chaudhuri, S. A. Khrapak, and G. E. Morfill. Ion drag force on a small grain in highly collisional weakly anisotropic plasma: Effect of plasma production and loss mechanisms. *Physics of Plasmas*, 15(5):053703, 2008.

[31] M. Chaudhuri, S. A. Khrapak, and G. E. Morill. A note on the electrical potential distribution around a test charge in anisotropic collisional plasmas. *Journal of Plasma Physics*, pages 1–4, Jan 2010.

[32] M. Chaudhuri, S.A. Khrapak, and G.E. Morfill. Electrostatic potential behind a macroparticle in a drifting collisional plasma: effect of plasma absorption. *Physics of Plasmas*, 14(2):22102–1–5, February 2007.

[33] M. Chaudhuri, R. Kompaneets, and G. E. Morfill. On the possibility of collective attraction in complex plasmas. *Physics of Plasmas*, 2010.

[34] Manis Chaudhuri, Sergey A. Khrapak, Roman Kompaneets, and Gregor E. Morfill. Shielding of a small charged particle in weakly ionized plasmas. *IEEE Transactions on Plasma Science*, Apr 2010.

[35] J. H. Chu and Lin I. Direct observation of coulomb crystals and liquids in strongly coupled rf dusty plasmas. *Phys. Rev. Lett.*, 72(25):4009–4012, Jun 1994.

[36] L. Couëdel, M. Mikikian, L. Boufendi, and A. A. Samarian. Residual dust charges in discharge afterglow. *Phys. Rev. E*, 74(2):026403, 2006.

[37] L. Couëdel, V. Nosenko, A. V. Ivlev, S. K. Zhdanov, H. M. Thomas, and G. E. Morfill. Direct observation of mode-coupling instability of two-dimensional plasma crystals. *Phys. Rev. Lett.*, 104(19):195001, May 2010.

[38] L. Couëdel, V. Nosenko, S. K. Zhdanov, A. V. Ivlev, H. M. Thomas, and G. E. Morfill. First direct measurement of optical phonons in 2d plasma crystals. *Phys. Rev. Lett.*, 103(21):215001, Nov 2009.

[39] L. Couëdel, A. Samarian, M. Mikikian, and L. Boufendi. Dust density effect on complex plasma decay. *Physics Letters A*, 372:5336–5339, 2008.

[40] L. Couëdel, A. A. Samarian, M. Mikikian, and L. Boufendi. Dust charge distribution in complex plasma afterglow. *EPL*, 84(3):35002, nov 2008.

[41] C. S. Cui and J. Goree. Fluctuations of the charge on a dust grain in a plasma. *IEEE Transactions on Plasma Science*, 22(2):151–158, APR 1994.

[42] N. D'Angelo and R. L. Merlino. Current-driven dust-acoustic instability in a collisional plasma. *Planetary and Space Science*, 44(12):1593 – 1598, 1996.

[43] J. E. Daugherty, R. K. Porteous, M. D. Kilgore, and D. B. Graves. Sheath structure around particles in low-pressure discharges. *J. Appl. Phys.*, 72(9):3934–3942, 1992.

[44] Kathleen De Bleecker, Annemie Bogaerts, and Wim Goedheer. Modeling of the formation and transport of nanoparticles in silane plasmas. *Phys. Rev. E*, 70(5):056407, Nov 2004.

[45] R.P. Donovan, editor. *Particle Control for Semiconductor Manufacturing*, New York, NY, USA, 1990 1990. Marcel Dekker. 19-21 April 1988, Research Triangle Park, NC, USA.

[46] K. G. Emeleus and A. C. Breslin. Notes on the effects of dust in positive columns. *International Journal of Electronics*, 29(1):1–18, 1970.

[47] Paul S. Epstein. On the resistance experienced by spheres in their motion through gases. *Phys. Rev.*, 23(6):710–733, Jun 1924.

[48] M A Fink, M Kretschmer, V Fortov, H Hfner, U Konopka, G Morfill, O Petrov, S Ratynskaia, A Usachev, and A Zobnin. Cooperative phenomena in laminar fluids: observation of streamlines. In Laïfa Boufendi, Maxime Mikikian, and P. K. Shukla, editors, *New Vistas in Dusty Plasmas*, volume 799, pages 295–298. AIP, 1 2005.

[49] V. E. Fortov, A. V. Ivlev, S. A. Khrapak, A. G. Khrapak, and G. E. Morfill. Complex (dusty) plasmas: Current status, open issues, perspectives. *Physics Reports*, 421(1-2):1–103, Dec 2005.

[50] V. E. Fortov, A. G. Khrapak, S. A. Khrapak, V. I. Molotkov, A. P. Nefedov, O. F. Petrov, and V. M. Torchinsky. Mechanism of dust–acoustic instability in a direct current glow discharge plasma. *Physics of Plasmas*, 7(5):1374–1380, 2000.

[51] V. E. Fortov, O. F. Petrov, V. I. Molotkov, M. Y. Poustylnik, V. M. Torchinsky, V. N. Naumkin, and A. G. Khrapak. Shock wave formation in a dc glow discharge dusty plasma. *Phys. Rev. E*, 71(3):036413, Mar 2005.

[52] Vladimir E. Fortov, Anatoli P. Nefedov, Vladimir M. Torchinsky, Vladimir I. Molotkov, Oleg F. Petrov, Alex A. Samarian, Andrew M. Lipaev, and Alexei G. Khrapak. Crystalline structures of strongly coupled dusty plasmas in dc glow discharge strata. *Physics Letters A*, 229(5):317 – 322, 1997.

[53] Andrew M. Fraser and Harry L. Swinney. Independent coordinates for strange attractors from mutual information. *Phys. Rev. A*, 33(2):1134–1140, Feb 1986.

[54] M Gadsden and M Taylor. Noctilucent clouds: anywhere, anytime? *Journal of the British Astronomical Association*, vol.113, no.2:77–83, 2003.

[55] J. Goree. Ion trapping by a charged dust grain in a plasma. *Phys. Rev. Lett.*, 69(2):277–280, Jul 1992.

[56] J. Goree, G. E. Morfill, V. N. Tsytovich, and S. V. Vladimirov. Theory of dust voids in plasmas. *Phys. Rev. E*, 59(6):7055–7067, Jun 1999.

[57] P. Grassberger and I. Procaccia. Characterization of strange attractors. *Phys. Rev. Lett.*, 50(5):346–349, 1983.

[58] T. C. Halsey, M. H. Jensen, L. P. Kadanoff, I. Procaccia, and B. I. Shraiman. Fractal measures and their singularities - the characterization of strange sets. *Phys. Rev. A*, 33(2):1141–1151, Feb 1986.

[59] S. Hamaguchi, R. T. Farouki, and D. H. E. Dubin. Triple point of yukawa systems. *Phys. Rev. E*, 56(4):4671–4682, Oct 1997.

[60] O Havnes, C La Hoz, A Biebricher, M Kassa, T Meseret, and L Naesheim. Investigation of the mesospheric pmse conditions by use of the new overshoot effect. *Physica Scripta T*, T107:70–78, 2004.

[61] Yasuaki Hayashi. Structure of a three-dimensional coulomb crystal in a fine-particle plasma. *Phys. Rev. Lett.*, 83(23):4764–4767, Dec 1999.

[62] Yasuaki Hayashi and Kunihide Tachibana. Observation of coulomb-crystal formation from carbon particles grown in a methane plasma. *Jpn. J. Appl. Phys.*, 33:L804–L806, 1994.

[63] G. A. Hebner, M. E. Riley, and B. M. Marder. Dynamic probe of dust wakefield interactions using constrained collisions. *Phys. Rev. E*, 68(1):016403, Jul 2003.

[64] R. Heidemann, S. Zhdanov, R. Sütterlin, H. M. Thomas, and G. E. Morfill. Dissipative dark soliton in a complex plasma. *Phys. Rev. Lett.*, 102(13):135002, 2009.

[65] A. Homann, A. Melzer, S. Peters, R. Mandani, and A. Piel. Laser–excited dust lattice waves in plasma crystals. *Physics Letters A*, 173:1–7, 1998.

[66] A. Homann, A. Melzer, S. Peters, and A. Piel. Determination of the dust screening length by laser-excited lattice waves. *Phys. Rev. E*, 56(6):7138–7141, Dec 1997.

[67] Lu-Jing Hou, You-Nian Wang, and Z. L. Mišković. Induced potential of a dust particle in a collisional radio-frequency sheath. *Phys. Rev. E*, 68(1):016410, Jul 2003.

[68] H. Ikezi. Coulomb solid of small particles in plasmas. *Physics of Fluids*, 29:1764–1766, Mar 1986.

[69] O. Ishihara and S.V. Vladimirov. Wake potential of a dust grain in a plasma with ion flow. *Physics of Plasmas*, 4(1):69, Jan 1997.

[70] Osamu Ishihara. Complex plasma: dusts in plasma. *J. Phys. D: Appl. Phys.*, 40:R121–R147, Apr 2007.

[71] A. V. Ivlev, U. Konopka, and G. Morfill. Influence of charge variation on particle oscillations in the plasma sheath. *Phys. Rev. E*, 62(2):2739–2744, Aug 2000.

[72] A. V. Ivlev, U. Konopka, G. Morfill, and G. Joyce. Melting of monolayer plasma crystals. *Phys. Rev. E*, 68(2):026405, Aug 2003.

[73] A. V. Ivlev and G. Morfill. Anisotropic dust lattice modes. *Phys. Rev. E*, 63(1):016409, Dec 2000.

[74] A. V. Ivlev, G. Morfill, and V. E. Fortov. Acoustic modes in a collisional dusty plasma: Effect of the charge variation. *Physics of Plasmas*, 7(4):1094–1102, 2000.

[75] A. V. Ivlev, G. E. Morfill, and U. Konopka. Coagulation of charged microparticles in neutral gas and charge-induced gel transitions. *Phys. Rev. Lett.*, 89(19):195502, Oct 2002.

[76] A. V. Ivlev, G. E. Morfill, H. M. Thomas, C. Räth, G. Joyce, P. Huber, R. Kompaneets, V. E. Fortov, A. M. Lipaev, V. I. Molotkov, T. Reiter, M. Turin, and P. Vinogradov. First observation of electrorheological plasmas. *Phys. Rev. Lett.*, 100(9), Mar 2008.

[77] A. V. Ivlev, V. Steinberg, R. Kompaneets, H. Höfner, I. Sidorenko, and G. E. Morfill. Non-newtonian viscosity of complex-plasma fluids. *Phys. Rev. Lett.*, 98(14):145003, 2007.

[78] A. V. Ivlev, R. Sütterlin, V. Steinberg, M. Zuzic, and G. Morfill. Nonlinear vertical oscillations of a particle in a sheath of a rf discharge. *Phys. Rev. Lett.*, 85(19):4060–4063, Nov 2000.

[79] A. V. Ivlev, S. K. Zhdanov, H. M. Thomas, and G. E. Morfill. Fluid phase separation in binary complex plasmas. *EPL*, 85(4):45001, feb 2009.

[80] A.V. Ivlev, M. Kretschmer, M. Zuzic, G. E. Morfill, H. Rothermel, H.M. Thomas, V. E. Fortov, V. I. Molotkov, A. P. Nefedov, A.M. Lipaev, O. F. Petrov, Yu.M. Baturin, A. I. Ivanov, and J. Goree. Decharging of complex plasmas: First kinetic observations. *Phys. Rev. Lett.*, 90:055003, 2003.

[81] F. Jamitzky, R. W. Stark, W. Bunk, S. Thalhammer, C. Räth, T. Aschenbrenner, G. E. Morfill, and W. M. Heckl. Scaling-index method as an image processing tool in scanning-probe microscopy. *Ultramicroscopy*, 86(1-2):241–246, Jan 2001. 2nd International Conference on Scanning Probe Microscopy, Sensors, and Nanostructures, Heidelberg, Germany, May 28-31, 2000.

[82] G. Kalman, M. Rosenberg, and H. E. DeWitt. Collective modes in strongly correlated yukawa liquids: Waves in dusty plasmas. *Phys. Rev. Lett.*, 84(26):6030–6033, Jun 2000.

[83] Namjun Kang, Soo ghee Oh, and Andre Ricard. Determination of the electron temperature in a planar inductive argon plasma with emission spectroscopy and electrostatic probe. *J. Phys. D: Appl. Phys.*, 41(15):155203 (6pp), 2008.

[84] P. K. Kaw and A. Sec:. Low frequency modes in strongly coupled dusty plasmas. *Physics of Plasmas*, 5(10):3552–3559, 1998.

[85] R. V Kennedy and J. E. Allen. The floating potential of spherical probes and dust grains. ii: Orbital motion theory. *Journal of Plasma Physics*, 69(6):485–506, 2003.

[86] S. A. Khrapak, M. Chaudhuri, and G. E. Morfill. Ion drag force in collisional plasmas. *IEEE Transactions on Plasma Science*, 37(4):487–493, Apr 2009.

[87] S. A. Khrapak, A. V. Ivlev, G. E. Morfill, and H. M. Thomas. Ion drag force in complex plasmas. *Phys. Rev. E*, 66(4):046414, Oct 2002.

[88] S. A. Khrapak and G. E. Morfill. A note on the binary interaction potential in complex (dusty) plasmas. *Physics of Plasmas*, 15(8), AUG 2008.

[89] S. A. Khrapak, S. V. Ratynskaia, A. V. Zobnin, A. D. Usachev, V. V. Yaroshenko, M. H. Thoma, M. Kretschmer, H. Höfner, G. E. Morfill, O. F. Petrov, and V. E. Fortov. Particle charge in the bulk of gas discharges. *Phys. Rev. E*, 72(1):016406, Jul 2005.

[90] B. A. Klumov, M. Rubin-Zuzic, and G. E. Morfill. Crystallization waves in a dusty plasma. *JETP Letters*, 84(10):542–546, Jan 2007.

[91] R. Kompaneets, G. E. Morfill, and A. V. Ivlev. Design of new binary interaction classes in complex plasmas. *Physics of Plasmas*, 16(4):043705, 2009.

[92] U. Konopka. *Wechselwirkungen geladener Staubteilchen in Hochfrequenzplasmen*. Fakultät für Physik und Astronomie der Ruhr–Universität–Bochum, Bochum, 2000.

[93] U. Konopka, G. E. Morfill, and L. Ratke. Measurement of the interaction potential of microspheres in the sheath of a rf discharge. *Phys. Rev. Lett.*, 84(5):891–894, Jan 2000.

[94] U. Konopka, L. Ratke, and H. M. Thomas. Central collisions of charged dust particles in a plasma. *Phys. Rev. Lett.*, 79(7):1269–1272, Aug 1997.

[95] V Koukouloyannis and I Kourakis. Existence of multisite intrinsic localized modes in one-dimensional debye crystals. *Phys. Rev. E*, 76(1):016402, 2007.

[96] I. Kourakis and P. K. Shukla. Weakly nonlinear vertical dust grain oscillations in dusty plasma crystals in the presence of a magnetic field. *Physics of Plasmas*, 11(7):3665–3671, 2004.

[97] M. Kretschmer, S. A. Khrapak, S. K. Zhdanov, H. M. Thomas, G. E. Morfill, V. E. Fortov, A. M. Lipaev, V. I. Molotkov, A. I. Ivanov, and M. V. Turin. Force field inside the void in complex plasmas under microgravity conditions. *Phys. Rev. E*, 71(5, Part 2), May 2005.

[98] M. Lampe, G. Joyce, and G. Ganguli. Structure and dynamics of dust in streaming plasma: dust molecules, strings, and crystals. *IEEE Transactions on Plasma Science*, 33(1):57–69, Feb 2005.

[99] M. Lampe, G. Joyce, G. Ganguli, and V. Gavrishchaka. Interactions between dust grains in a dusty plasma. *Physics of Plasmas*, 7:3851–3861, 2000.

[100] Martin Lampe. Limits of validity for orbital-motion-limited theory for a small floating collector. *Journal of Plasma Physics*, 65(3):171–180, 2001.

[101] Martin Lampe, Valeriy Gavrishchaka, Gurudas Ganguli, and Glenn Joyce. Effect of trapped ions on shielding of a charged spherical object in a plasma. *Phys. Rev. Lett.*, 86(23):5278–5281, Jun 2001.

[102] Martin Lampe, Rajiv Goswami, Zoltan Sternovsky, Scott Robertson, Valeriy Gavrishchaka, Gurudas Ganguli, and Glenn Joyce. Trapped ion effect on shielding, current flow, and charging of a small object in a plasma. *Physics of Plasmas*, 10:1500, May 2003.

[103] V. Land and W.J. Goedheer. Effect of large-angle scattering, ion flow speed and ion-neutral collisions on dust transport under microgravity conditions. *New Journal of Physics*, 8(1), January 2006.

[104] L. D. Landau. On the vibrations of the electronic plasma. *J. Phys. USSR*, 10:25, 1946.

[105] L.D. Landau and E.M. Lifshitz. *Mechanics*. Pergamon, Oxford, 1960.

[106] Irving Langmuir. Positive ion currents from the positive column of mercury arcs. *Science*, 58(1502):290–291, Oct 1923.

[107] Irving Langmuir. The interaction of electron and positive ion space charges in cathode sheaths. *Phys. Rev.*, 33(6):954–989, Jun 1929.

[108] Irving Langmuir, C. G. Found, and A. F. Dittmer. A new type of electric discharge: the streamer discharge. *Science*, 60(1557):392–394, Oct 1924.

[109] G. Lapenta. Linear theory of plasma wakes. *Phys. Rev. E*, 62:1175–1181, 2000.

[110] G. Lapenta. Nature of the force field in plasma wakes. *Phys. Rev. E*, 66:026409/1–6, 2002.

[111] D. S. Lemons, M. S. Murillo, W. Daughton, and D. Winske. Two-dimensional wake potentials in sub- and supersonic dusty plasmas. *Physics of Plasmas*, 7:2306–2313, 2000.

[112] F. Melandsø. Lattice waves in dust plasma crystals. *Physics of Plasmas*, 3(11):3890–3901, 1996.

[113] F. Melandsø, T. Aslaksen, and O. Havnes. A kinetic model for the dust-acoustic waves applied to planetary rings. *J. Geophys. Res.*, 98(A8):13315–13323, 1993.

[114] F. Melandsø, T. Aslaksen, and O. Havnes. A new damping effect for the dust–acoustic wave. *Planetary and Space Science*, 41(4):321–325, 1993.

[115] F. Melandsø and J. Goree. Polarized supersonic plasma flow simulation for charged bodies such as dust particles and spacecraft. *Phys. Rev. E*, 52(5):5312–5326, Nov 1995.

[116] A. Melzer, V. A. Schweigert, and A. Piel. Transition from attractive to repulsive forces between dust molecules in a plasma sheath. *Phys. Rev. Lett.*, 83(16):3194–3197, Oct 1999.

[117] A. Melzer, T. Trottenberg, and A. Piel. Experimental determination of the charge on dust particles forming coulomb lattices. *Physics Letters A*, 191:301–308, 1994.

[118] Robert L. Merlino. Dust-acoustic waves driven by an ion-dust streaming instability in laboratory discharge dusty plasma experiments. *Physics of Plasmas*, 16(12):124501, 2009.

[119] M. Mikikian, L. Boufendi, and A. Bouchoule. Spectroscopic analysis and instabilities observation during dust particle growth. In R. Koch and S. Lebedev, editors, *30th EPS Conf. on Contr. Fusion and Plasma Phys.*, volume 27A, pages 0–3.1B, 2003.

[120] M. Mikikian, L. Boufendi, A. Bouchoule, H. M. Thomas, G. E. Morfill, A. P. Nefedov, V. E. Fortov, and the PKE-Nefedov team. Formation and behaviour of dust particle clouds in a radio-frequency discharge: results in the laboratory and under microgravity conditions. *New Journal of Physics*, 5:19.1, 2003.

[121] M. Mikikian, M. Cavarroc, and L. Boufendi. Dust Growth Instabilities in a Dense Cloud of Particles. In L. Boufendi, M. Mikikian, and P. K. Shukla, editors, *New Vistas in Dusty Plasmas*, volume 799, pages 319–322. AIP, October 2005.

[122] M. Mikikian, M. Cavarroc, N. Chaumeix, and L. Boufendi. Instabilities in a dense cloud of grown dust particles. In P. Norreys and H. Hutchinson, editors, *Proceedings of the 31st EPS Conference on Plasma Physics*, volume 28G of ECA, pages 0–2.13, 2004.

[123] M. Mikikian, M. Cavarroc, N. Chaumeix, and L. Boufendi. Instabilities of the void region in a dense cloud of grown dust particles. In Laïfa Boufendi, Maxime Mikikian, and P. K. Shukla, editors, *New Vistas in Dusty Plasmas*, volume 799. AIP, 2005.

[124] M. Mikikian, L. Couëdel, M. Cavarroc, Y. Tessier, and L. Boufendi. Self-excited void instability in dusty plasmas: plasma and dust cloud dynamics during the heartbeat instability. *New Journal of Physics*, 9(8):268, 2007.

[125] Maxime Mikikian and Laïfa Boufendi. Experimental investigations of void dynamics in a dusty discharge. *Physics of Plasmas*, 11(8):3733, 2004.

[126] W. Miloch, J. Trulsen, and H. Pecseli. Numerical studies of ion focusing behind macroscopic obstacles in a supersonic plasma flow. *Phys. Rev. E*, 77(5):056408, 2008.

[127] C. J. Mitchell, M. Horányi, O. Havnes, and C. C. Porco. Saturn's spokes: Lost and found. *Science*, 311(5767):1587–1589, Jul 2006.

[128] S. Mitic, B. A. Klumov, M. Y. Pustylnik, and G. E. Morfill. Determination of electron temperature in low-pressure plasmas by means of optical emission spectroscopy. *Pis'ma v ZhETF*, 91:249–253, March 2010.

[129] S. Mitic, M. Y. Pustylnik, and G. E. Morfill. Spectroscopic evaluation of the effect of the microparticles on radiofrequency argon plasma. *New Journal of Physics*, 11, AUG 19 2009.

[130] V. I. Molotkov, A. P. Nefedov, and V. M. Torchinsky. Dust acoustic waves in a dc glow–discharge plasma. *JETP*, 89(3):477, 1999.

[131] R. A. Monetti, H. Böhm, D. Müller, E. Rummeny, T. Link, and C. Räth. Structural analysis of human proximal femur for the prediction of biomechanical strength 'in vitro'. the locally adapted scaling vector method. In Fitzpatrick, J. M. and Reinhardt, J. M., editor, *Medical Imaging 2005: Image Processing*, volume 5747 of *Proceedings*

of SPIE, pages 231–239, 1000 20th St, PO Box 10, Bellingham, WA 98227-0010 USA, 2005. SPIE, SPIE-Int Soc Optical Engineering. Medical Imaging 2005 Conference, San Diego, CA, Feb 15-17, 2005.

[132] R. A. Monetti, H. Böhm, D. Müller, E. Rummeny, T. M. Link, and C. Räth. Assessing the biomechanical strength of trabecular bone in vitro using 3d anisotropic non-linear texture measures: The scaling vector method. In Fitzpatrick, J. M. and Sonka, M., editor, *Medical Imaging 2004: Image Processing*, volume 5370 of *Proceedings of SPIE*, pages 215–224, 1000 20th St, PO Box 10, Bellingham, WA 98227-0010 USA, 2004. SPIE; Amer Assoc Phys Med; Amer Physiol Soc; Ctr Devices & Radiol Hlth; Soc Imaging Sci & Technol; Natl Elect Mfg Assoc, Diagnost Imaging & Therapy Syst Div; Radiol Soc N Amer; Soc Comp Applicat Radiol, SPIE-Int Soc Optical Engineering. Medical Imaging 2004 Conference, San Diego, CA, Feb 17-19, 2004.

[133] G. Morfill, V. Fortov, L. Boufendi, and N. Brenning. The plasma state of soft matter. *Europhysics News*, 39(3):30–32, may 2008.

[134] G. E. Morfill, S. A. Khrapak, A. V. Ivlev, B. A. Klumov, M. Rubin-Zuzic, and H. M. Thomas. From fluid flows to crystallization: new results from complex plasmas. *Physica Scripta T*, 107:59–64, 2004.

[135] G. E. Morfill, M. G. Kong, and J. L. Zimmermann. Focus on plasma medicine. *New Journal of Physics*, 11:115011, Nov 2009.

[136] G. E. Morfill, H. M. Thomas, U. Konopka, H. Rothermel, M. Zuzic, A. Ivlev, and J. Goree. Condensed plasmas under microgravity. *Phys. Rev. Lett.*, 83(8):1598–1601, Aug 1999.

[137] G. E. Morfill, H. M. Thomas, U. Konopka, and M. Zuzic. The plasma condensation: Liquid and crystalline plasmas. *Physics of Plasmas*, 6:1769–1780, 1999.

[138] Gregor E. Morfill and Alexei V. Ivlev. Complex plasmas: An interdisciplinary research field. *Reviews of Modern Physics*, 81(4):1353, 2009.

[139] Gregor E. Morfill, Uwe Konopka, Michael Kretschmer, Milenko Rubin-Zuzic, Hubertus M. Thomas, Sergej K. Zhdanov, and Vadim Tsytovich. The 'classical tunnelling effect' - observations and theory. *New Journal of Physics*, 8:7, 2006.

[140] Gregor E. Morfill, Milenko Rubin-Zuzic, Hermann Rothermel, Alexei V. Ivlev, Boris A. Klumov, Hubertus M. Thomas, Uwe Konopka, and Victor Steinberg. Highly resolved fluid flows: "liquid plasmas" at the kinetic level. *Phys. Rev. Lett.*, 92(17):175004, Apr 2004.

[141] H. M. Mott-Smith and Irving Langmuir. The theory of collectors in gaseous discharges. *Phys. Rev.*, 28(4):727–763, Oct 1926.

[142] A.H. Nayfeh and D.T. Mook. *Nonlinear Oscillation*. Wiley, New York, 1979.

[143] Anatoli P. Nefedov, Gregor E. Morfill, Vladimir E. Fortov, Hubertus M. Thomas, Hermann Rothermel, Tanja Hagl, Alexei V. Ivlev, Milenko Zuzic, Boris A. Klumov, Andrey M. Lipaev, Vladimir I. Molotkov, Oleg F. Petrov, Yuri P. Gidzenko, Sergey K. Krikalev, William Shepherd, Alexandr I. Ivanov, Maria Roth, Horst Binnenbruck, John A. Goree, and Yuri P. Semenov. Pke-nefedov: plasma crystal experiments on the international space station. *New Journal of Physics*, 5:33, 2003.

[144] S. Nunomura, J. Goree, S. Hu, X. Wang, and A. Bhattacharjee. Dispersion relations of longitudinal and transverse waves in two-dimensional screened coulomb crystals. *Phys. Rev. E*, 65(6):066402, Jun 2002.

[145] S. Nunomura, T. Misawa, N. Ohno, and S. Takamura. Instability of dust particles in a coulomb crystal due to delayed charging. *Phys. Rev. Lett.*, 83(10):1970–1973, Sep 1999.

[146] H. Ohta and S. Hamaguchi. Wave dispersion relations in yukawa fluids. *Phys. Rev. Lett.*, 84(26):6026–6029, Jun 2000.

[147] R. Ozaki, G. Uchida, S. Iizuka, and N. Sato. Vertical string structure of fine particles in a magnetized DC plasma. In Y. Nakamura, T. Yokota, & P. K. Shukla, editor, *Frontiers in Dusty Plasmas*, pages 457–+, 2000.

[148] Jr. P. J. Hargis, K. E. Greenberg, P. A. Miller, J. B. Gerardo, J. R. Torczynski, M. E. Riley, G. A. Hebner, J. R. Roberts, J. K. Olthoff, J. R. Whetstone, R. J. Van Brunt, M. A. Sobolewski, H. M. Anderson, M. P. Splichal, J. L. Mock, P. Bletzinger, A. Garscadden, R. A. Gottscho, G. Selwyn, M. Dalvie, J. E. Heidenreich, Jeffery W. Butterbaugh, M. L. Brake, M. L. Passow, J. Pender, A. Lujan, M. E. Elta, D. B. Graves, H. H. Sawin, M. J. Kushner, J. T. Verdeyen, R. Horwath, and T. R. Turner. The gaseous electronics conference radio-frequency reference cell: A defined parallel-plate radio-frequency system for experimental and theoretical studies of plasma-processing discharges. *Review of Scientific Instruments*, 65(1):140–154, 1994.

[149] G. Paladin and A. Vulpiani. Anomalous scaling laws in multifractal objects. *Phys. Rep.-Rev. Sec. Phys. Lett.*, 156(4):147–225, Dec 1987.

[150] S. Park, C. R. Seon, and W. Choe. Role of particle size and gas pressure on the nonlinear oscillatory behavior of a dust particle in a direct current discharge. *Physics of Plasmas*, 11(11):5095–5101, 2004.

[151] J. B. Pieper and J. Goree. Dispersion of plasma dust acoustic waves in the strong-coupling regime. *Phys. Rev. Lett.*, 77(15):3137–3140, Oct 1996.

[152] A. Yu. Pigarov, R. D. Smirnov, S. I. Krasheninnikov, T. D. Rognlien, M. Rosenberg, and T. K. Soboleva. Transport of dust particles in tokamak devices. *Journal of Nuclear Materials*, 363-365:216 – 221, 2007. Plasma-Surface Interactions-17.

[153] R. Pompl. *Quantitative Bildverarbeitung und ihre Anwendung auf melanozytäre Hautveränderungen*. Institut für Informatik der Technischen Universität München, München, 2000.

[154] B. Poppe. *Einführung gewichteter struktureller Komplexitätsmaße zur Analyse verrauschter Signale und deren Anwendung in der medizinischen Bildverarbeitung*. GCA-Verlag, Herdecke, 2001.

[155] G. Praburam and J. Goree. Experimental observation of very low-frequency macroscopic modes in a dusty plasma. *Physics of Plasmas*, 3(4):1212–1219, 1996.

[156] I. Prigogine. *From Begin To Becoming*. Freeman, San Francisco, 1980.

[157] P. N. Pusey. *Liquids, Freezing and the Glass Transition*. North Holland, Amsterdam, 1991.

[158] N. N. Rao, P. K. Shukla, and M. Y. Yu. Dust–acoustic waves in dusty plasmas. *Planetary and Space Science*, 38:543–546, 1990.

[159] C. Räth, W. Bunk, M. B. Huber, G. E. Morfill, J. Retzlaff, and P. Schücker. Analysing large-scale structure - I. Weighted scaling indices and constrained randomization. *Mon. Not. Roy. Astron. Soc.*, 337(2):413–421, Dec 2002.

[160] C. Räth and G. Morfill. Texture detection and texture discrimination with anisotropic scaling indices. *J. Opt. Soc. Am. A-Opt. Image Sci. Vis.*, 14(12):3208–3215, Dec 1997.

[161] C. W. Räth, D. Müller, H. F. Böhm, E. J. Rummeny, T. M. Link, and R. Monetti. Improving the textural characterization of trabecular bone structure to quantify its changes: the locally adapted scaling vector method. In Fitzpatrick, J. M. and Reinhardt, J. M., editor, *Medical Imaging 2005: Image Processing*, volume 5747 of *Proceedings of SPIE*, pages 240–248, 1000 20th St, PO Box 10, Bellingham, WA 98227-0010 USA, 2005. SPIE, SPIE-Int Soc Optical Engineering. Medical Imaging 2005 Conference, San Diego, CA, Feb 15-17, 2005.

[162] S. Ratynskaia, S. Khrapak, A. Zobnin, M. H. Thoma, M. Kretschmer, A. Usachev, V. Yaroshenko, R. A. Quinn, G. E. Morfill, O. Petrov, and V. Fortov. Experimental determination of dust-particle charge in a discharge plasma at elevated pressures. *Phys. Rev. Lett.*, 93(8):085001, Aug 2004.

[163] D. P. Resendes, J. T. Mendona, and P. K. Shukla. Formation of dusty plasma molecules. *Physics Letters A*, 239(3):181 – 186, 1998.

[164] M. Rex and H. Löwen. Lane formation in oppositely charged colloids driven by an electric field: Chaining and two-dimensional crystallization. *Phys. Rev. E*, 75(5):051402, May 2007.

[165] S. Robertson, M. Horányi, S. Knappmiller, Z. Sternovsky, R. Holzworth, and M. Shimogawa. Mass analysis of charged aerosol particles in nlc and pmse during the ecoma/mass campaign. *Annales geophysicae*, 27(3):1213–1232, 2009.

[166] M. Rosenberg. Ion– and dust–acoustic instabilities in dusty plasmas. *Planetary and Space Science*, 41(3):229–233, 1993.

[167] H. Rothermel, T. Hagl, G. E. Morfill, M. H. Thoma, and H. M. Thomas. Gravity compensation in complex plasmas by application of a temperature gradient. *Phys. Rev. Lett.*, 89(17):175001, Oct 2002.

[168] M. Rubin-Zuzic, G. E. Morfill, A. V. Ivlev, R. Pompl, B. A. Klumov, W. Bunk, H. M. Thomas, H. Rothermel, O. Havnes, and A. Fouquet. Kinetic development of crystallization fronts in complex plasmas. *Nature Physics*, 2(3):181–185, Mar 2000.

[169] A. Samarian, S. Vladimirov, and B. James. Wake-induced symmetry-breaking of dust particle arrangements in a complex plasma. *JETP Letters*, 82(12):758–762, 2005.

[170] D. Samsonov and J. Goree. Instabilities in a dusty plasma with ion drag and ionization. *Phys. Rev. E*, 59(1):1047–1058, Jan 1999.

[171] D. Samsonov and J. Goree. Particle growth in a sputtering discharge. *J. Vac. Sci. Technol. A-Vac. Surf. Films*, 17(5):2835–2840, SEP-OCT 1999.

[172] D. Samsonov, A. V. Ivlev, R. A. Quinn, G. Morfill, and S. Zhdanov. Dissipative longitudinal solitons in a two-dimensional strongly coupled complex (dusty) plasma. *Phys. Rev. Lett.*, 88(9):095004, Feb 2002.

[173] D. Samsonov, S. Zhdanov, and G. Morfill. Vertical wave packets observed in a crystallized hexagonal monolayer complex plasma. *Phys. Rev. E*, 71(2):026410, Feb 2005.

[174] J. R. Sanmarti and S. H. Lam. Far-wake structure in rarefield plasma flows past charged bodies. *Physics of Fluids*, 14(1):62, 1971.

[175] T. Sauer, J. A. Yorke, and M. Casdagli. Embedology. *J. Stat. Phys.*, 65(3-4):579–616, Nov 1991.

[176] H. Schollmeyer, A. Melzer, A. Homann, and A. Piel. Dust–dust and dust-plasma interactions of monolayer plasma crystals. *Physics of Plasmas*, 6(7):2693–2698, 1999.

[177] Walter Schottky. *Physikalische Zeitschrift*, 25:342, 1924.

[178] Thomas Schreiber and Andreas Schmitz. Improved surrogate data for nonlinearity tests. *Phys. Rev. Lett.*, 77(4):635–638, Jul 1996.

[179] M. Schwabe, M. Rubin-Zuzic, S. Zhdanov, H. M. Thomas, and G. E. Morfill. Highly resolved self-excited density waves in a complex plasma. *Phys. Rev. Lett.*, 99(9):095002, 2007.

[180] Mierk Schwabe, Sergey K. Zhdanov, Hubertus M. Thomas, Alexei V. Ivlev, Milenko Rubin-Zuzic, Gregor E. Morfill, Vladimir I. Molotkov, Andrey M. Lipaev, Vladimir E. Fortov, and Thomas Reiter. Nonlinear waves externally excited in a complex plasma under microgravity conditions. *New Journal of Physics*, 10(3):033037, 2008.

[181] I. V. Schweigert, V. A. Schweigert, V. M. Bedanov, A. Melzer, A. Homann, and A. Piel. Instability and melting of a crystal of microscopic particles in a radio–frequency discharge plasma. *JETP*, 87:905, 1998.

[182] V. A. Schweigert, I. V. Schweigert, A. Melzer, A. Homann, and A. Piel. Alignment and instability of dust crystals in plasmas. *Phys. Rev. E*, 54(4):4155–4166, Oct 1996.

[183] G. S. Selwyn, J. Singh, and R. S. Bennett. Insitu laser diagnostic studies of plasma-generated particulate contamination. *J. Vac. Sci. Technol. A-Vac. Surf. Films*, 7(4):2758–2765, Jul-Aug 1989.

[184] C. R. Seon, S. Park, W. Choe, C. H. Seo, H. Y. Park, K. B. Chai, and Y. H. Shin. Electron temperature and pressure dependences of nonlinear phenomena in dust particle oscillation in dc plasmas. *New Journal of Physics*, 10(1):013025 (12pp), 2008.

[185] R. D. Smirnov, A. Yu. Pigarov, M. Rosenberg, S. I. Krasheninnikov, and D. A. Mendis. Modelling of dynamics and transport of carbon dust particles in tokamaks. *Plasma Physics and Controlled Fusion*, 49(4):347, 2007.

[186] G. Sorasio, D. Resendes, and P. Shukla. Induced oscillations of dust grains in a plasma sheath under low pressures. *Physics Letters A*, 293(1-2):67–73, 2002.

[187] Lyman Spitzer. *Physical processes in the interstellar medium.* Wiley-Interscience, New York, 1978.

[188] V. Steinberg, R. Sütterlin, A. V. Ivlev, and G. Morfill. Vertical pairing of identical particles suspended in the plasma sheath. *Phys. Rev. Lett.*, 86(20):4540–4543, May 2001.

[189] E. Stoffels, W. W. Stoffels, G. M. W. Kroesen, and F. J. deHoog. Dust formation and charging in an Ar/SiH4 radio-frequency discharge. *J. Vac. Sci. Technol. A-Vac. Surf. Films*, 14(2):556–561, Mar-Apr 1996. Dusty Plasmas-95 Workshop on Generation, Transport, and Removal of Particles in Plasmas, Wickenburg, AZ, Oct 01-07, 1995.

[190] K. R. Sütterlin, H. M. Thomas, A. V. Ivlev, G. E. Morfill, V. E. Fortov, A. M. Lipaev, V. I. Molotkov, O. F. Petrov, A. Wysocki, and H. Löwen. Lane formation in driven

binary complex plasmas on the international space station. *IEEE Transactions on Plasma Science*, 99:1–8, Dec 2009.

[191] K. R. Sütterlin, A. Wysocki, A. V. Ivlev, C. Räth, H. M. Thomas, M. Rubin-Zuzic, W. J. Goedheer, V. E. Fortov, A. M. Lipaev, V. I. Molotkov, O. F. Petrov, G. E. Morfill, and H. Löwen. Dynamics of lane formation in driven binary complex plasmas. *Phys. Rev. Lett.*, 102(8):085003, Feb 2009.

[192] K. R. Sütterlin, A. Wysocki, A. V. Ivlev, C. Räth, H. M. Thomas, M. Rubin-Zuzic, W. J. Goedheer, V. E. Fortov, A. M. Lipaev, V. I. Molotkov, O. F. Petrov, G. E. Morfill, and H. Löwen. Erratum: Dynamics of lane formation in driven binary complex plasmas [phys. rev. lett. 102, 085003 (2009)]. *Phys. Rev. Lett.*, 102(14):149901, Apr 2009.

[193] Kazuo Takahashi, Tomoko Oishi, Ken-ichi Shimomai, Yasuaki Hayashi, and Shigehiro Nishino. Analyses of attractive forces between particles in coulomb crystal of dusty plasmas by optical manipulations. *Phys. Rev. E*, 58(6):7805–7811, Dec 1998.

[194] R. J. Taylor, K. R. MacKenzie, and H. Ikezi. A large double plasma device for plasma beam and wave studies. *Rev. Sci. Instrum.*, 43:1675, Aug 1972.

[195] H. Thomas and G. E. Morfill. Melting dynamics of a plasma crystal. *Nature*, 379(6568):806–809, Feb 1996.

[196] H. Thomas, G. E. Morfill, V. Demmel, J. Goree, B. Feuerbacher, and D. Möhlmann. Plasma crystal: Coulomb crystallization in a dusty plasma. *Phys. Rev. Lett.*, 73(5):652–655, Aug 1994.

[197] H. M. Thomas, G. E. Morfill, V. E. Fortov, A. V. Ivlev, V. I. Molotkov, A. M. Lipaev, T. Hagl, H. Rothermel, S. A. Khrapak, R. K. Suetterlin, M. Rubin-Zuzic, O. F. Petrov, V. I. Tokarev, and S. K. Krikalev. Complex plasma laboratory PK-3 Plus on the International Space Station. *New Journal of Physics*, 10(3):033036 (14pp), 2008.

[198] C. Thompson, A. Barkan, N. D'Angelo, and R. L. Merlino. Dust acoustic waves in a direct current glow discharge. *Physics of Plasmas*, 4(7):2331–2335, 1997.

[199] C. M. Ticos, P. W. Smith, and P. K. Shukla. Experimental wake-induced oscillations of dust particles in a rf plasma. *Physics Letters A*, 319(5-6):504 – 509, 2003.

[200] Lewi Tonks and Irving Langmuir. A general theory of the plasma of an arc. *Phys. Rev.*, 34(6):876–922, Sep 1929.

[201] Lewi Tonks and Irving Langmuir. Oscillations in ionized gases. *Phys. Rev.*, 33(2):195–210, Feb 1929.

[202] A. Usachev, A. Zobnin, O. Petrov, V. Fortov, M. Thoma, M. Kretschmer, S. Ratynskaia, R. Quinn, H. Höfner, and G. Morfill. The project "Plasmakristall-4" (PK-4) - a dusty plasma experiment in a combined dc/rf discharge plasma under microgravity conditions. *Czechoslovak Journal of Physics*, 54(Part 4):C639–C647, 2004. 21st Symposium on Plasma Physics and Technology, Prague, Czech Republic, Jun 14-17, 2004.

[203] O. S. Vaulina, S. A. Khrapak, A. P. Nefedov, and O. F. Petrov. Charge-fluctuation-induced heating of dust particles in a plasma. *Phys. Rev. E*, 60(5):5959, 1999.

[204] S. V. Vladimirov and A. A. Samarian. Stability of particle arrangements in a complex plasma. *Phys. Rev. E*, 65(4):046416, Apr 2002.

[205] S. V. Vladimirov, V. N. Tsytovich, and G. E. Morfill. Stability of dust voids. *Physics of Plasmas*, 12:052117, 2005.

[206] C. L. Wang, G. Joyce, and D. R. Nicholson. Debye shielding of a moving test charge in plasma. *Journal of Plasma Physics*, 25(APR):225–231, 1981.

[207] Xiaogang Wang, A. Bhattacharjee, and S. Hu. Longitudinal and transverse waves in yukawa crystals. *Phys. Rev. Lett.*, 86(12):2569–2572, Mar 2001.

[208] You-Nian Wang, Lu-Jing Hou, and Xiaogang Wang. Self-consistent nonlinear resonance and hysteresis of a charged microparticle in a rf sheath. *Phys. Rev. Lett.*, 89(15):155001, Sep 2002.

[209] Y. Watanabe. Formation and behaviour of nano/micro-particles in low pressure plasmas. *J. Phys. D: Appl. Phys.*, 39(19):R329–R361, Oct 2006.

[210] D. Winske. Nonlinear wake potential in a dusty plasma. *IEEE Transactions on Plasma Science*, 29:191–197, 2001.

[211] M. Wolter, M. Haass, T. Ockenga, J. Blazec, R. Basner, and H. Kersten. Micro-Particles as Electrostatic Probes for Plasma Sheath Diagnostic. In J. Tito & P. K. Shukla, editor, *American Institute of Physics Conference Series*, volume 1041 of *American Institute of Physics Conference Series*, pages 259–260, September 2008.

[212] A. Wysocki and H. Löwen. Instability of a fluid-fluid interface in driven colloidal mixtures. *Journal of Physics: Condensed Matter*, 16(41):7209–7224, 2004.

[213] V. Yaroshenko, H. Thomas, and G. Morfill. The 'dipole instability' in complex plasmas and its role in plasma crystal melting. *New Journal of Physics*, 8, 2006.

[214] V. V. Yaroshenko, M. H. Thoma, H. M. Thomas, and G. E. Morfill. Double layer formation at the interface of complex plasmas. *Physics of Plasmas*, 15(8):082104, 2008.

[215] C. Zafiu, A. Melzer, and A. Piel. Nonlinear resonances of particles in a dusty plasma sheath. *Phys. Rev. E*, 63(6):066403, May 2001.

[216] Z. Zakrzewski and T. Kopiczynski. Effect of collisions on positive ion collection by a cylindrical langmuir probe. *Plasma Physics*, 16:1195–1198, 1974.

[217] S. Zhdanov, R. Heidemann, M. H. Thoma, R. Sütterlin, H. M. Thomas, H. Höfner, K. Tarantik, G. E. Morfill, A. D. Usachev, O. F. Petrov, and V. E. Fortov. Dissipative dark solitons in a dc complex plasma. *EPL*, 89(2):25001, 2010.

[218] S. Zhdanov, A. Ivlev, and G. Morfill. Mode-coupling instability of two-dimensional plasma crystals. *Physics of Plasmas*, 16(8):083706, 2009.

[219] S. Zhdanov, R. A. Quinn, D. Samsonov, and G. E. Morfill. Large-scale steady-state structure of a 2d plasma crystal. *New Journal of Physics*, 5:74, 2003.

[220] Sergey Zhdanov, Mierk Schwabe, Ralf Heidemann, R. Sütterlin, H. M. Thomas, Milenko Rubin-Zuzic, Hermann Rothermel, Tanja Hagl, Alexei V. Ivlev, Gregor Morfill, V. I. Molotkov, Andrey M. Lipaev, Oleg F. Petrov, Vladimir E. Fortov, and Thomas Reiter. Auto-oscillations in complex plasmas. *New Journal of Physics*, March 2010.

[221] A. V. Zobnin, A. P. Nefedov, V. A. Sinelshchikov, and V. E. Fortov. On the charge of dust particles in a low-pressure gas discharge plasma. *JETP*, 91:483–487, 2000.

[222] M. Zuzic, A. V. Ivlev, J. Goree, G. E. Morfill, H. M. Thomas, H. Rothermel, U. Konopka, R. Sütterlin, and D. D. Goldbeck. Three-dimensional strongly coupled plasma crystal under gravity conditions. *Phys. Rev. Lett.*, 85(19):4064–4067, Nov 2000.

[223] M. Zuzic, H. M. Thomas, and G. E. Morfill. Wave propagation and damping in plasma crystals. *J. Vac. Sci. Technol. A*, 14(2):496–500, Mar 1996.

Nonlinear Vertical Oscillations of a Particle in a Sheath of a rf Discharge

A. V. Ivlev,* R. Sütterlin, V. Steinberg,† M. Zuzic, and G. Morfill
Max-Planck-Institut für Extraterrestrische Physik, D-85740 Garching, Germany
(Received 30 March 2000)

A new simple method to measure the spatial distribution of the electric field in the plasma sheath is proposed. The method is based on the experimental investigation of vertical oscillations of a single particle in the sheath of a low-pressure radio-frequency discharge. It is shown that the oscillations become strongly nonlinear as the amplitude increases. The theory of anharmonic oscillations provides a good quantitative description of the data and gives estimates for the first two anharmonic terms in an expansion of the sheath potential around the particle equilibrium.

PACS numbers: 52.25.Zb, 52.25.Gj, 52.35.–g, 52.80.Pi

There are various experimental methods on the plasma sheath diagnostic in low-pressure gas discharges (see, e.g., [1–3], and references therein). Most of the methods are based on optical emission spectroscopy and temporally resolved probe measurements and are rather complicated technically. We propose an "alternative" simple method to measure the spatial distribution of the electric field in the plasma sheath based on investigation of "large-amplitude" vertical oscillations of micron sized particles.

So far, investigation of the particle oscillations in the sheath of a radio-frequency (rf) discharge was one of the methods used to determine the particle charge [4,5]. This method is based on the assumption that the vertical distribution of the sheath potential can be approximated by a parabolic profile [6], so that the oscillations are always harmonic. This assumption is reasonable for sufficiently high gas pressure, when the mean free path of ions is much less than the vertical spatial scale of the sheath field [6]: For example, the model of a parabolic rf sheath in an argon plasma can be applied for pressures above $\simeq 20$ Pa. But for $p \lesssim 10$ Pa the sheath profile might deviate strongly from a parabolic one. In this case, the oscillations are harmonic only if their amplitude is very small.

In this Letter, we report experimental and theoretical investigations of nonlinear (large-amplitude) vertical oscillations of a single particle in the sheath of a low-pressure rf discharge. Comparing the experimental results to the theory of anharmonic oscillations we estimate the first two anharmonic terms in an expansion of the sheath potential around the particle equilibrium height. This allows us to reconstruct the distribution of the vertical electric field in the wide region of the sheath.

Experimental setup and results.—The experiments are performed in a so-called Gaseous Electronic Conference rf reference cell [7] with the electrode system modified as shown in Fig. 1. The lower aluminum electrode, 230 mm in diameter, is capacitively coupled to a rf generator providing a peak-to-peak voltage $\simeq 70$ V (rf power $\simeq 2$ W). A ring-shaped upper grounded electrode with an outer diameter of 200 mm and a thickness of 10 mm is located 50 mm above the lower electrode. A 2 mm thick copper ring with a 40 mm inner diameter is placed on the lower electrode to confine the particle above the center. Argon gas at a pressure of 0.5 Pa is used for the discharge. For this pressure, a self-bias voltage $\simeq -33$ V on the lower electrode provides the sheath with a (visible) thickness of $\simeq 20$ mm and causes a spherical polystyrene particle (density 1.05 g/cm^3, diameter 7.6 ± 0.1 μm) to levitate $\simeq 14$ mm above the electrode.

At a height 8 mm above the lower electrode a horizontal wire of 0.5 mm diameter and 80 mm length is placed directly below the levitated particle. A low-frequency sinusoidal voltage of amplitude U_{ex} is applied to this wire to excite the vertical oscillations of the particle. The frequency $\omega/2\pi$ of the voltage was varied from 0.1 up to 40 Hz and back in 0.1 Hz steps. To determine the oscillation amplitude, we illuminated the particle with a vertical laser sheet of $\simeq 140$ μm thickness and imaged it from the side by an external digital charge-coupled device camera (maximum field rate is 50 fields/s; resolution is 768×576 pixels).

For small excitation voltage ($U_{ex} \lesssim 30$ mV), we observed the usual linear (harmonic) oscillations: The amplitude has a single symmetric narrow maximum at the resonance frequency $\omega_0/2\pi \simeq 17.0$ Hz (primary resonance). However, for larger U_{ex} the dependence clearly exhibits nonlinearity (see, e.g., [8]). Compare Figs. 2(a) and 2(b) for $U_{ex} = 100$ and 200 mV: When ω increases [Fig. 2(a)], the amplitude grows continuously until a certain frequency (ω_+) is reached; then it "jumps"

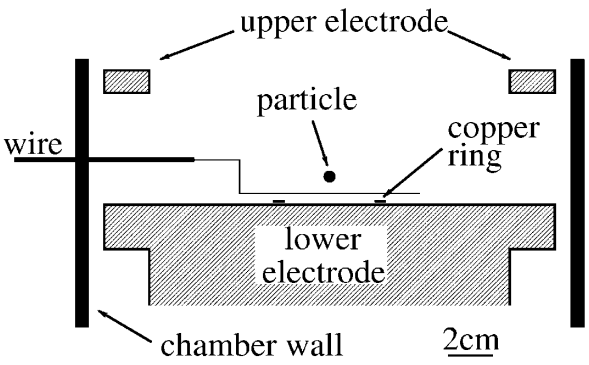

FIG. 1. Experimental setup.

 0031-9007/00/85(19)/4060(4)$15.00

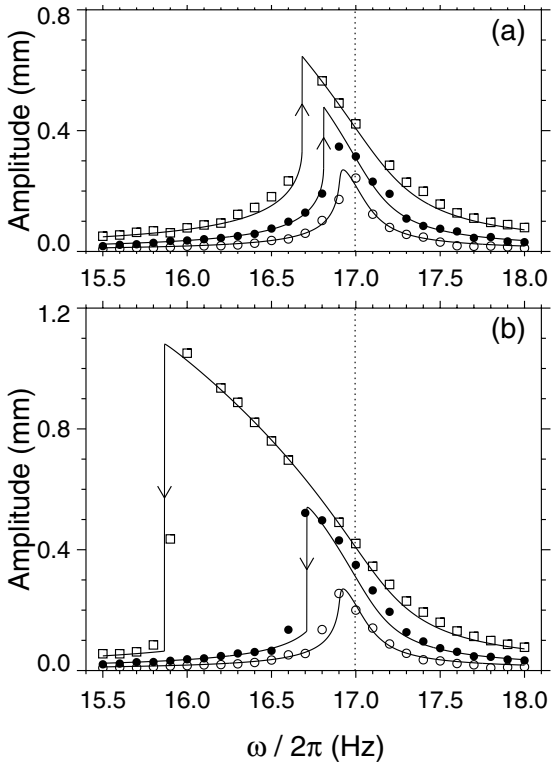

FIG. 2. Variation of the amplitude of particle oscillations close to the primary resonance for increasing (a) and decreasing (b) frequency of excitation, ω, and for different magnitudes of the excitation voltage U_{ex}: 50 mV (open circles), 100 mV (closed circles), and 200 mV (squares). Solid lines show the least-squares fit of the points using Eq. (4) for a. The vertical dotted line indicates the position of the resonance frequency, ω_0, obtained from the fit.

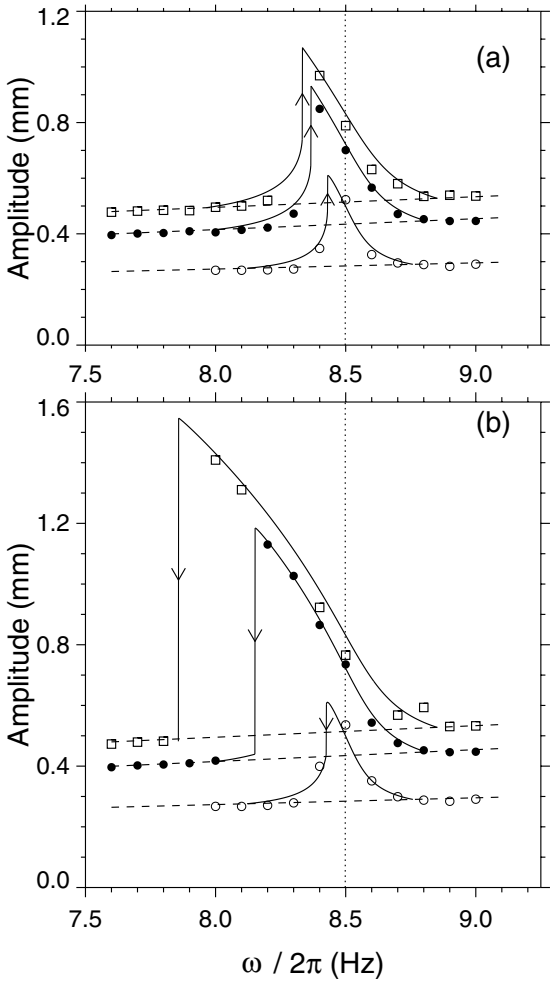

FIG. 3. Variation of the amplitude of particle oscillations close to the superharmonic resonance for increasing (a) and decreasing (b) frequency of excitation, ω, and for different magnitudes of the excitation voltage U_{ex}: 4 V (open circles), 6 V (closed circles), and 7 V (squares). Solid lines show the least-squares fit of the points using Eq. (6) for a_2. The tilted dashed lines represent the linear amplitude offset a_1. The vertical dotted line indicates the position of the half resonance frequency, $\frac{1}{2}\omega_0$, obtained from the fit.

upward and thereafter decreases monotonically as ω is further increased. On the "way back" [Fig. 2(b)], the amplitude grows continuously until another frequency (ω_-) is reached. Then it spontaneously jumps downward and continues to decrease as ω is reduced further. We found that ω_+ is always larger than ω_-. Outside this "hysteresis zone," the experimental points obtained for increasing and decreasing frequencies practically overlap. The shift of the maximum, as well as the width of the hysteresis zone rapidly increases with U_{ex}.

Another peculiarity of the oscillations is the secondary resonances—two maxima at $\omega \simeq \frac{1}{2}\omega_0$ and $\omega \simeq 2\omega_0$, which are observed for sufficiently high U_{ex}. Figure 3 shows the peak in the vicinity $\omega \simeq \frac{1}{2}\omega_0$ (superharmonic resonance) for different values of U_{ex}. There is a finite offset with some slope (marked by the dashed line), which represents the low-frequency tail of the primary resonance. The shape of the peaks resembles that of the primary resonance. In contrast, for the subharmonic resonance at $\omega \simeq 2\omega_0$ (Fig. 4) the behavior is qualitatively different. When U_{ex} is below a certain threshold, we see only the offset—the high-frequency tail of the primary resonance. However, when U_{ex} exceeds this threshold a peak appears with an amplitude which increases monotonically with U_{ex}. With increasing ω [Fig. 4(a)] we found that a jump in amplitude occurs at some ω_*, followed by a rapid decrease back to the offset. For decreasing ω [Fig. 4(b)], the amplitude follows the same resonance curve down to ω_*, but then for $\omega < \omega_*$, the amplitude increases continuously until the particle is ejected from the sheath.

Theory and discussion.—The particle oscillations are determined by the spatial distribution of the electrostatic potential, $\phi(z)$, in the sheath. Without excitation, a particle is levitated in the minimum of the potential well ($z = 0$), where the gravitational force, Mg, is balanced by the electrostatic force, $Q(0)E(0) \equiv Q_0E_0$. We assume that the equilibrium particle charge, $Q(z)$, changes weakly with z [compared to the electric field of

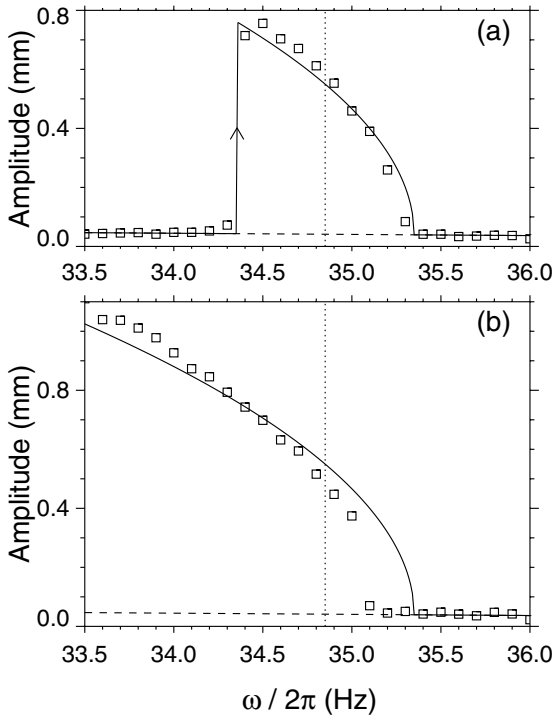

FIG. 4. Variation of the amplitude of particle oscillations close to the subharmonic resonance for increasing (a) and decreasing (b) frequency of excitation, ω. The excitation voltage $U_{\rm ex} = 2$ V. Solid lines show the least-squares fit of the points using Eq. (8) for a_2. The tilted dashed lines represent the linear amplitude offset a_1. The vertical dotted line indicates the position of the double resonance frequency, $2\omega_0$, obtained from the fit.

the sheath, $E(z)$], so that we can set $Q \simeq Q_0 = \text{const}$. The particle collision experiments [9] in Ar discharge at pressures $p \sim 1$ Pa confirm this assumption: Typically, the spatial scale of the field change is approximately 1 order smaller than that of the charge change [10]. The electrostatic energy of the particle, $\mathcal{U} = Q\phi$, can be expanded around $z = 0$ in the series $\mathcal{U}(z) = \mathcal{U}_0' z + \frac{1}{2}\mathcal{U}_0'' z^2 + \frac{1}{6}\mathcal{U}_0''' z^3 + \frac{1}{24}\mathcal{U}_0^{(4)} z^4 + O(z^5)$. Using the equilibrium condition $Mg = QE_0 \equiv -\mathcal{U}_0'$ and the definition of the resonance frequency, $M\omega_0^2 = -QE_0' \equiv \mathcal{U}_0''$, we rewrite it as follows:

$$\mathcal{U}(z) \simeq M(-gz + \tfrac{1}{2}\omega_0^2 z^2 + \tfrac{1}{3}\alpha z^3 + \tfrac{1}{4}\beta z^4), \quad (1)$$

where $\alpha = \mathcal{U}_0'''/2M$ and $\beta = \mathcal{U}_0^{(4)}/6M$ are the anharmonic coefficients. Keeping only the first two anharmonic coefficients is (in practice) sufficient to describe all major peculiarities of a nonlinear oscillator [8,11]. Using Eq. (1), we obtain the equation for the particle oscillation,

$$\ddot{z} + 2\gamma\dot{z} + \omega_0^2 z + \alpha z^2 + \beta z^3 = \frac{F(z)}{M}\cos\omega t. \quad (2)$$

Here γ is the damping rate due to neutral gas friction; F is the excitation force acting from the wire. This force presumably depends on the vertical position of the particle, and we expand it up to quadratic terms, $F(z) \simeq F_0 + F_0' z + \frac{1}{2}F_0'' z^2$.

First, let us consider the primary resonance $\omega \simeq \omega_0$. Nonlinear effects are stronger when the oscillation amplitude is larger, and therefore we are interested in a narrow region $\epsilon = \omega - \omega_0$ around the resonance frequency, where $|\epsilon| \ll \omega_0$. This approach is normally valid in the limit $\gamma \ll \omega_0$ and is justified for our case: The calculated $\gamma/2\pi \simeq 0.068$ Hz (see [12]) is much less than the measured $\omega_0/2\pi \simeq 17.0$ Hz. Then, we obtain from Eq. (2),

$$\ddot{z} + 2\gamma\dot{z} + \omega_0^2 z + \alpha z^2 + \beta z^3 = \omega_0^2 A\cos(\omega_0 + \epsilon)t, \quad (3)$$

where $A = F_0/M\omega_0^2 \equiv kU_{\rm ex}$ and k is a "scale factor" of the oscillation amplitude. In Eq. (3) we omit the higher order terms in $F(z)$, because for the primary resonance they are not important when the inequality $A|F_0'/F_0| \ll 1$ is satisfied (this condition always holds in our case). In accordance with the method of successive approximations for anharmonic oscillations [8,11], the first term in the solution of Eq. (3) is $z(t) \simeq a\cos(\omega_0 + \epsilon)t$, and the dependence of the amplitude a on ϵ and A is given by

$$a^2[(\epsilon - \kappa a^2)^2 + \gamma^2] = \tfrac{1}{4}\omega_0^2 A^2, \quad (4)$$

where $\kappa = 3\beta/8\omega_0 - 5\alpha^2/12\omega_0^3$ characterizes a nonlinear shift of the primary resonance frequency. The least-squares fit of the experimental points for the low-amplitude (linear) primary resonance yields the resonance frequency $\omega_0/2\pi = 17.0$ Hz, the damping rate $\gamma/2\pi = 0.067$ Hz, and the amplitude scale factor $k = 0.042$ mm/V (note that the fitted damping rate is very close to $\gamma/2\pi = 0.068$ Hz evaluated from the theory [12]). Using these values, we fit the points for the nonlinear oscillations in Fig. 2 to the function $a(\epsilon, A)$ from Eq. (4). The solid lines represent the least-squares fit with $\kappa/2\pi = -0.96$ Hz/mm^2. If each curve is fitted independently, this value varies within 5%. The hysteresis appears when A exceeds the critical value: $A_{\rm cr}^2 = \frac{32}{3\sqrt{3}}(\gamma^3/|\kappa|\omega_0^2) \simeq (2.4 \times 10^{-3}\ \text{mm})^2$, which corresponds to $U_{\rm ex} \simeq 60$ mV.

Second, for the superharmonic resonance $\omega \simeq \frac{1}{2}\omega_0$, we set $\epsilon = \omega - \frac{1}{2}\omega_0$. The solution of Eq. (2) is approximately a sum of the first- and second-order terms [8], $z(t) \simeq z_1(t) + z_2(t)$. The first (linear) term is $z_1(t) = a_1\cos(\frac{1}{2}\omega_0 + \epsilon)t$, where $a_1 \simeq \frac{4}{3}(1 + \frac{4}{3}\epsilon/\omega_0)A$ represents the amplitude offset (dashed line in Fig. 3), and z_2 describes the nonlinear resonance peak. Substituting the expression for $z_1(t)$ in Eq. (2), we get the resonance terms $z_1^2 \propto \cos(\omega_0 + 2\epsilon)t$ in the resulting equation for z_2 (see Ref. [8]). Retaining these terms, we obtain

$$\ddot{z}_2 + 2\gamma\dot{z}_2 + \omega_0^2 z_2 + \alpha z_2^2 + \beta z_2^3 = -\tfrac{8}{9}\alpha_{(\omega/2)}A^2\cos(\omega_0 + 2\epsilon)t, \quad (5)$$

where $\alpha_{(\omega/2)} = \alpha - \frac{3}{4}\omega_0^2/\ell$ and $\ell = F_0/F_0' < 0$ is the spatial scale of change of the excitation force. In Eq. (5)

we omit the small terms $O(A^2/\ell^2)$. Formally, Eq. (5) is similar to that for the primary resonance [see Eq. (3)], and therefore shapes of the corresponding curves are qualitatively the same. Assuming $z_2(t) \simeq a_2 \cos(\omega_0 + 2\epsilon)t$, we obtain for the superharmonic resonance,

$$a_2^2[(2\epsilon - \kappa a_2^2)^2 + \gamma^2] = \frac{16}{81}\left(\frac{\alpha_{(\omega/2)}}{\omega_0}\right)^2 A^4. \quad (6)$$

The independent least-squares fit of the experimental points in Fig. 3 using Eq. (6) gives for each curve values of ω_0 and γ, which are nearly the same as those for the primary resonance (deviation within $\simeq 0.5\%$), $\kappa/2\pi = -1.0 \pm 5\%$ Hz/mm^2, and $|\alpha_{(\omega/2)}|/(2\pi)^2 = 32 \pm 10\%$ Hz^2/mm. The critical value of A for the hysteresis is $A_{\rm cr}^4 = \frac{9\sqrt{3}}{2}(\gamma^3\omega_0^2/|\kappa|\alpha_{(\omega/2)}^2) \simeq (0.14\ \text{mm})^4$, which corresponds to $U_{\rm ex} \simeq 3.5$ V.

Third, for the subharmonic resonance $\omega \simeq 2\omega_0$, we set $\epsilon = \omega - 2\omega_0$. The first-order term is $z_1(t) = -a_1 \cos(2\omega_0 + \epsilon)t$ with the amplitude offset $a_1 \simeq \frac{1}{3}(1 - \frac{4}{3}\epsilon/\omega_0)A$. Retaining the necessary terms (see Ref. [8]), we derive from Eq. (2) the equation for z_2,

$$\ddot{z}_2 + 2\gamma\dot{z}_2 + \omega_0^2[1 - \tfrac{2}{3}(\alpha_{(2\omega)}A/\omega_0^2)\cos(2\omega_0 + \epsilon)t]z_2 + \alpha z_2^2 + \beta z_2^3 = 0, \quad (7)$$

where $\alpha_{(2\omega)} = \alpha + \frac{3}{2}\omega_0^2/\ell$. We see that Eq. (7) is an equation of a nonlinear parametric oscillator, and therefore the subharmonic resonance appears due to a parametric instability [8]. Putting $z_2(t) \simeq a_2 \cos(\omega_0 + \frac{1}{2}\epsilon)t$ we get

$$a_2^2[(\tfrac{1}{2}\epsilon - \kappa a_2^2)^2 + \gamma^2] = \frac{1}{36}\left(\frac{\alpha_{(2\omega)}}{\omega_0}\right)^2 A^2 a_2^2. \quad (8)$$

The solution of Eq. (8) has the following peculiarities [8]: If A is less than the threshold value $A_{\rm th} = 6\gamma\omega_0/|\alpha_{(2\omega)}|$, then Eq. (8) has only the zero solution $a_2 = 0$, and thus just the offset $a_1(\omega)$ can be observed. For sufficiently high $U_{\rm ex}$ ($A > A_{\rm th}$), a nonzero solution exists for $\epsilon_{\rm b1} < \epsilon < \epsilon_{\rm b2}$, where $\epsilon_{\rm b1,2} = \mp 2\gamma\sqrt{A^2/A_{\rm th}^2 - 1}$. The least-squares fit of the points in Fig. 4 ($U_{\rm ex} = 2.0$ V) with Eq. (8) gives us $\kappa/2\pi = -0.95$ Hz/mm^2 and $|\alpha_{(2\omega)}|/(2\pi)^2 = 320$ Hz^2/mm. Thus, $A_{\rm th} \simeq 0.02$ mm, which corresponds to $U_{\rm ex} \simeq 0.5$ V. The fit for the center $\epsilon = 0$ yields 34.85 Hz, which is $\simeq 2\%$ larger than the double value of ω_0 obtained for the primary and superharmonic resonance.

Finally we can reconstruct the sheath potential, $\phi(z)$. Using the fitted values $|\alpha_{(\omega/2)}| = |\alpha - \frac{3}{4}\omega_0^2/\ell| \simeq (2\pi)^2 \times 30$ Hz^2/mm and $|\alpha_{(2\omega)}| = |\alpha + \frac{3}{2}\omega_0^2/\ell| \simeq (2\pi)^2 \times 320$ Hz^2/mm, we evaluate the first anharmonic coefficient and the spatial scale of the excitation force: $\alpha/(2\pi)^2 \simeq -130$ Hz^2/mm and $\ell \simeq -2$ mm. With this value for α and $\kappa/2\pi = -0.95$ Hz/mm, we estimate the second anharmonic coefficient: $\beta/(2\pi)^2 \simeq 20$ Hz^2/mm^2. Then, using Eq. (1) we evaluate the potential energy of a particle in the sheath field (z in mm),

$$\mathcal{U}(z) \simeq M\omega_0^2(-0.9z + \tfrac{1}{2}z^2 - \tfrac{1}{3}0.5z^3 + \tfrac{1}{4}0.07z^4) \propto \phi(z). \quad (9)$$

We see that the first anharmonic term results in a significant deviation of the sheath potential from a parabolic one, and therefore the oscillations become strongly nonlinear when the amplitude reaches a few tenths of mm, or more. At the same time the obtained coefficients of the series converge rapidly, so that for $|z| \lesssim 2$ mm we can limit ourselves to expansion (1). Thus, Eq. (9) provides a convenient analytical expression for the electric field in a rather wide vicinity of the equilibrium particle position.

In this Letter, we have presented one example of nonlinear particle oscillations in the sheath of a low-pressure rf discharge and its quantitative analysis. The proposed simple method opens the possibility to retrieve the profile of the electric field in the wide region of the sheath, using particles of different masses (and thus levitating at different heights). Analysis for each particle allows us to reconstruct the electric field in a range of a few mm, and therefore it is sufficient to use just a few different particles to get a rather precise field distribution in the whole sheath range. Hence, we believe that experiments with excitation of nonlinear oscillations might be an effective way to study the sheath.

*Electronic address: ivlev@mpe.mpg.de.
†Present address: Department of Physics of Complex Systems, Weizmann Institute of Science, Rehovot 76100, Israel.

[1] U. Czarnetzki, D. Luggenhölscher, and H. F. Döbele, Plasma Sources Sci. Technol. **8**, 230 (1999).
[2] A. H. Sato and M. A. Lieberman, J. Appl. Phys. **68**, 6117 (1990).
[3] C. M. O. Mahony, R. Al Wazzan, and W. G. Graham, Appl. Phys. Lett. **71**, 608 (1997).
[4] A. Melzer, T. Trottenberg, and A. Piel, Phys. Lett. A **191**, 301 (1994).
[5] H. Schollmeyer *et al.,* Phys. Plasmas **6**, 2693 (1999).
[6] E. B. Tomme *et al.,* Phys. Rev. Lett. **85**, 2518 (2000).
[7] P. J. Hargis, Jr. *et al.,* Rev. Sci. Instrum. **65**, 140 (1994).
[8] L. D. Landau and E. M. Lifshitz, *Mechanics* (Pergamon, Oxford, 1960).
[9] U. Konopka, G. E. Morfill, and L. Ratke, Phys. Rev. Lett. **84**, 891 (2000).
[10] U. Konopka, Ph.D. thesis, Ruhr-Universität Bochum, 2000.
[11] A. H. Nayfeh and D. T. Mook, *Nonlinear Oscillations* (Wiley, New York, 1979).
[12] P. Epstein, Phys. Rev. **23**, 710 (1924).

Vertical Pairing of Identical Particles Suspended in the Plasma Sheath

V. Steinberg,* R. Sütterlin, A. V. Ivlev, and G. Morfill
Max-Planck-Institut für Extraterrestrische Physik, D-85740 Garching, Germany
(Received 9 May 2000; revised manuscript received 24 January 2001)

It is shown experimentally that vertical pairing of two identical microspheres suspended in the sheath of a radio-frequency (rf) discharge at low gas pressures (a few Pa) appears at a well-defined instability threshold of the rf power. The transition is reversible, but with significant hysteresis on the second stage. A simple model which uses measured microsphere resonance frequencies and takes into account, in addition to the Coulomb interaction between negatively charged microspheres, their interaction with positive-ion-wake charges, seems to explain the instability threshold quite well.

DOI: 10.1103/PhysRevLett.86.4540 PACS numbers: 52.27.Lw, 52.27.Gr

Recent interest in the properties of complex plasmas—charged monodisperse microparticles suspended in an electron-ion environment, is partially due to the possibility to model condensed matter phenomena on an "atomic" level [1–3]. The particles are charged negatively in a radio-frequency (rf) discharge (up to 10^3–10^4 elementary charges) and levitate in the lower plasma sheath, where gravity can be balanced by an inhomogeneous vertical electric field. The particles repel each other via a screened Coulomb interaction. Inside a confining horizontal potential they arrange themselves either into an ordered structure—the "plasma crystal," or form disordered, liquid- or gaslike, states [4–6].

At low gas pressures one has typically only a very few layers (as few as one) for these structures. Ion streaming motion in the plasma sheath produces a nonequilibrium environment, which is reflected in the properties of the complex plasma structures and makes them rather different from the known equilibrium ones [7,8]. One of the striking observations at sufficiently low gas densities (such that the ion-neutral mean free path is not small compared with a typical distance between microspheres) is an unusual "stacking" of the particles such that adjacent horizontal layers are located on top of each other [2,5,9]. This vertical "polarization" of the dusty plasma was ascribed to the attractive forces which result from the focusing of the ion flux under each particle (ion wake effect, see, e.g., Ref. [10]). Thus, the attractive interaction between the horizontal layers in a plasma crystal is asymmetric, such that the attractive force is communicated only downstream in the direction of the ion flow [10]. The same arguments were applied to predict a "binding" force for a possible "dust molecule" formation [11]. This theoretical prediction was verified recently by experimental studies of the competition between repulsive and attractive forces acting on two *different* dust particles levitated on *different* levels in the plasma sheath [12].

In this Letter we present experiments on a new instability which is observed for two *identical* microspheres suspended initially on the *same* level in the plasma sheath. In this Letter we report on the quantitative investigations involving (for simplicity) only two microspheres, which were undertaken to clarify the basic behavior for many identical particles. The instability appears first as a continuous (forward) bifurcation to a state of the vertically separated microspheres and then to a discontinuous vertical pairing. Depending on gas pressure, the last stage—the pairing—can be either strongly hysteretic (for lower pressure) or weakly hysteretic (for higher pressure).

The experiments were performed in a standard Gaseous Electronics Conference (GEC) rf reference cell [13] with the lower electrode powered at 13.56 MHz and the upper electrode grounded (see Fig. 1). Argon gas at various pressures between 1 and 7 Pa was used, and the discharge power (or a rf peak-to-peak voltage, U_{pp}) was the control parameter of the instability described. The electron temperature and density were measured at the center of the discharge with a rf-compensated passive Langmuir probe. At these conditions the electron temperature T_e was found to be within 2–5 eV, while the electron density n_e ranged from 10^7 to 8×10^8 cm^{-3}, so that the electron Debye length varied from $\lambda_{De} \simeq 0.5$ mm (high U_{pp}) to $\lambda_{De} \simeq 5$ mm (low U_{pp}). These values of the Debye length are comparable to or larger than the separation distances measured, and thus Debye shielding plays only a minor role in this rather low-density plasma. The microspheres, suspended in the plasma, were illuminated by a laser sheet of about 100 μm thickness, and their imaging was performed by external CCD cameras from the top and from the side (in both cases via 300 mm

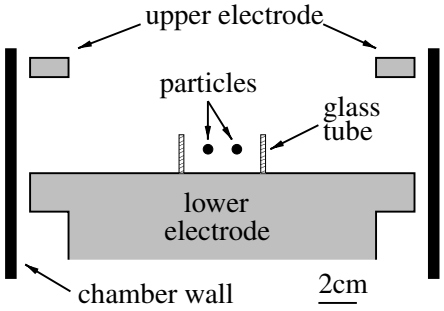

FIG. 1. Experimental setup using a quartz glass cylinder as a confining electrode.

 0031-9007/01/86(20)/4540(4)$15.00

objectives). We used polystyrene (density 1.05 g/cm^3) microspheres with diameter 7.6 ± 0.1 μm and mass $M \simeq 2.4 \times 10^{-10}$ g. In order to confine the microspheres horizontally we placed a quartz glass cylinder of 20 mm height and 50 mm diameter on the lower electrode (see Fig. 1). In contrast to a copper ring normally used to confine particles, the glass cylinder produces extremely flat, almost "square well" confining potential. The latter conclusion is based on our observation of an unusually flat shape of 2D plasma crystal, particularly up to its edges, contrary to the trap formed by a standard metal ring. The square well confining potential provides us the opportunity to study two identical microspheres suspended in the plasma sheath on the same initial height.

In order to quantitatively investigate the pairing instability and to verify that it is indeed symmetry breaking, we conducted experiments with two identical microspheres at different pressures. Figure 2 shows how, at a pressure of 2 Pa, the relative position of one microsphere, which eventually moves below and then under the other (i.e., downstream) with respect to the eventual upstream microsphere, varies as the power (or U_{pp}) decreases. As long as U_{pp} exceeds the threshold value $U_{pp}^{th} \simeq 55$ V, both particles are located on the same level (initial position 1). When U_{pp} decreases below the threshold, vertical separation starts (position 2) and grows continuously up to position 3. A further small U_{pp} decrease causes the lower particle to "jump" to a position directly beneath the upper one and to create a vertical pair (final position 4). By reversing the process, i.e., increasing U_{pp}, the particles revert back to their initial horizontal configuration. The transition is strongly hysteretic with respect to U_{pp}. Further measurements showed that the threshold, U_{pp}^{th}, rapidly increases with pressure, while the relative width of the hysteresis decreases with pressure.

Figure 3 represents the forward (positions 1–5) and the reverse (positions 6 and 7) transitions at $p = 7$ Pa. The instability (vertical separation) starts at $U_{pp}^{th} \simeq 200$ V and develops continuously until position 4. Then a small U_{pp} decrease is accompanied by the discontinuous vertical pairing (position 5). When the voltage is increased back, the particles remain vertically paired until position 6 is reached, and then the lower particle jumps to position 7. In Fig. 4 the vertical separation distance is plotted against the control parameter, $U_{pp}^{th} - U_{pp}$, at $p = 7$ Pa. As in the low pressure case, the transition is divided into two stages: (i) continuous transition from the horizontal configuration and (ii) discontinuous, hysteretic transition to the final vertical pairing. It is worth noting that at the onset of the continuous transition strong *symmetrical* fluctuations of the vertical particle separation are observed in the experiments. This means that the pairing instability may be initiated with equal probability by either microsphere in the pair. Therefore, this transition is related to the symmetry breaking.

In the experiments both U_{pp} (at the fixed p) and p (at the fixed U_{pp}) were used as the control parameters

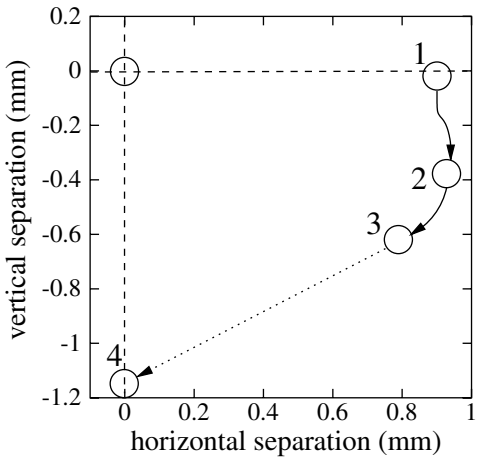

FIG. 2. Sequence of the relative particle positions during the pairing instability as U_{pp} decreases (pressure $p = 2$ Pa). The steps are (1) $U_{pp} \geq U_{pp}^{th} \simeq 55$ V—horizontal configuration, (2) $U_{pp} \simeq 45$ V, (3) $U_{pp} \simeq 37$ V—continuous separation, and (4) $U_{pp} \simeq 36$ V—discontinuous vertical pairing.

of the instability. But in a subsequent analysis, presented below, it is much more convenient to use the resonance frequencies of vertical, ω_z, and horizontal, ω_r, oscillations of a single particle in the sheath as the control parameters. The resonance frequencies are certain functions of U_{pp} and p and can be determined experimentally [14].

We first examine the simplest model without wake effects. The model uses the measured values of ω_z and ω_r as the control parameters and provides an order of magnitude estimate for the instability threshold. We consider a pair of two identical particles of mass M and (negative) charge $-Q$, electrostatically confined in the harmonic potential

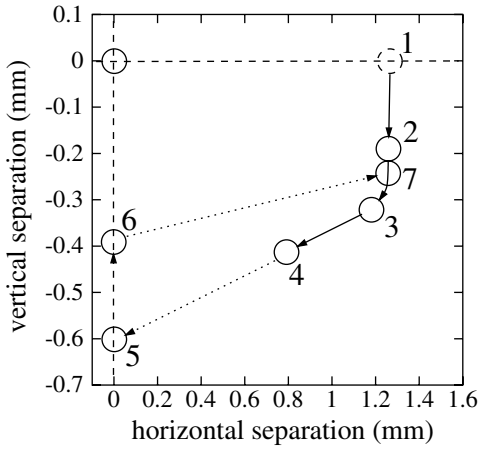

FIG. 3. Sequence of the relative particle positions during the pairing instability as U_{pp} decreases (1–5) and increases back (6 and 7) (pressure $p = 7$ Pa). For decreasing voltage the steps are (1) $U_{pp} \geq U_{pp}^{th} \simeq 200$ V—horizontal configuration, (2) $U_{pp} \simeq 110$ V, (3) $U_{pp} \simeq 85$ V, (4) $U_{pp} \simeq 78$ V—continuous separation, and (5) $U_{pp} \simeq 76$ V—discontinuous vertical pairing. For increasing voltage the steps are (6) $U_{pp} \simeq 93$ V—continuous vertical movement and (7) $U_{pp} \simeq 95$ V—discontinuous reversibility of the pair configuration.

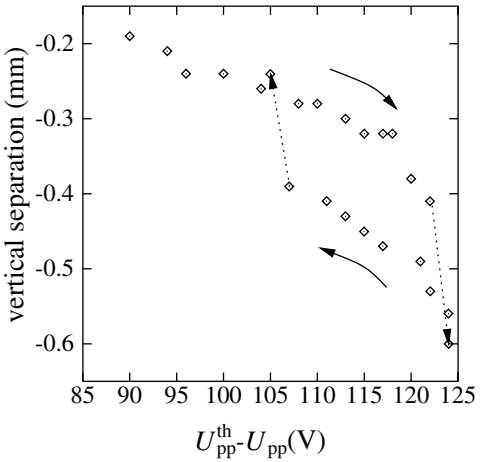

FIG. 4. Vertical separation of a particle pair vs the control parameter, $U_{pp}^{th} - U_{pp}$, for two stages of the pairing transition at $p = 7$ Pa. The hysteretic nature of the second stage is obvious from the plot. The arrows denote the direction of the variation observed.

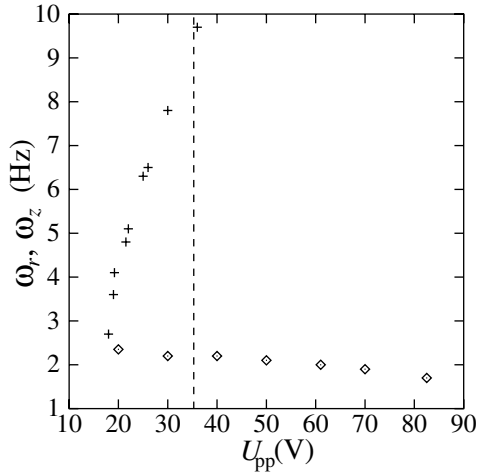

FIG. 5. Horizontal, ω_r ($\diamond$), and vertical, ω_z (+), resonance frequencies of a single particle as a function of U_{pp} (at a pressure $p = 1$ Pa). The vertical dashed line shows the threshold voltage $U_{pp}^{th} \simeq 35$ V (onset of the vertical separation).

well. If the particles are separated horizontally by R and vertically by δ (i.e., each particle is displaced at $R/2$ and $\delta/2$ from the center), then their energy in the confinement is $\frac{1}{4}M(\omega_z^2\delta^2 + \omega_r^2R^2)$. Since the Debye length is relatively large, the bare coupling energy of two unshielded particles, $Q^2(R^2 + \delta^2)^{-1/2}$, should be added to the confinement energy. This system has two stable configurations—horizontally (when $\omega_z > \omega_r$) or vertically (when $\omega_z < \omega_r$) aligned at distances of $R = (2Q^2/M\omega_r^2)^{1/3}$ or $\delta = (2Q^2/M\omega_z^2)^{1/3}$, respectively.

Our model is characterized in terms of the measured resonance frequencies. Thus, it is necessary to trace these frequencies as the control parameter, $U_{pp}^{th} - U_{pp}$, is varied. The typical dependence of ω_r and ω_z on the value of U_{pp} at $p = 1$ Pa is shown in Fig. 5. One can see that the frequencies converge rapidly as U_{pp} decreases. Comparison of Figs. 4 and 5 shows (albeit for different pressures) that the transition starts *continuously* when ω_z still *considerably exceeds* ω_r. This implies that the harmonic approximation with the isotropic particle field is too simple. Thus, we have to include the wake effect in its simplest form. For consistency in the nonlinearity analysis, we must also take into consideration the anharmonicity of the potential well in the vertical direction [15]. The corresponding expression for the total potential energy of a particle pair in a 2D confinement is

$$\mathcal{W}_{pair} \simeq \frac{M}{4}\left(\omega_r^2R^2 + \omega_z^2\delta^2 + \frac{\beta^*}{8}\delta^4\right) + \frac{Q^2}{\sqrt{R^2 + \delta^2}} - \frac{Qq}{2\sqrt{R^2 + (\Delta + \delta)^2}} - \frac{Qq}{2\sqrt{R^2 + (\Delta - \delta)^2}}. \quad (1)$$

In writing Eq. (1) the simplest two-microsphere model of the wake is used (see Fig. 6). We treat the excessive positive charge of the wake, q, as pointlike, located under the particle at distance Δ. We assume also that since both the particle and the wake charges vary only slightly with variation in R and δ, so that Q and q are approximately constant. The last two terms in Eq. (1) represent the particle-wake interaction, and cross terms of the particle-wake and wake-wake (qq) interactions are neglected [12]. Since the coefficients multiplying the terms δ^3 cancel out for a pair of identical particles, the lowest order vertical anharmonicity in Eq. (1) is the fourth order term with coefficient $\beta^* > 0$ but whose value is here unknown, since it was not feasible to measure it by technique used elsewhere [15].

The dependence $R(\delta)$ is determined from the equilibrium condition in the radial direction, $\partial\mathcal{W}_{pair}/\partial R = 0$:

$$\frac{2Q^2}{(R^2 + \delta^2)^{3/2}} - Qq\left(\frac{1}{[R^2 + (\Delta + \delta)^2]^{3/2}} + \frac{1}{[R^2 + (\Delta - \delta)^2]^{3/2}}\right) = M\omega_r^2. \quad (2)$$

The equilibrium value of δ is given by the condition $\partial\mathcal{W}_{pair}/\partial\delta = 0$. A linear combination of this condition and Eq. (2) gives

$$M(\omega_z^2 - \omega_r^2)\delta + \frac{M\beta^*}{4}\delta^3 + Qq\Delta\left(\frac{1}{[R^2 + (\Delta + \delta)^2]^{3/2}} - \frac{1}{[R^2 + (\Delta - \delta)^2]^{3/2}}\right) = 0. \quad (3)$$

First, we expand Eq. (3) to a third power in δ. Then we obtain from Eq. (2) an expression for $R(\delta)$ up to a second order expansion in δ (an even expansion) and substitute it into the coefficients of terms of first and third powers in δ in the expansion of Eq. (3). This approach provides the following expression which is a typical stationary equation for the vertical displacement as the order parameter:

$$\left(\frac{\omega_z^2}{\omega_r^2} - \Omega^2\right)\tilde{\delta} + \frac{\beta^* R_0^2}{4\omega_r^2}\,\tilde{\delta}^3 - \frac{35(\Omega^2 - 1)\tilde{\Delta}^2}{6(1 + \tilde{\Delta}^2)^2}\left(\frac{1 + \frac{8}{7}\frac{q/Q}{(1+\tilde{\Delta}^2)^{5/2}}}{1 - \frac{q/Q}{(1+\tilde{\Delta}^2)^{5/2}}}\right)\tilde{\delta}^3 = 0\,. \tag{4}$$

Here we have introduced the dimensionless parameters, $\tilde{\delta} = \delta/R_0$ and $\tilde{\Delta} = \Delta/R_0$ [normalized by $R_0 = R|_{\delta=0}$ from Eq. (2)], and the critical frequency ratio,

$$\Omega \equiv \sqrt{1 + \frac{6Qq\tilde{\Delta}^2}{M\omega_r^2 R_0^3 (1 + \tilde{\Delta}^2)^{5/2}}}\,. \tag{5}$$

The instability criterion $(\omega_z/\omega_r)_{\rm cr} = \Omega$ is obtained from Eq. (4) by setting the coefficient of $\tilde{\delta}$ equal to zero. At $\omega_z/\omega_r > \Omega$, the energy $\mathcal{W}_{\rm pair}(\delta)$ has a minimum at $\delta = 0$ and the equilibrium configuration is horizontal. In the opposite case, $\omega_z/\omega_r < \Omega$, the $\delta = 0$ state becomes unstable, and the particles start separating vertically. From Fig. 5 we note that the separation starts at $(\omega_z/\omega_r)_{\rm cr} \simeq 4$ (when $U_{\rm pp} \lesssim U_{\rm pp}^{\rm th}$). Assuming $Q \sim q$ and substituting Eq. (2) at $\delta = 0$ into Eq. (5), one gets Ω as a function of $\tilde{\Delta}$ only. Then at $\tilde{\Delta} \sim 1$ we obtain $\Omega \sim 3$. Thus, the threshold of the pairing instability is adequately described by the model. A saturation of the order parameter, $\tilde{\delta}$, above the instability threshold in the first continuous stage of the transition (see Fig. 4) could be reached if the sum of both coefficients of $\tilde{\delta}^3$ in Eq. (4) is positive. By using the expression $\Omega(\tilde{\Delta})$ and the value of the ratio $Q/q \sim 1$ we achieve this condition at $\beta^* R_0^2/\omega_r^2 \gtrsim 7$, or $\beta^*/(2\pi)^2 \gtrsim 20\ \mathrm{Hz^2/mm^2}$. Our recent experiments [15] indicate that at pressures below ~10 Pa the anharmonic coefficients become relatively large: For example, $\beta/(2\pi)^2 \simeq 20\ \mathrm{Hz^2/mm^2}$ at $p \sim 1$ Pa and $U_{\rm pp} \simeq 70$ V. At smaller $U_{\rm pp}$, the whole vertical structure of the sheath changes dramatically, because the Debye length increases by the order of magnitude. Hence, the anharmonic coefficients should also increase rapidly as $U_{\rm pp}$ decreases, and it is plausible that β^* will provide the instability saturation. Then, as follows from Eq. (4), $\tilde{\delta} \propto \sqrt{\Omega - \omega_z/\omega_r}$ close to the threshold. However, failing an accurate experimental determination of the shape of the sheath potential for the actual conditions of the experiment, further testing of the model via the experimental value of δ is not feasible here.

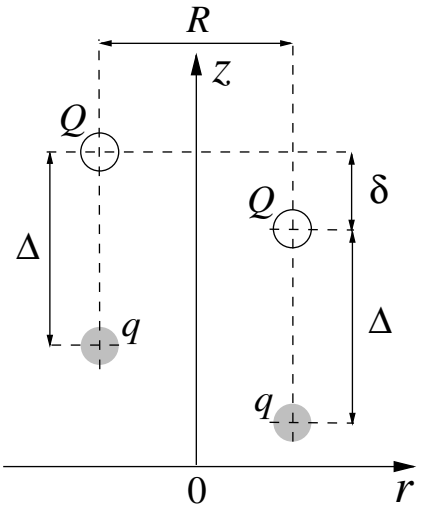

FIG. 6. Schematics of the simplified model of the wake potential.

The modeling of the second (discontinuous) stage of the instability is a rather complicated problem: When the lower particle approaches the wake, its actual "shape" becomes crucial, and the approximation of the pointlike wake charge cannot be used. This very nonlinear second stage will almost certainly involve nonlinear wake dynamics, and these can probably be adequately treated only by three-dimensional numerical simulations. We point out that the effect of the wake is stronger at lower p and $U_{\rm pp}$, when λ_{De} is larger. At the same time, the ion mean free path should exceed λ_{De} (otherwise, the wake effect weakens due to the ion scattering on neutrals). Both these requirements are well satisfied in our experiments.

V. S. is grateful for the support of the Alexander von Humboldt Foundation, Germany, during his stay at MPE.

*Also at Department of Physics of Complex Systems, Weizmann Institute of Science, Rehovot, 76100, Israel.

[1] H. Thomas *et al.,* Phys. Rev. Lett. **73**, 652 (1994).
[2] J. H. Chu and Lin I, Phys. Rev. Lett. **72**, 4009 (1994).
[3] Y. Hayashi and K. Tachibana, Jpn. J. Appl. Phys. **33**, L804 (1994).
[4] H. Thomas and G. Morfill, Nature (London) **379**, 806 (1996).
[5] A. Melzer, A. Homann, and A. Piel, Phys. Rev. E **53**, 2757 (1996).
[6] R. A. Quinn *et al.,* Phys. Rev. E **53**, R2049 (1996).
[7] S. V. Vladimirov and M. Nambu, Phys. Rev. E **52**, 2172 (1995).
[8] F. Melandsø and J. Goree, Phys. Rev. E **52**, 5312 (1995).
[9] K. Takahashi *et al.,* Phys. Rev. E **58**, 7805 (1998).
[10] V. A. Schweigert *et al.,* Phys. Rev. E **54**, 4155 (1996).
[11] D. P. Resendes, J. T. Mendonca, and P. Shukla, Phys. Lett. A **239**, 181 (1998).
[12] A. Melzer, V. A. Schweigert, and A. Piel, Phys. Rev. Lett. **83**, 3194 (1999); Phys. Scr. **61**, 494 (2000).
[13] P. J. Hargis, Jr. *et al.,* Rev. Sci. Instrum. **65**, 140 (1994).
[14] A. Melzer, T. Trottenberg, and A. Piel, Phys. Lett. A **191**, 301 (1994); A. Homann, A. Melzer, and A. Piel, Phys. Rev. E **59**, R3835 (1999).
[15] A. V. Ivlev *et al.,* Phys. Rev. Lett. **85**, 4060 (2000).

Dynamics of Lane Formation in Driven Binary Complex Plasmas

K. R. Sütterlin,[1] A. Wysocki,[2] A. V. Ivlev,[1] C. Räth,[1] H. M. Thomas,[1] M. Rubin-Zuzic,[1] W. J. Goedheer,[3] V. E. Fortov,[4] A. M. Lipaev,[4] V. I. Molotkov,[4] O. F. Petrov,[4] G. E. Morfill,[1] and H. Löwen[2]

[1]*Max Planck Institute for Extraterrestrial Physics, 85741 Garching, Germany*
[2]*Heinrich-Heine-Universität Düsseldorf, 40225 Düsseldorf, Germany*
[3]*FOM-Institute for Plasma Physics Rijnhuizen, 3430 BE Nieuwegein, The Netherlands*
[4]*Joint Institute for High Temperatures, 125412 Moscow, Russia*

(Received 23 December 2008; published 25 February 2009)

The dynamical onset of lane formation is studied in experiments with binary complex plasmas under microgravity conditions. Small microparticles are driven and penetrate into a cloud of big particles, revealing a strong tendency towards lane formation. The observed time-resolved lane-formation process is in good agreement with computer simulations of a binary Yukawa model with Langevin dynamics. The laning is quantified in terms of the anisotropic scaling index, leading to a universal order parameter for driven systems.

DOI: 10.1103/PhysRevLett.102.085003 PACS numbers: 52.27.Lw

The formation of lanes is a ubiquitous phenomenon occurring in nature when two species of particles are driven against each other. When the driving forces are strong enough, like-driven particles form ''stream lines'' and move collectively in lanes. Typically, the lanes exhibit a considerable anisotropic structural order accompanied by an enhancement of their (unidirectional) mobility. The phenomenon is most commonly known from pedestrian dynamics in highly populated pedestrian zones [1], but also occurs in different systems of driven particles, such as colloidal dispersions [2–4], lattice gases [5], and molecular ions [6]. In other words, it is a ubiquitous generic process of considerable interest in different branches of physics. It is also a genuine nonequilibrium transition [5] which depends on the details of the particle interactions and their dynamics [7].

Recently, particle laning was also observed in complex plasmas [8]. In fact, complex plasmas [9,10] occupy the important intermediate dynamical regime between undamped fluids and fully damped colloidal suspensions: the ''atomistic'' dynamics associated with the interparticle interaction is virtually undamped whereas the large-scale hydrodynamics is determined by friction.

In this Letter we report on comprehensive experimental studies of lane formation in complex plasmas, that were carried out under microgravity conditions with the radio frequency (rf) discharge chamber PK-3 Plus [11]. The motivation for this research is fourfold. First, we demonstrate that complex plasmas are indeed an ideal system for studying nonequilibrium phase transitions such as laning. Second, the experiments enable us to investigate the dynamical onset of lane formation in detail. Third, we achieve a quantitative understanding of the structural correlation during the onset of laning by comparison with particle-resolved Langevin simulations. Fourth, based on the anisotropic scaling index analysis of the obtained data, we suggest a universal order parameter for nonequilibrium phase transitions in driven systems.

Experiments.—A series of dedicated experiments was carried out on the International Space Station. These involved various combinations of ''big'' and ''small'' monodisperse particles (2.55, 6.8, 9.2, and 14.9 μm diameter for big, and 1.55, 2.55, and 3.4 μm for small), with different neutral gases and pressures (argon between 10 and 60 Pa and neon at 60 Pa), and for different rf discharge powers. First a stable spheroidal cloud of big particles was produced. Second, small particles were injected into this cloud. The force field pulls the small particles through the cloud of big particles towards the center, thus making such systems perfectly suited to study lane formation.

Figure 1 shows a characteristic example of lane formation observed in experiments with 3.4 and 9.2 μm particles at pressure of 30 Pa. When a fraction of individual small particles enters the interface of the fairly homogeneous cloud formed by big particles, the subsequent penetration is accompanied by a remarkable self-organization sequence: (a) Big particles are pushed collectively by the inflowing cloud of small particles, the latter form ''strings'' drifting on averaging along the force field; (b) as the particles approach the center of the chamber, the field decreases and the strings organize themselves into larger ''streams.'' At the later stage, when the field almost vanishes, the streams merge to form a spheroidal droplet with a well-defined surface, indicating the transition to the regime when surface tension plays the primary role. We restrict ourselves to the first two stages [12]. It is noteworthy that during stage (b) big particles also form well-defined strings. Small and big particles create an ''array'' of interpenetrating strings. After the flux of small particles is exhausted, the big-particle strings slowly dissolve [13].

Computer simulations.—First, the distribution of the characteristic parameters of the discharge plasma, such

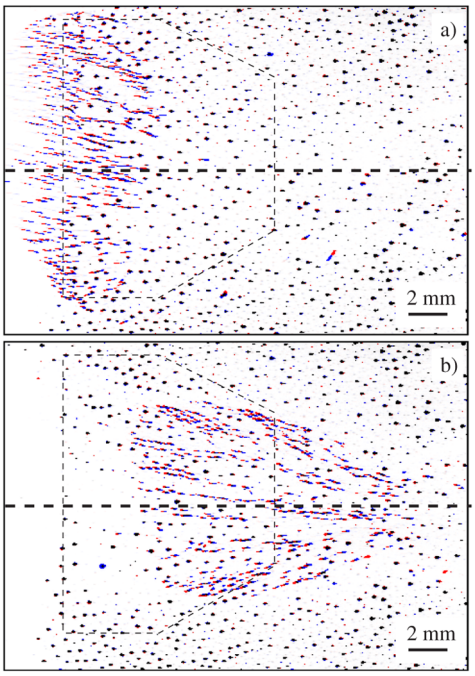

FIG. 1 (color online). Lane formation in complex plasmas. A short burst of small (3.4 μm) particles is injected into a cloud of big (9.2 μm) background particles (close to the midplane of the chamber, indicated by horizontal dashed line). Small particles are driven towards the center, stages of (a) initial lane formation and (b) merging of lanes into larger streams are shown. Particles are illuminated by a thin laser sheet of $\simeq$0.35 mm; each figure is a superposition of two consecutive images (1/50 s apart), the time difference between them is $\simeq$1.2 s. At the stage (b) big particles also form well-defined lanes. The frame indicates the region used for the analysis of big-particle dynamics.

as plasma density, electron temperature, and electric fields, was deduced from 2D simulations of the PK-3 Plus discharge chamber. We used a plasma fluid code (described in Ref. [14]), which provides a self-consistent coupling of dust species to the discharge plasma, including particle charging, plasma absorption, redistribution of volume charges or ambipolar fields, etc. These simulations suggest that in the midplane of the chamber the cloud of big particles is "self-confined" at its edges due to the self-consistent plasma field, as illustrated in Fig. 13 of Ref. [14], whereas inside the cloud the electric and ion drag forces practically compensate each other. On the other hand, since these two forces have different scaling on the particle size, the net force on small particles is nonzero inside the cloud. For the experiment shown in Fig. 1, the simulations yield a force of $f_s = 0.3 \pm 0.1$ pN pushing a small particle towards the center.

Next, particle-resolved molecular dynamics (MD) simulations were performed on the Langevin level [15] for a binary mixture of 5759 small and 12 287 big particles. The simulation box with periodic boundary conditions has dimensions of 4.4 cm in the x direction and 0.8 cm in the y and z directions. The particles interact via a Yukawa pair potential with a screening length $\lambda = 100$ μm (based on results of our plasma discharge simulations) and effective charges $Z_s = 3000e$ (based on experiment [16]) and $Z_b = 8117e$, proportional to the respective particle diameter, $\sigma_s = 3.4$ μm and $\sigma_b = 9.2$ μm. The mass density of the particles is 1.5 g/cm^3 and the corresponding friction rates are $\nu_s = 250$ s^{-1} and $\nu_b = (\sigma_s/\sigma_b)\nu_s = 92.4$ s^{-1}. The mean interparticle distances are deduced from the experiment, $\Delta_s = 464$ μm (before the penetration) and $\Delta_b = 493$ μm, the temperature is $T = 0.024$ eV.

Our plasma simulations show that big particles do not experience a net external force in the bulk. Therefore, in our MD simulation we confine them in the x direction by a parabolic external potential at two edges (with a width of 2.2 cm) and adjust the confinement strength, so that the measured interparticle distance Δ_b is reproduced. Similarly, a portion of small particles, separated from the big particles, was prepared (with a width of 0.7 cm). Then the constant driving force f_s was instantaneously applied, leading to penetration of small particles into the cloud of big ones. Simulation snapshots are shown in Fig. 2, revealing a qualitative agreement with the experiment [13].

Anisotropic scaling index and order parameter.—In order to identify and quantify the stringlike structures in our experimental data and the simulations, a suitable order parameter has to be employed that is sensitive to the changing particle structures. Conventional approaches, e.g., binary correlation or bond orientation functions, Legendre polynomials, etc., turned out to be too insensitive. Much more satisfactory results were obtained by implementing an *anisotropic scaling index* method—a local nonlinear measure for structure characterization. This method has already been used to characterize electrorheological complex plasmas [17], large-scale distribution of galaxies [18], or bone structure [19].

For a given set of particle positions, $\{\mathbf{r}_i\}$, $i = 1, \ldots, N$, we define a local density $\rho(\mathbf{r}_i, R) = \sum_{j=1}^{N} s(d_{ij}/R)$, where $d_{ij} = |\mathbf{r}_i - \mathbf{r}_j|$ and s is a certain shaping function characterized by the spatial scale R. The scaling index α is the logarithmic derivative of the density with respect to the spatial scale, $\alpha = \partial \log\rho(\mathbf{r}_i, R)/\partial \log R$. Hence, $\alpha(\mathbf{r}_i, R)$

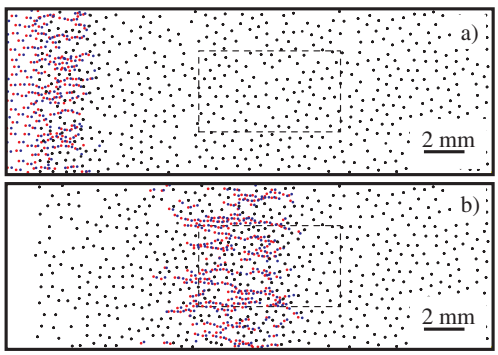

FIG. 2 (color online). Lane formation in MD simulation corresponding to the experiment shown in Fig. 1. Two snapshots illustrate (a) the initial injection stage and (b) the steady state.

characterizes the dimensionality of the local structure around point $\mathbf{r}_i$, in the vicinity determined by the scale R. For example, $\alpha(\mathbf{r}_i, R) \simeq 1$ means that the local structure is close to a straight line at the spatial scale R, for $\alpha(\mathbf{r}_i, R) \simeq 2$ it is an element of a plane, and so on. Using the Gaussian shaping function $s = e^{-(d_{ij}/R)^2}$ we derive

$$\alpha(\mathbf{r}_i, R) = \frac{2\sum_{j=1}^{N}(d_{ij}/R)^2 e^{-(d_{ij}/R)^2}}{\sum_{j=1}^{N} e^{-(d_{ij}/R)^2}}. \quad (1)$$

Thus, the spatial scale R is an important mesoscopic measure of the local environment. In the range of relevant scales α is practically independent of R.

In order to characterize anisotropic structures, we use a ''stretch metric'' for the distance measure d_{ij}. On a 2D plane, the metric is determined by the aspect ratio ϵ (>1), which is the relative stretching of two principal axes, and by the unit vector $\mathbf{u} = (\cos\theta, \sin\theta)$ in the direction of stretching. Then the resulting anisotropic scaling index, $\alpha(\mathbf{r}_i, R, \theta)$, can be directly obtained from Eq. (1). We propose a ''uniaxial vector characterization'': Each point $\mathbf{r}_i$ is associated with the unit vector $\mathbf{u}_i$ which points to a ''preferred'' direction of the local anisotropy. This direction is determined by the angle θ_i at which the ''anisotropic contrast'' $\alpha(\mathbf{r}_i, R, \theta_i + \pi/2) - \alpha(\mathbf{r}_i, R, \theta_i)$ is maximized. The directions $\mathbf{u}_i$ and $-\mathbf{u}_i$ are equivalent, so that below they are defined for the range $-\frac{\pi}{2} \le \theta_i \le \frac{\pi}{2}$.

Thus, each point can now be considered as a uniaxial ''molecule'' (simple rod) with the direction $\mathbf{u}_i$. Therefore, the global laning on a 2D plane can be characterized with the second-rank tensor $Q_{\alpha\beta} = 2N^{-1}\sum_{i=1}^{N} \mathbf{u}_i \otimes \mathbf{u}_i - \delta_{\alpha\beta}$, analogous to that used to quantify order of the nematic phase. The direction of the global laning, $\langle \mathbf{u} \rangle$, is then the eigenvector (''nematic director'') corresponding to the largest eigenvalue of $Q_{\alpha\beta}$, which in turn is the laning order parameter, S. Obviously, $S = 1$ for a perfect alignment and $S = 0$ for a disordered phase, when individual vectors $\mathbf{u}_i$ are uncorrelated. We finally define the global laning angle Θ via the relation $\cos\Theta = \langle \mathbf{u} \rangle \cdot \mathbf{e}_x$.

Comparison of experiments and simulations.—For the analysis of the MD simulations, we divided the volume of the simulation box in the z direction (perpendicular to the driving force in the x direction) into several slabs of 0.35 mm width, which is about the thickness of the laser sheet used to record the experimental data. Hence, the average number of particles and their average density, as well as the magnitude of their fluctuations in this ''reduced'' simulation data set, were similar to those in the experiment. The obtained results were analyzed and compared using the anisotropic scaling index method. The relevant range of spatial scales R was about $(2.5–4)\Delta_b$ for big particles and $(3–5)\Delta_b$ for small particles, the anisotropic aspect ratio ϵ was 5 and 7, respectively.

Discrimination of big and small particles in the experimental data was performed in terms of their velocities: During the stages of the lane evolution illustrated in Fig. 1, small particles drift relatively fast with respect to big particles. They gradually slow down and near the center their velocities become too low, so that small and big particles are no longer distinguishable.

(i) Small particles.—We first identified the boundaries of the self-contained big- and small-particle clouds. Then the dynamics and structural evolution of small particles was analyzed in the overlap region (where interpenetration exists). There are two distinct phases characterizing formation and evolution of small-particle lanes [approximately correspond to Figs. 1(a) and 1(b), respectively]: An ''injection stage'' (I) starts at the moment when small particles first penetrate the cloud of big ones. During this phase, the number of small particles for the analysis increases from zero to the average number per slab, and therefore significant fluctuations are possible due to poor statistics. After about 1 s, there is a crossover to a ''steady-state stage'' (II), when the average number of small particles remains constant and the driving force can be considered constant as well. In the simulations the duration of the steady-state phase is sufficiently long (2 s, due to an appropriate choice of the simulation box). In the experiment, however, this phase is 2–3 times shorter, because the driving force and hence the particle velocities decrease as they approach the center of chamber.

The order parameter $S_s(t)$ calculated for small particles is plotted in Fig. 3(a). Although in the beginning of stage I it exhibits significant fluctuations due to poorer statistics, one can see that the formation of small-particle lanes is practically ''instantaneous'' at time scales corresponding to the video frame rate (50 frames/s). The magnitude of the order parameter in the experiment is almost half that of the MD simulation. We believe that this discrepancy is due to the fact that the discrimination procedure allows us to identify only 70%–80% of small particles in the experimental data, which results in an artificial ''thinning'' of the small-particle lanes. Random elimination of 30% small particles in the MD data decreases S_s down to the experimental level, clearly supporting this hypothesis. Figure 3(b) shows the evolution of the global laning angle $\Theta_s(t)$ for small particles, which exhibits narrow dispersion and demonstrates that the ''nematic director'' practically coincides with the driving vector. Note the increasing broadening and deflection of $\Theta_s(t)$ observed in the experiment at the ''steady-state'' stage II [coinciding with a slight decrease in $S_s(t)$], which is related to the convergence of small-particle lanes towards the chamber center as the driving force gradually decreases.

(ii) Big particles.—In order to diminish a possible influence of the boundary effects, we defined fixed regions in the bulk of the big-particle cloud, as indicated in Figs. 1 and 2. In terms of the size and shape, these regions approximately correspond to the ''overlap regions'' used for the analysis of small-particle dynamics.

The evolution of the order parameter and of the global laning angle for big particles is shown in Figs. 3(c) and 3(d), respectively. Initially, there is no anisotropy in the

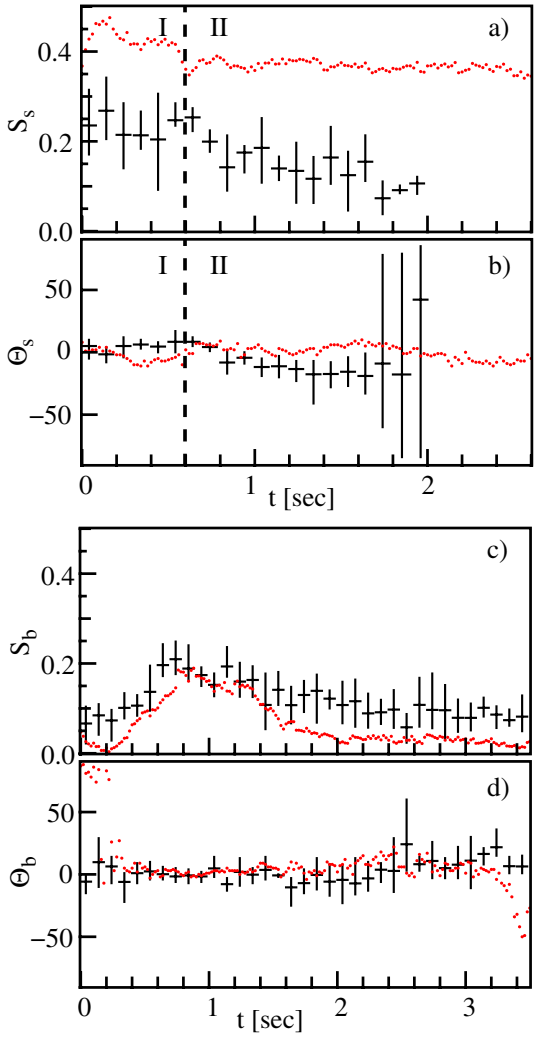

FIG. 3 (color online). Dynamics of laning. Shown are the evolution of the "nematic" order parameter for small and big particles, S_s (a) and S_b (c), respectively, as well as the corresponding global laning angle, Θ_s (b) and Θ_b (d), as obtained from the anisotropic scaling index analysis of the experiment (crosses) and MD simulation (dots). For small particles, injection stage I and steady-state stage II are indicated.

simulation, whereas in the experiment $S_b \simeq 0.05$ and $\Theta_b \to 0$, due to a weak inhomogeneity in the big-particle density. Once the cloud of small particles reaches the fixed region used for the analysis, S_b starts growing and the angular distribution narrows around $\Theta_b = 0$, due to the increasing number of small particles causing the formation of big-particle strings. Then S_b reaches a maximum and starts falling off, reflecting the onset of string relaxation when small particles leave the region. The initial relaxation occurs at a characteristic time scale of ~ 1 s which is an order of magnitude shorter than the self-diffusion time scale for the big particles ($\sim m_b \nu_b \Delta_b^2 / T$). Note that after this rapid relaxation $S_b(t)$ tends to some intermediate plateau, and the laning angle $\Theta_b(t)$ keeps the anisotropy, indicating that the structural relaxation is apparently not complete. This suggests that the ultimate equilibration might involve some metastable states.

Thus, binary complex plasmas provide us with new insights into the dynamical regime of laning—between classic undamped fluids and fully damped colloidal suspensions. By combining the experimental studies and the particle-resolved Langevin simulations, we investigated the dynamical onset of lane formation in driven complex plasmas. Furthermore, we proposed a universal order parameter for the characterization of nonequilibrium phase transitions in driven systems. The approach is based on the anisotropic scaling index analysis that is exceptionally sensitive to symmetry changes occurring in particle ensembles. The use of such a sensitive order parameter is very useful for studying the onset of nonequilibrium phase transitions. In particular, it appears well suited to resolve the principal issue of the order of such phase transitions, characterize possible universality, identify dynamical regimes of structural relaxation, etc. As immediate next steps, one can think of employing the proposed approach to investigate laning in periodically driven [20] and crystalline [21] systems.

We thank J. Dzubiella, R. Monetti, and M. Rex for helpful discussions. This work was supported by DLR/BMWi (Grant No. 50WP0203), SFB TR6, and RFBR (Grant No. 08-02-00444).

[1] D. Helbing, I. J. Farkas, and T. Vicsek, Phys. Rev. Lett. **84**, 1240 (2000).
[2] J. Dzubiella, G. P. Hoffmann, and H. Löwen, Phys. Rev. E **65**, 021402 (2002).
[3] M. E. Leunissen *et al.*, Nature (London) **437**, 235 (2005).
[4] C. Reichhardt and C. J. Olson Reichhardt, Phys. Rev. E **74**, 011403 (2006).
[5] B. Schmittmann and R. K. P. Zia, Phys. Rep. **301**, 45 (1998).
[6] R. R. Netz, Europhys. Lett. **63**, 616 (2003).
[7] M. Rex and H. Löwen, Eur. Phys. J. E **26**, 143 (2008).
[8] G. E. Morfill *et al.*, New J. Phys. **8**, 7 (2006).
[9] V. E. Fortov *et al.*, Phys. Rep. **421**, 1 (2005).
[10] P. K. Shukla and A. A. Mamun, *Introduction to Dusty Plasma Physics* (IOP, Bristol, 2001).
[11] H. M. Thomas *et al.*, New J. Phys. **10**, 033036 (2008).
[12] Droplet formation is governed by different physical mechanisms and will therefore be considered elsewhere.
[13] Movies of the experiment and simulation can be viewed at http://www.mpe.mpg.de/pke/lane-formation/.
[14] V. Land and W. J. Goedheer, New J. Phys. **8**, 8 (2006).
[15] A. V. Ivlev *et al.*, Phys. Plasmas **12**, 092104 (2005).
[16] S. V. Annibaldi *et al.*, New J. Phys. **9**, 327 (2007).
[17] A. V. Ivlev *et al.*, Phys. Rev. Lett. **100**, 095003 (2008).
[18] C. Räth *et al.*, Mon. Not. R. Astron. Soc. **337**, 413 (2002).
[19] C. Räth *et al.*, New J. Phys. **10**, 125010 (2008).
[20] L. Corte *et al.*, Nature Phys. **4**, 420 (2008).
[21] Y. Roichman, V. Wong, and D. G. Grier, Phys. Rev. E **75**, 011407 (2007).

Erratum: Dynamics of Lane Formation in Driven Binary Complex Plasmas [Phys. Rev. Lett. 102, 085003 (2009)]

K. R. Sütterlin, A. Wysocki, A. V. Ivlev, C. Räth, H. M. Thomas, M. Rubin-Zuzic, W. J. Goedheer, V. E. Fortov, A. M. Lipaev, V. I. Molotkov, O. F. Petrov, G. E. Morfill, and H. Löwen

(Received 18 March 2009; published 8 April 2009)

DOI: 10.1103/PhysRevLett.102.149901 PACS numbers: 52.27.Lw, 99.10.Cd

(i) There was a typographical error. The force f_s (acting on the small particles) used in the MD simulations was 0.08 pN.

(ii) Additional simulations with an improved code have resulted in slightly revised optimum fit parameters for the Yukawa interactions: Small-particle charge $Z_s = 4000e$ (corresponding to $Z_b = 11\,000e$) and the screening length $\lambda = 150\ \mu$m. All conclusions remain unchanged, of course.

Lane Formation in Driven Binary Complex Plasmas on the International Space Station

K. Robert Sütterlin, Hubertus M. Thomas, Alexei V. Ivlev, Gregor E. Morfill, Vladimir E. Fortov, Andrey M. Lipaev, Vladimir I. Molotkov, Oleg F. Petrov, Adam Wysocki, and Hartmut Löwen

***Abstract*—We conducted a series of experiments to study lane formation in complex plasma, using the PK-3 Plus Laboratory in the International Space Station. In our experiments, small (driven) microparticles penetrate into a cloud of large (background) particles, revealing a strong tendency toward lane formation: When the driving force is strong enough, particles of both sorts form interpenetrating lines. Typically, the lanes exhibit a considerable anisotropic structural order accompanied by an enhancement of their (unidirectional) mobility. Laning is quantified locally in terms of the anisotropic scaling index. Using a "nematic" order parameter, the observed time-resolved lane-formation process is compared to a set of computer simulations of a binary Yukawa model with Langevin dynamics. This not only yields a best fit but also reveals a strong influence of the initial experimental conditions on the dynamics of lane formation.**

***Index Terms*—Complex plasma, lane formation, non-equilibrium phase transition.**

I. Introduction

THE LABORATORY PK-3 Plus [1] onboard the International Space Station (ISS) allows the research of complex plasmas under microgravity conditions. This research complements the work on the ground and is mandatory for certain precision experiments. Under gravity conditions, the dust is usually pushed into the plasma sheath, where it is levitated by the strong electric field. Thus, the complex plasma is usually compressed and under substantial stress in the direction of the gravitational force. In addition, ions attain huge velocities—even supersonic—in the sheath region, resulting in a very strong ion drag, and the particle interaction potential becomes highly anisotropic.

Manuscript received July 28, 2009. This work was supported in part by DLR/BMWi under Grant 50WP0203, by DFG through the SFB TR6, and by RFBR under Grant 08-02-00444.

K. R. Sütterlin, H. M. Thomas, A. V. Ivlev, and G. E. Morfill are with the Max Planck Institute for Extraterrestrial Physics, 85741 Garching, Germany (e-mail: robert@mpe.mpg.de; thomas@mpe.mpg.de; ivlev@mpe.mpg.de; gem@mpe.mpg.de).

V. E. Fortov, A. M. Lipaev, V. I. Molotkov, and O. F. Petrov are with the Joint Institute for High Temperature of RAS, 125412 Moscow, Russia (e-mail: fortov@ras.ru; lipaev@ihed.ras.ru; molotkov@ihed.ras.ru; ofpetrov@ihed.ras.ru).

A. Wysocki and H. Löwen are with the Heinrich-Heine-Universität Düsseldorf, 40225 Düsseldorf, Germany (e-mail: adam@thphy.uni-duesseldorf.de; hlowen@thphy.uni-duesseldorf.de).

Color versions of one or more of the figures in this paper are available online at http://ieeexplore.ieee.org.

Digital Object Identifier 10.1109/TPS.2009.2035504

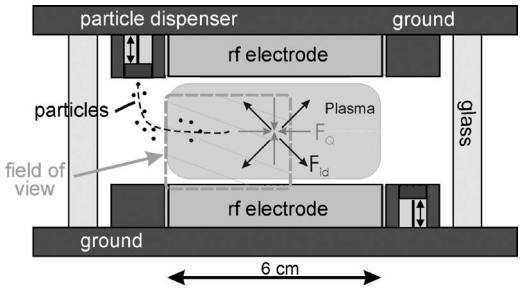

Fig. 1. Three-dimensional sketch of the PK-3 Plus setup. The dashed rectangular box indicates the field of view (see Fig. 2).

PK-3 Plus is the second-generation laboratory on the ISS already. Compared with its precursor PKE-Nefedov, it has advanced hardware and software. Much better diagnostics and a particularly much better homogeneity of the complex plasma allow more detailed investigations. Fig. 1 shows a schematic view of the experimental setup. PK-3 Plus offers a wide variety of parameters. Argon and neon can be used to produce an RF discharge. Neutral gas pressure, i.e., damping, as well as discharge power, can be changed by two orders of magnitude. Particles of six different sizes, from 1.55 to 14.9 μm in diameter, can be injected to form a complex plasma. All these factors are used to tune the details of (inter)particle dynamics. The possibility to resolve single-particle motion in complex-plasma experiments allows fully kinetic analysis.

One investigation, which uses these special features, is lane formation. This phenomenon can be found everywhere in nature when two species of particles are driven against each other. It is a genuine nonequilibrium phase transition [2], which depends on the details of the particle interactions and their dynamics [3], and is of considerable interest in different branches of physics. Lane formation is most commonly known from pedestrian dynamics in highly populated pedestrian zones [4] and also occurs in different systems of driven particles, such as colloidal dispersions [5]–[7], lattice gases [2], and molecular ions [8]. Particle laning in complex plasmas [9] occupies the important intermediate dynamical regime between undamped fluids and fully damped colloidal suspensions [10], [11]: The "atomistic" dynamics associated with the interparticle interaction is virtually undamped, whereas the large-scale (long-term) fluid pattern is determined by friction.

While steady-state lanes have been studied in detail, the dynamical pathway toward the laning is still under debate. PK-3 Plus offers the perfect system to study the dynamics of lane formation [12]. Under microgravity conditions, the

dominant forces (see Fig. 1) are the electrostatic force F_Q arising from an electric potential with a maximum in the center and the ion drag force $F_{\rm id}$. The latter is due to the drift of positive ions along the electric field out from the center and the resulting momentum transfer to the particles. Both these forces depend on particle size and distance from the center. For a given particle size, there is a position, where the net force becomes zero, that defines the equilibrium inner boundary of a complex plasma formed by this particle species. For small particles, this position is closer to the center than for large particles.

For laning experiments, we start by filling almost the whole chamber with large particles that form a stable background. Then, smaller particles are injected from outside. The net force pulls the small particles through the cloud of large particles toward the center of the chamber. Under certain conditions, this penetration appears in lanes, in order to avoid mutual collisions. A series of dedicated experiments was carried out on the ISS. These involved various combinations of "large" and "small" monodisperse particles (2.55-, 6.8-, 9.2-, and 14.9-μm diameters for large particles and 1.55-, 2.55-, and 3.4-μm diameters for small particles), with different neutral gases and pressures (argon between 10 and 60 Pa and neon at 60 Pa to control the friction rate) and for different RF discharge powers (to control the screening length and, accordingly, the particle interaction).

II. Experiments

In this paper, we analyze experiments at a pressure of 30 Pa using a background complex plasma formed by large 9.2-μm-diameter particles. The particles are illuminated by a thin laser sheet of $\simeq$0.35 mm.[1] The scattered light is recorded under 90 $^\circ$ using a 50-frames/s PAL progressive-scan CCD camera. Experimental conditions keep the background in a liquid state. In addition, large-scale vortex motion, with a period of a few minutes, is constantly mixing the background particles [13]. Into this, a single short burst of small particles with 3.4-μm diameter is injected in plane with the illumination.

Fig. 2 shows an overlay of consecutive frames highlighting the lanes formed by small particles while they penetrate the cloud of large particles. Closer inspection reveals that the mostly inert large particles are combed into lanes, too. Thereby, small and large particles form an array of interpenetrating strings. After the small particles have passed by, the strings formed by large particles slowly dissolve.

For a full kinetic analysis of the development of lanes, the trajectories of all visible particles were extracted from the images. This is particularly difficult for the small particles. First, they scatter less light than the large particles. Second, they are quite fast, particularly before entering the background, leaving long (small particles travel interparticle distances of the background cloud per frame) and very faint traces on the images. Third, the small particles are scattered violently in collisions with large particles, often out of the illuminated volume. Standard

[1]We see just a thin layer of particles around the center of the chamber. There are 3000–4000 illuminated particles in the field of view, while the whole system consists of about half a million of particles.

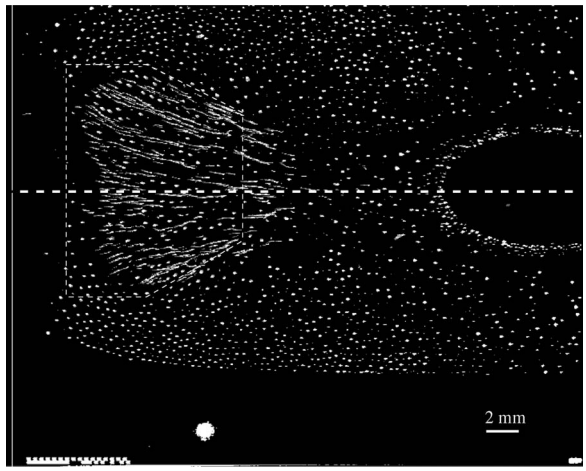

Fig. 2. Lane formation in complex plasmas. A short burst of small (3.4-μm) particles is injected into a cloud of large (9.2-μm) background particles. Small particles are driven toward the center, forming lanes. The particles are illuminated by a thin laser sheet of $\simeq$0.35 mm. The picture is a superposition of consecutive images: The fast small particles can be identified as long tracks, and the inert large particles look like points. One can clearly see that also the large particles are arranged into lanes. The dashed line indicates the midplane of the PK-3 Plus chamber, and the dashed box marks the measurement area for lane formation of large particles (see Section IV-A-1).

tracking algorithms that first find objects in single frames and then try to identify objects in consecutive frames are unable to track the small particles. For this paper, we had to develop a different tracking algorithm. Particles are identified by the complete light curve that they leave in the movie. These light curves are processed carefully to make sure that one curve is produced by exactly one particle. To these light curves, a simple model—cubic splines—of particle motion is fitted to extract particle position, velocity, and acceleration at each time step.

After extracting the full kinetic information, particles are sorted by their velocities into two groups. Particles moving toward the center with large-enough velocity are considered to be small. All other particles are considered to be large. This proves to be a very good selection algorithm, providing no false positives, i.e., large particles wrongly identified as small. Unfortunately, this criterion results in 30% false negatives, i.e., small particles wrongly identified as large.

III. Data Analysis

To quantify lane formation in terms of nonequilibrium phase transitions, we need a suitable order parameter. The local anisotropy of lanes lends itself to using the anisotropic scaling index method [14]. On top of this local measure, we define a global "nematic" order parameter. To calibrate our measures and to get some insight into experimental parameters that are not directly measurable, we resort to numerical simulations.

A. Anisotropic Scaling Index

The scaling index $\alpha = \partial \log \rho(\mathbf{r}_i, R)/\partial \log R$ is the logarithmic derivative of a local density $\rho(\mathbf{r}_i, R) = \sum_{j=1}^{N} s(d_{ij}/R)$ for a set of points $\{\mathbf{r}_i\}, i = 1, \ldots N$. s is a certain shaping function,

and d_{ij} is a distance measure. We use $s = \mathrm{e}^{-(d_{ij}/R)^2}$ which gives

$$\alpha(\mathbf{r}_i, R) = \frac{2\sum_{j=1}^{N}(d_{ij}/R)^2 \mathrm{e}^{-(d_{ij}/R)^2}}{\sum_{j=1}^{N}\mathrm{e}^{-(d_{ij}/R)^2}}. \quad (1)$$

$\alpha(\mathbf{r}_i, R)$ determines the dimensionality of the point distribution around $\mathbf{r}_i$ in a vicinity defined by the scale R. For example, $\alpha(\mathbf{r}_i, R) \simeq 1$ means that the local structure is close to a straight line. The spatial scale R is an important mesoscopic measure of the local environment. In the range of relevant scales, α is practically independent of R.

To define the anisotropic scaling index, we use a "stretch metric" for the distance measure d_{ij}: Given a direction $\mathbf{u}$ and the relative stretching of two principal axes $\epsilon(>1)$

$$d_{ij} = \sqrt{((\mathbf{r}_i - \mathbf{r}_j)\cdot\mathbf{u})^2 + (\epsilon\,(\mathbf{r}_i - \mathbf{r}_j)\cdot\mathbf{u}_\perp)^2}. \quad (2)$$

In 2-D, the metric is determined by ϵ, and the direction $\mathbf{u} = (\cos\theta, \sin\theta)$, $\mathbf{u}_\perp = (\sin\theta, -\cos\theta)$. The anisotropic scaling index $\alpha(\mathbf{r}_i, R, \epsilon, \theta)$ is derived directly from (1).

The anisotropic scaling index will become more sensitive to perfectly aligned structures as ϵ gets larger. ϵ can initially be guessed between two and ten. To select the optimal ϵ for a given problem, similar to determining the optimal mesoscopic scale R, one does a multiscale analysis. Then, one searches for a range of ϵ where α is stable and shows a significant dependence on θ. If such an ϵ cannot be found, the local structure is not anisotropic.

B. Nematic Order Parameter

Using the anisotropic scaling index method, we associate each point $\mathbf{r}_i$ with the unit vector $\mathbf{u}_i$ in the "preferred" direction of the local anisotropy, as determined by the angle θ_i at which the "anisotropic contrast" $\alpha(\mathbf{r}_i, R, \epsilon, \theta_i + \pi/2) - \alpha(\mathbf{r}_i, R, \epsilon, \theta_i)$ is maximized.[2] For each point, we define a corresponding rod with the direction $\mathbf{u}_i$.

The global laning on a 2-D plane can be characterized with the second-rank tensor $Q_{\alpha\beta} = 2N^{-1}\sum_{i=1}^{N}\mathbf{u}_i \otimes \mathbf{u}_i - \delta_{\alpha\beta}$ analogous to that used to quantify the order of the nematic phase. The largest eigenvalue of $Q_{\alpha\beta}$ defines the laning-order parameter S, with $S = 1$ for a perfect alignment and $S = 0$ for a disordered phase. The corresponding eigenvector ("nematic director") $\langle\mathbf{u}\rangle$ defines the direction of the global laning, and the global laning angle via $\cos\Theta = \langle\mathbf{u}\rangle \cdot \mathbf{e}_x$.

C. Numeric Simulations

To complement our complex-plasma experiments, we used two independent numerical simulations. First, a 2-D simulation of the PK-3 Plus discharge chamber using a plasma fluid code (described in [15], where dust was also treated as a fluid species), providing self-consistent coupling of dust species to the discharge plasma. This provided us with parameters of the discharge plasma, such as plasma density, electron temperature, and electric fields. For the background complex plasma, this simulation also suggested that the cloud of large particles is "self-confined" at its edges due to the self-consistent plasma field (cf. [15, Fig.13]), whereas inside the cloud, the electric and ion drag forces practically compensate each other. For the small particles, it predicted a nonzero net force inside the background: For the experiment discussed here, a force of $f_s = 0.08$ pN pushing a small particle toward the center is predicted by the simulation.

[2]By definition, the directions $\mathbf{u}_i$ and $-\mathbf{u}_i$ are equivalent, so that we consider the range $-\pi/2 \le \theta_i \le \pi/2$.

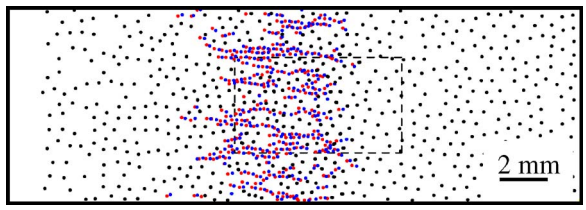

Fig. 3. Lane formation in MD simulation corresponding to the experiment shown in Fig. 2. The simulation is fully 3-D. To get highest similarity between experimental and simulation data, the latter are cut in slices of 0.366-mm width, which are analyzed individually. The dashed box marks the measurement area for lane formation of large particles (see Section IV-A-1).

Second, we input these results (and measurements of previous experiments [16]) in a particle-resolved molecular-dynamics (MD) simulation performed on the Langevin level [17] for a binary mixture of 5759 small and 12 287 large particles (cf. Fig. 3). Whereas the 2-D plasma fluid code mainly provided us with experimental parameters that cannot be measured in PK-3 Plus onboard the ISS, the 3-D MD simulation was used to calibrate our local structure measures and global order parameter. Unlike in the experiment, we can directly control all parameters defining particle interaction individually and independently. Additionally initial conditions, particularly relaxation time before the injection, can be varied. Comparing the measurements of different simulations allows us to identify the most important players in the dynamics of lane formation. The divergence from measurements of the experimental data allows us to separate the influence of coupled parameters, e.g., particle charge and screening length, that define the interparticle potential.

There are three main differences between the MD simulation and the experiment. First, the experiment has a cylindrical symmetry, where the simulation is perfectly uniaxial. Second, the complex plasma is externally confined on all surfaces in three dimensions, and the small particles penetrate only ∼1/10 of the background, where the simulation only has surfaces in x-direction and periodic boundary conditions in y- and z-directions and the small particles penetrate the whole background. Third, the interaction potential of particles in the experiment is *generally considered* to be of Yukawa type, where the interaction potential in the simulation is *defined* to be Yukawa.

In the experiments, the cylindrical configuration leads to lane formation pointing toward the center of the chamber, as can be seen from Fig. 2. This makes the detection of global laning more difficult in the experiment than in the simulation. The individual lanes also merge with each other, finally forming a blob or droplet of small paticles that moves collectively through the background formed by large particles. This basically limits the time during which laning can be investigated in the experiment.

The background complex plasma in the experiment can easily adjust to the "missing volume" filled by the small particles, changing its shape and volume by rearranging its outer boundary. In the simulation, we have periodic boundary conditions in y- and z-directions. Therefore, we cannot reproduce any density gradients present in the experiment. Furthermore, volume adjustments are only possible by changing the x-size of the large-particle complex plasma. Comparing the motion of the free large particles—i.e., those not in contact with small particles—these perform circular motion in the experiment, while they are pushed in the x-direction away from the bulk of small particles in the simulation.

The real interaction potential of microparticles in a complex plasma is still under discussion. Even though there are several theories proposing non-Yukawa particle interaction potential, experiments, so far, were unable to distinguish between the real potential and purely Yukawa type within experimental errors. Current high-precision experiments on the ISS will allow to discriminate different theoretical models and will give more accurate measurements on the real interaction potential. We specifically used the generally assumed Yukawa-type interaction potential for the simulations as it is agnostic to particle species and, thus, neutral in terms of collective effects such as self-organization.

All differences in the simulation were chosen to remove as many side effects as possible to allow for clear interpretation of the analysis and easy separation of the influence of external parameters while still allowing tuning to relevant experimental conditions.

IV. Results

To get the "best fit" numerical simulations, we first put all measured variables of the experiment, geometries, and all relevant physics into our simulations and use theoretical estimates to get the most faithful representation of experimental conditions.

There are basically only two free parameters left to tune the simulation: 1) the decomposition of the coupling parameter Γ into particle charge and screening length and 2) the initial state of the background complex plasma, into which the smaller particles are injected. In principle, the initial state of the small particles could also have some influence. In our case, due to the much bigger inertia of the background particles, there is no influence, as all structural order in the cloud of injected small particles is completely lost upon impact.

First, we compare the best fit simulations to the actual experimental data. Second, using the possibilities of numeric experiments, we investigate the influence of initial conditions on the dynamics of lane formation and verify our choices for particle charge and screening length, which cannot be measured directly in the experiment.

A. Best Fit of Simulations and Experiment

As explained in Section III-C, we used measurements of previous experiments for the particle charge of small particles $Q_s = -4000e$, and the charge of large particles is derived by the size ratio to be $Q_L = -11\,000e$. The screening length is calculated from the plasma density as given by the plasma fluid code $\lambda = 150\ \mu$m.

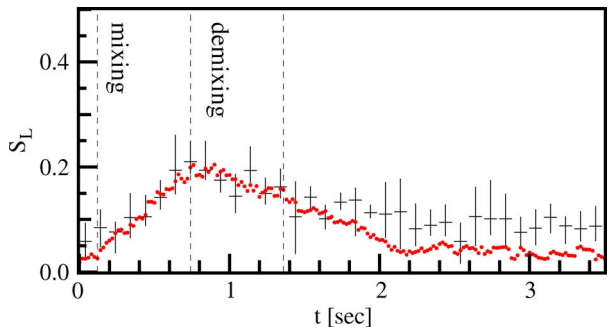

Fig. 4. Evolution of the nematic order parameter for large particles S_L, as obtained from the anisotropic scaling index analysis of the (crosses) experiment and (dots) MD simulation. The dashed lines highlight the time it takes small particles to fill (mixing) and then leave (demixing) the measurement area where S_L is determined (cf. Figs. 2 and 3).

1) Large Particles: For the analysis of laning in the cloud of large particles, a fixed measurement box (cf. Figs. 2 and 3) well within the cloud was used, both for experiments and simulations. This is necessary to remove the edge effects of the scaling index method and, in the case of experiments, to remove unaffected parts of the cloud from statistics.

To analyze the dynamics of laning in the background complex plasma using anisotropic scaling index, we used a stretching of $\epsilon = 5$ and a spatial scale $R = 1200\ \mu$m.

A comparison of the temporal evolution of lanes in the background complex plasma between experiment and best fit simulations is shown in Fig. 4. The important features are the initial nonzero value of the order parameter for the experimental data, the rise and fall times, the nonvanishing "final" value of the order parameter, and the continuous variation of the order parameter.

Initially, there is no anisotropy in the simulation data, but still, the experiment already shows some nonzero initial value of the order parameter. This results from a density gradient in the experimental data, which is not present in the simulation.

The rise time is basically identical to the mixing time, i.e., the time necessary for the small particles to completely fill the measurement box. That means that, within the temporal resolution of the experiment, lanes in the background complex plasma are formed "immediately" by the small particles streaming through it. This can also be confirmed visually: Stream lines once formed do not evolve (or improve) while more small particles stream through.

The fall time consists of three parts. First is the demixing time needed for the last small particles to leave the measurement box. As the small-particle velocity is almost constant, this time is basically identical to the mixing time. One sees immediately that lanes in the background cloud persist after the small particles are gone. Second, these lanes decay at a characteristic timescale of $\sim$1 s (which is much slower than would be expected from the self-diffusion timescale $\sim m_L \nu_L \Delta_L^2 / T$).[3] Third, after this fast relaxation, $S_L(t)$ stays

[3]With mass m_L, friction constant ν_L, mean particle separation Δ_L, and thermal energy of the dust particles T.

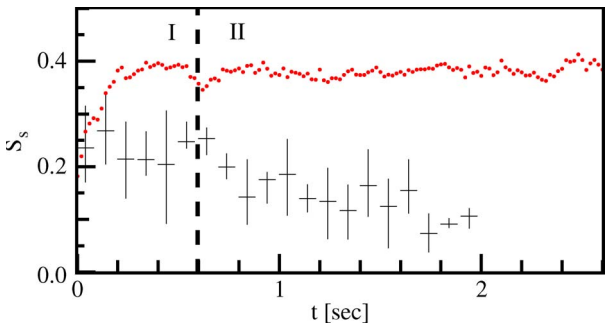

Fig. 5. Evolution of the nematic order parameter for small particles S_s, as obtained from the anisotropic scaling index analysis of the (crosses) experiment and (dots) MD simulation. Injection stage I and steady-state stage II are indicated. For the experiment, we cannot analyze lanes for more than 2 s, because particles approach the center of the chamber where the driving force vanishes.

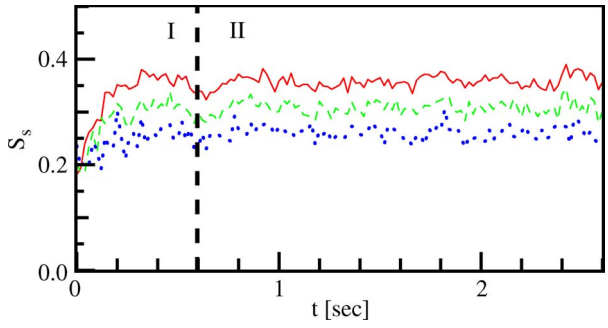

Fig. 6. Influence of random thinning of the simulation data on the value of S_s. The order parameter is decreasing with increased thinning fraction: (solid line) 10%, (dashed) 30%, and (dotted) 50%.

on some intermediate plateau, indicating that the structural relaxation is not complete. Thus, the process of complete relaxation might involve metastable states.

Therefore, the results point at a continuous second-order phase transition.

2) Small Particles: Similar to the large particles aforementioned, we did not take all small particles into account for the analysis. Only small particles within the cloud of large particles are considered. This is necessary for the experimental data, as here, small particles outside the cloud of large particles are either completely out of the field of view or much too fast to be detected in the movie. In Fig. 5, the evolution of $S_s(t)$ is divided in two parts, the first being the injection of the cloud of small particles into the background where the number of particles taken into account is increasing and the second part being the steady state when the small particles are all embedded within the cloud of large particles.

We used a stretching of $\epsilon = 7$ and a spatial scale $R = 2200$ μm for the detection of lanes formed by small particles. Unlike the large particles, the formation of lanes in small particles, i.e., $S_s(t)$ (cf. Fig. 5), has no rise or fall times (at least for the simulation). For the experimental data, we might derive a slight but steady decay of the order parameter (cf. Section IV-B2). In addition, the order parameter seems to indicate much lower structural ordering for experimental data than for the simulations (see Section IV-B1).

The order parameter S_s has a high value from the very beginning, initially varying strongly due to statistical fluctuations as the number of particles analyzed is rising from zero to a few hundreds.

This means that small particles entering the cloud of large particles are immediately—i.e., on the order of the time resolution of the experiment or faster—sorted into lanes or enter into channels created by earlier small particles. As they are very fast during initial impact, lanes are created within the first few interparticle distances of the background complex plasma.

B. Optimizing Simulation Parameters

1) Artificial Thinning: For experimental data, the order parameter of small particles S_s is suppressed compared with the simulation data. This is mainly an effect of the dynamical cuts applied to the experimental data for the selection of small particles. As explained in the description of the experiment (see Section II), we lose a substantial number of small particles from the analysis, which influences the anisotropic scaling index of the small particles and hinders efficient detection of lanes. Fig. 6 shows the influence of the random "thinning" of the simulation data for small particles, leading to a systematic decrease of the nematic order parameter.

2) Particle Charge: Not all parameters of the simulation could be fixed by measurements or derived with high accuracy from theory or simulation. In particular, the particle charge and the screening length have substantial error margins.

In the MD numerical simulation, we can change particle charge and screening length individually and independently. For this paper, we vary them in such a way that the resulting coupling parameter Γ stays constant,[4] i.e., without changing the phase of the background. Thus, changes in dynamical behavior indicate which set of parameters is closest to the experimental conditions. We consider three parameter sets.

- $Q^0\lambda^0$: The best fit, derived from measurements, using plasma parameters from the 2-D fluid code and tuning the MD simulation to give the same kinematics, i.e., velocity distribution, as the experiment. Here, small particles have a charge of $Q_s^0 = -4000e$, large particles have $Q_L^0 = -11\,000e$, and the screening length $\lambda^0 = 150$ μm. This is represented by a solid line in the plots of Fig. 7.
- $Q^+\lambda^-$: Particle charge is increased $Q_s^+ = -8278e$ and $Q_L^+ = -25\,100e$. The screening length is decreased appropriately to $\lambda^- = 100$ μm. Plotted with dashed line.
- $Q^-\lambda^+$: Here, particle charge is lower $Q_s^- = -3000e$ and $Q_L^- = -8117e$, whereas the screening length $\lambda^+ = 182$ μm is longer. Represented by a dotted line.

There are two main differences: (a) the velocity distribution and mobility of the small particles within the cloud of large particles and (b) the characteristics of lane formation for small and large particles.

a) The mobility of small particles within the background cloud strongly depends on the dynamics of the large particles. Here, $Q^0\lambda^0$ provides the highest mobility.

[4]It is defined as $\Gamma = (Q^2/T\Delta)\mathrm{e}^{-\kappa}$, with particle charge Q, mean particle separation $\Delta = n^{-1/3}$ in terms of the particle number density n, lattice parameter $\kappa = \Delta/\lambda$, screening length λ, and thermal energy of the dust particles T.

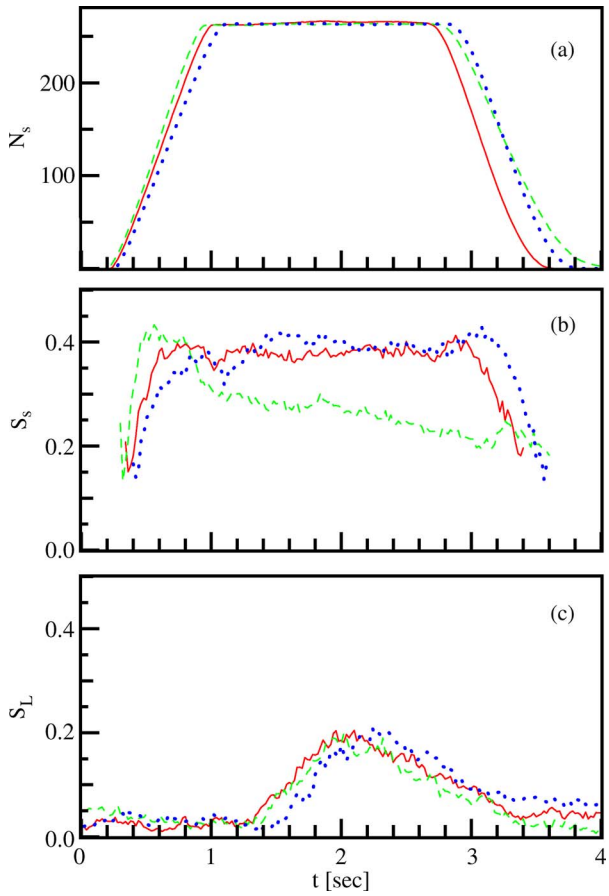

Fig. 7. Influence of particle charge and screening length on the dynamics of lane formation. The charge and screening length are varied in the MD simulations, so that the coupling parameter Γ is kept constant. (Solid) $Q^0\lambda^0$: $Q_s^0 = -4000e$, $Q_L^0 = -11\,000e$, and $\lambda^0 = 150$ μm. (Dashed) $Q^+\lambda^-$: $Q_s^+ = -8278e$, $Q_L^+ = -25\,100e$, and $\lambda^- = 100$ μm. (Dotted) $Q^-\lambda^+$: $Q_s^- = -3000e$, $Q_L^- = -8117e$, and $\lambda^+ = 182$ μm. Shown are (a) the number of small particles inside the background cloud of large particles and the temporal evolution of the order parameter for (b) small and (c) large particles.

Comparing the mobility and velocity distribution of the three simulations to the experimental results, $Q^0\lambda^0$ represents the particle dynamics most faithfully; thus, it is called best fit.

b) $Q^0\lambda^0$ is able to reproduce the dynamics of laning measured in the experiment fairly well, particularly for the large particles. In the case of $Q^+\lambda^-$, the lanes formed by small particles during injection slowly decay while they propagate through the background cloud. The experimental data might hint to such a trend (see Fig. 5), indicating that we could have underestimated particle charge or did not choose a perfect coupling parameter. Yet, the evolution of S_L is lacking the plateau. This plateau and also all timescales of the formation of lanes in large particles are very well reproduced by $Q^-\lambda^+$, which is slightly better even than by the best fit. For small particles, this parameter set shows a slow increase of the order parameter during injection which is not at all supported by experimental data.

It is obvious that dynamics of lane formation depend very sensitively on complex-plasma properties. More variations of particle charge and coupling parameter must be investigated using MD simulations to better identify which aspects of the dynamics of lane formation are influenced by specific parameters.

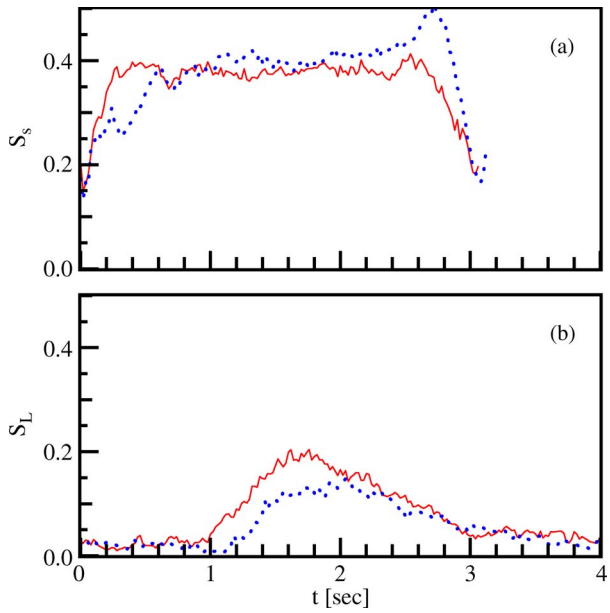

Fig. 8. Initial conditions influence lane formation. Small particles are injected into a background of large particles that has (solid line) just been thermally equilibrated for 2 s, as compared with (dots) an almost fully crystalline background. Shown is the temporal evolution of the laning-order parameter for (a) small and (b) large particles.

3) Initial Conditions: The main influence of initial conditions on the results is through the spatial configuration and phase state of the large particle cloud before the small particles are injected.

For the best fit parameter set, we let the numerical simulations equilibrate the background complex plasma for 2 s. This removes all initial heat, induced by the random initial positions and velocities, from the system. However, the system still contains lots of internal energy and is far from a crystalline state. As far as we can tell, this portrays the experimental conditions very well. We compare this configuration to numerical simulations that equilibrate the background for 1000 s. After such a long time, the system is, except for the center, in a crystalline state, close to its minimal energy configuration. The large particles form layers parallel to the external confinement.

Fig. 8 shows the main differences in dynamic behavior. First of all, in the case of an almost crystalline background, S_s rises slowly during the injection of small particles into the background of large particles, reaching its steady state only after all small particles are inside the background cloud. Moreover, as can be seen from Fig. 8(b), the mobility of small particles is much lower, reaching the measurement area at a later time. The large particles are much less influenced by the passage of small particles, resulting in a lower peak value of S_L. Interestingly, the decay of lanes in the background media is basically unmodified from what we see in the best fit data set. Even though the large particles do not reach the same level of laning order, the processes of decay of local structure are not influenced much by the (initial) state or internal energy of the large particle cloud. Still it seems that there is no—or a much lower—plateau in the decay of large particle lanes for the

crystalline background. (This might be because equilibration of local order is not going to a generic liquid state but to an already quite well-defined layered crystalline structure.) The peak in $S_s(t)$ evolution (at about $t = 2.8$ s), when the small particles leave the cloud of large particles, indicates that the later batches of small particles are better aligned than the forerunners (which would be in agreement with the difficulty of forming lanes during injection).

V. Conclusion and Outlook

Binary complex plasmas provide us with new insights into the dynamical regime of laning—between classic undamped fluids and fully damped colloidal suspensions. By combining the experimental studies and the particle-resolved Langevin simulations, we have investigated the dynamical onset of lane formation in driven complex plasmas. The use of a very sensitive order parameter proved valuable in studying the onset of these nonequilibrium phase transitions and in distinguishing the influence of different complex-plasma parameters on the dynamics of lane formation. We will continue to analyze more experiments and perform a full parameter scan using MD simulations, particularly to investigate laning in periodically driven [18] and crystalline [19] systems.

Acknowledgment

The authors would like to thank G. Joyce for his support in preparing this manuscript and C. Räth for the helpful discussions.

References

[1] H. M. Thomas, G. E. Morfill, V. E. Fortov, A. V. Ivlev, V. I. Molotkov, A. M. Lipaev, T. Hagl, H. Rothermel, S. A. Khrapak, R. K. Suetterlin, M. Rubin-Zuzic, O. F. Petrov, V. I. Tokarev, and S. K. Krikalev, "Complex plasma laboratory PK-3 Plus on the International Space Station," *New J. Phys.*, vol. 10, p. 033036, Mar. 2008.

[2] B. Schmittmann and R. K. P. Zia, "Driven diffusive systems. An introduction and recent developments," *Phys. Rep.*, vol. 301, no. 1–3, pp. 45–64, Jul. 1998.

[3] M. Rex and H. Löwen, "Influence of hydrodynamic interactions on lane formation in oppositely charged driven colloids," *Eur. Phys. J. E*, vol. 26, no. 1/2, pp. 143–150, May/Jun. 2008.

[4] D. Helbing, I. J. Farkas, and T. Vicsek, "Freezing by heating in a driven mesoscopic system," *Phys. Rev. Lett.*, vol. 84, no. 6, pp. 1240–1243, Feb. 2000.

[5] J. Dzubiella, G. P. Hoffmann, and H. Löwen, "Lane formation in colloidal mixtures driven by an external field," *Phys. Rev. E, Stat. Phys. Plasmas Fluids Relat. Interdiscip. Top.*, vol. 65, no. 2, p. 021402, Feb. 2002.

[6] M. E. Leunissen, C. G. Christova, A.-P. Hynninen, C. P. Royall, A. I. Campbell, A. Imhof, M. Dijkstra, R. van Roij, and A. van Blaaderen, "Ionic colloidal crystals of oppositely charged particles," *Nature*, vol. 437, no. 7056, pp. 235–240, Sep. 8, 2005, DOI:10.1038/nature03946 Letter.

[7] C. Reichhardt and C. J. Olson Reichhardt, "Cooperative behavior and pattern formation in mixtures of driven and nondriven colloidal assemblies," *Phys. Rev. E, Stat. Phys. Plasmas Fluids Relat. Interdiscip. Top.*, vol. 74, no. 1, p. 011403, Jul. 2006.

[8] R. R. Netz, "Conduction and diffusion in two-dimensional electrolytes," *Europhys. Lett.*, vol. 63, no. 4, pp. 616–622, Aug. 2003.

[9] G. E. Morfill, U. Konopka, M. Kretschmer, M. Rubin-Zuzic, H. M. Thomas, S. K. Zhdanov, and V. Tsytovich, "The 'classical tunnelling effect'—Observations and theory," *New J. Phys.*, vol. 8, p. 7, Jan. 2006.

[10] V. E. Fortov, A. V. Ivlev, S. A. Khrapak, A. G. Khrapak, and G. E. Morfill, "Complex (dusty) plasmas: Current status, open issues, perspectives," *Phys. Rep.*, vol. 421, no. 1/2, pp. 1–103, Dec. 2005.

[11] P. K. Shukla and A. A. Mamun, *Introduction to Dusty Plasma Physics*. Bristol, U.K.: IOP, 2001.

[12] K. R. Sütterlin, A. Wysocki, A. V. Ivlev, C. Räth, H. M. Thomas, M. Rubin-Zuzic, W. J. Goedheer, V. E. Fortov, A. M. Lipaev, V. I. Molotkov, O. F. Petrov, G. E. Morfill, and H. Löwen, "Erratum: Dynamics of lane formation in driven binary complex plasmas," *Phys. Rev. Lett.*, vol. 102, no. 14, p. 149 901 (E), Apr. 2009.

[13] M. Rubin-Zuzic, H. M. Thomas, S. K. Zhdanov, and G. E. Morfill, "Circulation' dynamo in complex plasma," *New J. Phys.*, vol. 9, p. 39, Feb. 2007.

[14] C. Räth, W. Bunk, M. B. Huber, G. E. Morfill, J. Retzlaff, and P. Schuecker, "Analysing large-scale structure—I. Weighted scaling indices and constrained randomization," *Mon. Not. R. Astron. Soc.*, vol. 337, no. 2, pp. 413–421, Dec. 2002.

[15] V. Land and W. J. Goedheer, "Effect of large-angle scattering, ion flow speed and ion-neutral collisions on dust transport under microgravity conditions," *New J. Phys.*, vol. 8, p. 8, Jan. 2006.

[16] S. V. Annibaldi, A. V. Ivlev, U. Konopka, S. Ratynskaia, H. M. Thomas, G. E. Morfill, A. M. Lipaev, V. I. Molotkov, O. F. Petrov, and V. E. Fortov, "Dust-acoustic dispersion relation in three-dimensional complex plasmas under microgravity," *New J. Phys.*, vol. 9, p. 327, Sep. 2007.

[17] A. V. Ivlev, S. K. Zhdanov, B. A. Klumov, and G. E. Morfill, "Generalized kinetic theory of ensembles with variable charges," *Phys. Plasmas*, vol. 12, no. 9, p. 092104, Sep. 2005.

[18] L. Corté, P. M. Chaikin, J. P. Gollub, and D. J. Pine, "Random organization in periodically driven systems," *Nat. Phys.*, vol. 4, no. 5, pp. 420–424, May 2008.

[19] Y. Roichman, V. Wong, and D. G. Grier, "Colloidal transport through optical tweezer arrays," *Phys. Rev. E, Stat. Phys. Plasmas Fluids Relat. Interdiscip. Top.*, vol. 75, no. 1, p. 011407, Jan. 2007.

K. Robert Sütterlin was born in Munich, Germany, in 1969. He received the Diploma degree in physics from the Ludwig-Maximilians-Universität München, Munich, in 1998. He is currently working toward the Ph.D. degree at the Max Planck Institute for Extraterrestrial Physics, Garching, Germany.

Since 2001, he has been a Project Scientist for the PKE-Nefedov and PK-3 Plus experiments. His research interests are complex plasmas, nonlinear effects, and data analysis.

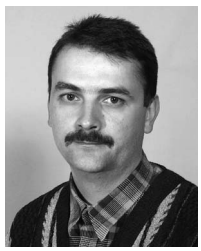

Hubertus M. Thomas was born in Cologne, Germany, in 1965. He received the Diploma degree from the University of Cologne, Cologne, Germany, in 1992 and the Ph.D. degree from the Ludwig-Maximilians-Universität München, Munich, Germany, in 1996.

Since 1992, he has been with the Max Planck Institute for Extraterrestrial Physics, Garching, Germany. He is the Scientist responsible for the complex-plasma projects PKE-Nefedov and PK-3 Plus, the first- and second-generation laboratories, respectively, operated on the International Space Station since 2001. He is leading the research group "Experimental Complex Plasmas." He is the author of more than 90 publications. His research interests are low-temperature plasmas and complex plasmas.

Alexei V. Ivlev was born in Chernogolovka, Russia, in 1971. He received the M.Sc. degrees in physics as well as in applied mathematics and the Ph.D. degree in physics from Moscow State Technical University, Moscow, Russia, in 1993 and 1997, respectively.

In 1994, he was a Research Fellow with the High Energy Density Research Center, Moscow, and since 1998, he has been with the theory group of the Max Planck Institute for Extraterrestrial Physics, Garching, Germany, where he currently holds the position of Senior Scientist. He is the author of more than 100 scientific papers. His research interests are in the fields of complex plasmas, astrophysical plasmas, and soft matter.

Gregor E. Morfill was born in Oberhausen, Germany, in 1945. He received the B.Sc. degree in physics and the Ph.D. degree in space plasma physics from Imperial College, London, U.K., in 1967 and 1970, respectively, and the Honorary Doctorate degree from the Technical University of Berlin, Berlin, Germany, in 2003.

Since 1984, he has been the Director of the Max Planck Institute for Extraterrestrial Physics, Garching, Germany. He also holds honorary professorships with the University of Leeds, Leeds, U.K., and the University of Arizona, Tucson. He is the author of more than 500 scientific papers. His present scientific interests are mostly focused on complex (dusty) plasmas, astrophysical plasmas, and plasma applications in medicine.

Prof. Morfill is a foreign member of the Russian Academy of Sciences. He is the recipient of a number of important prizes, including the Patten Prize, Bavarian Innovation Prize, Wissenschaftpreis of the German "Stifterverband," Gagarin Medal, Ziolkowski Medal, etc.

Vladimir E. Fortov was born in Moscow, Russia, on January 23, 1946. He received the M.Sc. degree and the Ph.D. degree in strongly coupled plasma physics from the Moscow Institute of Physics and Technology, Moscow, in 1968 and 1971, respectively, and the Ph.D. degree in "physics of strongly coupled plasma generated by intense shock waves" and the Professor's degree in physics and chemistry from the Russian Academy of Sciences (RAS), Moscow, in 1976 and 1978.

He performed pioneering experimental investigations on physical properties of hot dense matter at megabar pressure range. He carried out the new and detailed measurements of the physical properties of strongly coupled plasmas with strong interparticle interactions. He has made key contributions to the understanding and expanded knowledge of the basic properties of matter under extreme conditions. Since 1978, he has been the Director of the Institute for High Energy Density, RAS. He was also the Head of Laboratory of the Institute of Chemical Physics, RAS, and then the Department Head of the Institute. He was appointed Professor of chemical physics and plasma physics in 1978. In 1987, he became a Corresponding Member of USSR Academy of Sciences, where he became a member in 1991. In the same year, he was appointed Professor of High Energy Density Physics and the Chief of the Chair of the Moscow Institute of Physics and Technology, Dolgoprudny, Russia. Since 2007, he has been the Director of the Joint Institute for High Temperature, RAS.

Dr. Fortov has been a member of the European Academy of Sciences, Arts and Letters (Paris, France; since 1998), Academia Europaea (London, U.K.), International Academy of Astronautics (since 2000), and Max Plank Society (since 2000); a Fellow of the American Physical Society (since 2001); a Foreign Member of the National Academy of Engineering (USA, since 2002); and a Foreign Fellow of the Royal Engineering Academy (U.K., since 2003) and the Royal Academy of Engineering Sciences (Sweden, since 2004). He is the recipient of numerous prestigious international awards, including the A. P. Karpinsky–Toepfer Scientific Award in physics and chemistry (1997); the P. Bridgeman Prize for Achievements in High Pressure Physics and Chemistry (1999); the A. Einstein Medal of UNESCO for Scientific Achievements (2000); the Max-Plank Award in Physics for Pioneering Investigations of Strongly Coupled Plasmas (2002); the Alfven Prize in Plasma Physics for Outstanding Research of High Energy Density Plasmas (2003); the APS Prize in Shock Compression Science for Pioneering Research in High Energy Density Physics (2005); the A. Einstein Gold Medal of UNESCO for Achievements in Science and International Collaboration (2005); the Order of Merit of the Federal Republic of Germany (Bundesverdienstkreuz) for Achievements in Science and Collaboration with German Researchers (2006); the Honoured Legion Order, France (2006); and the GlassMemory Award for Achievements in Shock Wave Science from Nagoya University, Japan (2009).

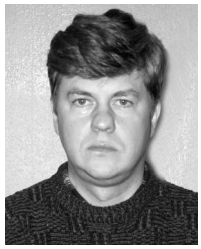

Andrey M. Lipaev received the Ph.D. degree in plasma physics from the Joint Institute for High Temperatures, Russian Academy of Sciences, Moscow, Russia.

He is currently a Senior Research Scientist with the Joint Institute for High Temperatures. He is the author of more than 30 refereed papers. His research interests include experimental investigations of strongly coupled complex plasmas, particularly the phenomena in complex plasmas under microgravity conditions.

Dr. Lipaev has participated in many plasma physics conferences.

Vladimir I. Molotkov received the Ph.D. degree in plasma physics and chemistry from the Joint Institute for High Temperatures, Russian Academy of Sciences (RAS), Moscow, Russia.

He is currently the Head of the Gas Discharge Dusty Plasma Laboratory, Joint Institute for High Temperatures. He is the author of more than 50 refereed papers. His current research interests include strongly coupled dusty plasmas and experimental studies of complex-plasma phenomena under microgravity conditions.

Dr. Molotkov has participated in many conferences on plasma physics.

Oleg F. Petrov was born in Yevpatoria, Crimea, USSR, in 1961. He received the Diploma and Ph.D. degrees from the Moscow Institute of Physics and Technology, Moscow, Russia, in 1985 and 1988, respectively, and the Dr.Sci. degree in experimental physics from the Institute for High Energy Density, Russian Academy of Sciences (RAS), Moscow, in 2000.

Since 1988, he has been a Research Scientist, Senior Research Scientist, Head of Laboratory, Deputy Director, and Head of Department of the Joint Institute for High Temperatures, RAS, where he has been a member since 2008. He is also the Head of Department of the Moscow Institute of Physics Science and Technology, Dolgoprudny, Russia. He is the author of more than 100 refereed papers in scientific journals and 170 conference papers on topics related to low-temperature plasma processing and dusty plasmas. His scientific interests are focused on strongly coupled dusty plasmas, probe and optical diagnostics of plasma, dusty plasma under microgravity, and plasma applications in medicine.

Adam Wysocki was born in Czarnowasy, Poland, in 1975. He received the Diploma and Ph.D. degrees from the Heinrich-Heine-Universität Düsseldorf, Düsseldorf, Germany, in 2003 and 2009, respectively.

He is currently with the Heinrich-Heine-Universität Düsseldorf. His research interests are nonequilibrium phenomena of soft condensed matter.

Hartmut Löwen received the Ph.D. degree in physics (on phase transitions in polaron systems) from the University of Dortmund, Dormund, Germany, in 1987.

He then moved to the Ludwig-Maximilians-Universität München, Munich, Germany, where he worked on surface melting and classical density functional theory. During a postdoctoral stay in Lyon, France, he started to do research on colloidal dispersions. Since 1995, he has been a Full Professor for Theoretical Physics with the Heinrich-Heine-Universität Düsseldorf, Düsseldorf, Germany. He is the Coordinator of the German–Dutch collaborative research center SFB-TR6 "Physics of Colloidal Dispersions in External Fields." His research concerns theoretical descriptions and computer simulations of soft-matter systems.